[redacted]

Last for file

Russian Original Vol. 41, No. 1, July, 1976

January, 1977

SATEAZ 41(1) 605-686 (1976)

SOVIET ATOMIC ENERGY

АТОМНАЯ ЭНЕРГИЯ
(ATOMNAYA ÉNERGIYA)

TRANSLATED FROM RUSSIAN

c/b CONSULTANTS BUREAU, NEW YORK

SOVIET ATOMIC ENERGY

Soviet Atomic Energy is a cover-to-cover translation of *Atomnaya Énergiya*, a publication of the Academy of Sciences of the USSR.

An agreement with the Copyright Agency of the USSR (VAAP) makes available both advance copies of the Russian journal and original glossy photographs and artwork. This serves to decrease the necessary time lag between publication of the original and publication of the translation and helps to improve the quality of the latter. The translation began with the first issue of the Russian journal.

Consultants Bureau journals appear about six months after the publication of the original Russian issue. For bibliographic accuracy, the English issue published by Consultants Bureau carries the same number and date as the original Russian from which it was translated. For example, a Russian issue published in December will appear in a Consultants Bureau English translation about the following June, but the translation issue will carry the December date. When ordering any volume or particular issue of a Consultants Bureau journal, please specify the date and, where applicable, the volume and issue numbers of the original Russian. The material you will receive will be a translation of that Russian volume or issue.

Subscription
$107.50 per volume (6 Issues)
2 volumes per year
Prices somewhat higher outside the United States.

Single Issue: $50
Single Article: $7.50

CONSULTANTS BUREAU, NEW YORK AND LONDON

227 West 17th Street
New York, New York 10011

Published monthly. Second-class postage paid at Jamaica, New York 11431.

Soviet Atomic Energy is abstracted or indexed in *Applied Mechanics Reviews, Chemical Abstracts, Engineering Index, INSPEC—Physics Abstracts and Electrical and Electronics Abstracts, Current Contents,* and *Nuclear Science Abstracts.*

SOVIET ATOMIC ENERGY

A translation of *Atomnaya Énergiya*

January, 1977

Volume 41, Number 1 July, 1976

CONTENTS

CONTENTS

(continued)

The Russian press date (podpisano k pechati) of this issue was 6/23/1976. Publication therefore did not occur prior to this date, but must be assumed to have taken place reasonably soon thereafter.

ARTICLES

NATURAL NUCLEAR REACTOR IN OKLO (GABON)

A. K. Kruglov, V. A. Pchelkin,
M. F. Sviderskii, N. G. Moshchanskaya,
O. K. Chernetsov, and Yu. M. Dymkov

UDC 539.17:549.514.87

When in the middle of 1972 the workers of the French Atomic Energy Commission prepared an operational uranium reference, they observed an abnormally low concentration of the ^{235}U isotope. Search work and other investigations have established that the anomaly stems from ore of the Oklo site (Gabon). A careful investigation of the ore-bearing region has shown that the ^{235}U concentration in the ore of the site reaches only 0.621% and even only 0.440% [1-3]. Such substantial isotope anomalies were observed for the first time in natural beddings.

Investigations of the isotope shifts which occur in nature have been for a long time the object of intent attention of Russian scientists. Various suggestions have been made to explain the small isotope shifts which reach less than 20% of the Clarke ratios. The explanations were based on natural isotope fractionation, biogeochemical separation, radioactive release in α decay, etc. [4, 5].

However, in addition to the small shifts, a spread of the isotope concentration reaching 10^3-10^{10}% was established in the case of He, Xe, Ne, and Sm [6, 7]. Even samples with a ratio $^{239}Pu/U = 10^{-6}$ [8] were found; ^{244}Pu was found in natural samples in amounts exceeding the calculated amounts 10^6-10^8 times [6]; a ^{235}U excess of the order of 0.3-0.02% was observed [1, 2, 6, 7].

Various hypotheses, among them the hypothesis of an annihilating explosion [9], were made to explain the Oklo effect and the above anomalies. The hypothesis of a natural nuclear reactor is the best explanation of the isotope anomalies [3, 10]. The hypothesis is corroborated by the fact that 2 billion years ago the ^{235}U

TABLE 1. Minimal Critical Masses for Enriched Uranium

^{235}U concn. (%) in the material	Critical mass (kg) of ^{235}U		Critical mass (kg) of U	
	heterog. system with reflec.	homog. system without reflec.	heterog. system with reflec.	homog. system without reflect.
0,8	150	∞	18750	∞
1,0	15	∞	1500	∞
2,0	3,8	6,0	190	300
3,0	2,31	4,0	78,7	133
4,0	2,0	3,3	50	82,5
5,0	1,8	2,8	36	56
6,0	1,75	2,6	20	43
7,0	1,5	2,5	21	36
8,0	1,4	2,3	18	29
9,0	1,3	2,2	14	24
10,0	1,2	2,1	12	21
20,0	1,05	1,9	5,25	9,5
30,0	1,0	1,8	3,33	6,0
40,0	0,95	1,75	2,4	4,4
50,0	0,9	1,7	1,8	3,4
60,0	0,87	1,65	1,45	2,75
70,0	0,86	1,60	1,23	2,29
80,0	0,85	1,55	1,06	1,94
90,0	0,82	1,50	0,91	1,67
100,0	0,8	1,45	0,8	1,45

Translated from Atomnaya Énergiya, Vol. 41, No. 1, pp. 3-9, July, 1976. Original article submitted September 19, 1975.

TABLE 2. Long-Lived and Stable Isotopes Which Accumulated upon Neutron Irradiation of the Uranium in the (n, γ) Reaction

Name	Initial material		Reaction		Intermediate isotope			Isotopes accumulating upon irradiation				Isotopes forming after reaction				Isotope preserved to now	
	half-life (years)	quantity (g)	reaction type	cross section, b	name	decay type	half-life	quantity (g)	half-life	quantity (g)	decay type	name	half-life (years)	quantity (g)	type of decay	name	quantity (g)
^{238}U	$4{,}51\cdot10^{9}$	972	n, γ	2,75	^{239}U	β	23,4 min	^{239}Np	2,35 d	2,65	β	^{239}Pu	24360	0,154	α	^{235}U	0,435
^{235}U	$7{,}13\cdot10^{8}$	28	n, γ	101	—		—	^{236}U	$2{,}39\cdot10^{7}$ y	2,82	α	^{236}U	$2{,}32\cdot10^{7}$	2,81	α	^{232}Th	2,55
^{234}U	$2{,}5\cdot10^{5}$	0,052	n, γ	105	—		—	^{235}U	$7{,}13\cdot10^{8}$ y	0,005	α	^{235}U	$7{,}13\cdot10^{8}$	0,005	α	^{207}Pb	0,044
^{230}Th	$7{,}52\cdot10^{4}$	0,013	n, γ	23	^{231}Th	β	25,64 h	^{231}Pa	$3{,}45\cdot10^{4}$ y	$3{,}6\cdot10^{-4}$	α	^{231}Pa	$3{,}45\cdot10^{4}$	$2{,}9\cdot10^{-4}$	α	^{207}Pb	$3{,}2\cdot10^{-4}$
^{231}Pa	$3{,}45\cdot10^{4}$	0,003	n, γ	200	^{232}Pa	β	1,32 d	^{232}U	73,6 y	$5{,}9\cdot10^{-4}$	α	^{208}Pb	Stable	$6{,}2\cdot10^{-4}$	Stable	^{208}Pb	$6{,}2\cdot10^{-4}$
^{227}Ac	22	$6{,}5\cdot10^{-5}$	n, γ	800	^{228}Ac		6,13 h	^{228}Th	1,91 y	$5{,}3\cdot10^{-5}$	α	^{208}Pb	Stable	$4{,}8\cdot10^{-5}$	Stable	^{208}Pb	$4{,}8\cdot10^{-5}$
^{239}Pu	24360	2,65	n, γ	300	—		—	^{240}Pu	6580 y	0,8	α	^{232}Th	$1{,}39\cdot10^{10}$	0,84	α	^{232}Th	0,77
^{240}Pu	6580	0,8	n, γ	270	^{241}Pu	β	13,32 y	^{241}Am	458 y	0,216	α	^{237}Np	$2{,}14\cdot10^{6}$	0,213	α	^{209}Bi	0,187
^{242}Pu	$3{,}74\cdot10^{5}$	0,086	n, γ	20	^{243}Pu	β	4,98 h	^{243}Am	7950 y	$1{,}73\cdot10^{-3}$	α	^{239}Pu	24360	$1{,}7\cdot10^{-3}$	α	^{235}U	$1{,}65\cdot10^{-3}$
^{236}U	$2{,}39\cdot10^{7}$	2,82	n, γ	6	^{237}U	β	6,75 d	^{237}Np	$2{,}14\cdot10^{6}$ y	0,014	α	^{237}Np	$2{,}14\cdot10^{6}$	0,014	α	^{209}Bi	0,012
^{243}Am	7950	$1{,}73\cdot10^{-5}$	n, γ	100	^{244}Am	β	10,1 h	^{244}Cm	18,4 y	$1{,}73\cdot10^{-5}$	α	^{236}U	$2{,}39\cdot10^{7}$	$1{,}67\cdot10^{-4}$	α	^{232}Th	$1{,}6\cdot10^{-4}$

Remark. Uranium quantity 1 kg; neutron flux 10^{21} neutrons/cm^2; irradiation time 10^5 years.

concentration reached 3.64% in place of the present 0.72%, because the half-lives of ^{235}U and ^{238}U are 0.707 and 4.5 billion years, respectively.

Table 1 lists the values of the minimal critical mass for an isotope mixture dependent on the ^{235}U concentration [11] in heterogeneous and homogeneous systems. It was established in experiments that for an at most 3% uranium enrichment, the critical mass decreases when the uranium is heterogeneously distributed in a moderator. A self-sustaining chain reaction cannot occur when the enrichment is less than 0.7% in heterogeneous systems or less than 1% in homogeneous systems. It follows from Table 1 that the critical mass amounts to 79 kg for 3% ^{235}U concentration in the case of heterogeneous systems; the critical mass is 133 kg in the case of homogeneous systems, which corresponds to 222 kg for ore with a 60% uranium concentration in homogeneous systems.

The geological structure of the site, the conditions of its formation, and the presence of water as a moderator favored the development of the reactor in the crust and guaranteed critical reactor conditions for large uranium quantities. The scientists of the entire world took interest in this unique phenomenon to which the International Symposium of June, 1975, in Libreville was devoted. The Soviet Union participated in the Symposium [12]. In the last few years ample experimental data confirming the hypothesis of a natural nuclear reactor were accumulated.

We present in the present paper some results of isotopic, radiochemical, and mineralogical investigations of the ores of the Oklo site. The samples which we have are distinguished by both uranium and ^{235}U concentrations. The scheme of the sample picking is shown in Fig. 1.

Figure 1 shows that samples 1410, 1414, and 1418 are of the zone of the chain reaction and are characterized by high uranium concentration (in excess of 40%) and low ^{235}U concentration; the other samples are from the zone of contamination. Based on data concerning the age of the site and the degree of ^{235}U burnup, the neutron flux of the natural nuclear reactor could be calculated; the flux proved to be 10^{21}

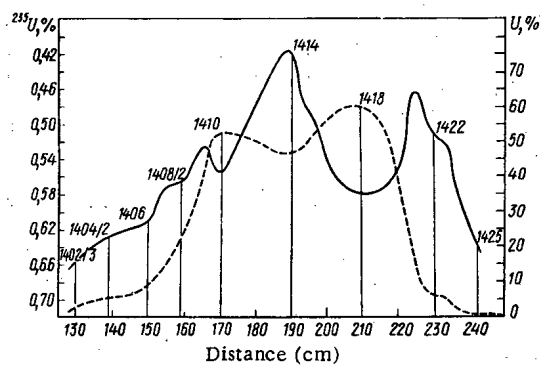

Fig. 1. Scheme of sample picking: — — —) U; ——) ^{235}U.

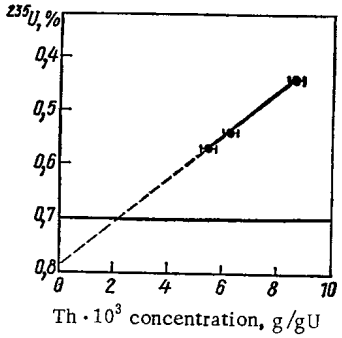

Fig. 2

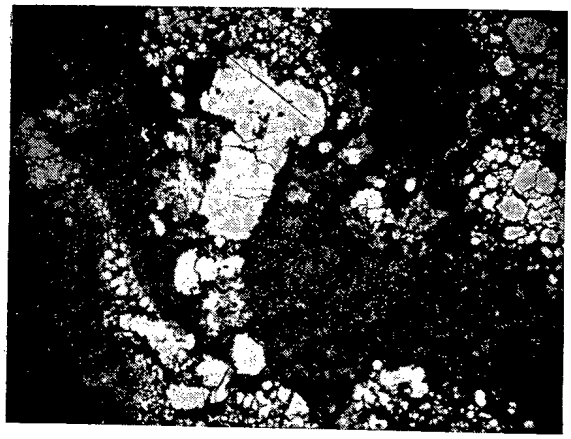

Fig. 3

Fig. 2. ^{232}Th amount per gram of uranium in dependence upon the ^{235}U burnup.

Fig. 3. Prismatic pseudomorphs and granular accumulations of uraninite (white) and phyllite (gray). Polished section (×200).

neutrons/cm^2. This value was used to calculate the accumulation of certain isotopes in the natural uranium (Table 2).*

It follows from Table 2 that ^{232}Th, ^{207}Pb, ^{208}Pb, ^{209}Bi, and ^{235}U can be the end products which reach the present from (n, γ) reactions. We note that ^{208}Pb can result from both ^{232}Th and ^{232}U decays. The ^{208}Pb quantity resulting from the ^{232}U decay is negligibly small relative to the ^{208}Pb from ^{232}Th and cannot be detected at the present time.

The ^{232}Th quantity formed in the reaction $^{235}U(n, \gamma)\ ^{236}U \xrightarrow{\alpha} {}^{232}Th \ldots {}^{208}Pb$ is about 0.3% of the uranium quantity. The fact that the ^{235}U quantity, which was formed again by ^{239}Pu decay, can reach several per cent deserves particular attention.

The fact that thorium is present in samples with high (>40%) uranium concentration suggests that the thorium resulted from the reaction $^{235}U(n, \gamma)^{236}U \xrightarrow{\alpha} {}^{232}Th$. Table 3 lists the results of uranium, thorium, and lead determinations made on several samples. The dependence of the amount of thorium per gram uranium upon the degree of the ^{235}U burnup is linear (Fig. 2), which means that the thorium can accumulate by the conversion $^{235}U(n, \gamma)^{236}U \xrightarrow{\alpha} {}^{232}Th$. This process can occur only in a high neutron flux. When the straight line is extrapolated to the abscissa, the straight line does not pass through the coordinate origin, and, this obviously means that there exists a small thorium concentration which is not associated with uranium minerals.

The burnup of ^{238}U, ^{235}U, and ^{232}Th during the activity of the natural nuclear reactor must reduce the concentrations of ^{206}Pb, ^{207}Pb, and ^{208}Pb which are the end products of the decay of the mother isotopes. The later the nuclear reaction began, the greater the amount of lead corresponding to the initial undisturbed amount of the mother isotopes. This process must be very clearly noticeable in the case of ^{207}Pb, because the burnup of the ^{235}U isotope is most clearly noticeable in the ore of the Oklo site.

*Most of the investigations of the scientists of the French Atomic Energy Commission dealt with the accumulation and analysis of isotopes resulting from fission.

TABLE 3. Concentrations of Uranium, Thorium, and Lead in Samples of the Oklo Site.

Sample No.	Uranium concentration (%)	$\frac{^{235}U}{^{238}U+^{235}U}$	^{235}U concentration (g/g)	Thorium concentration		Lead concentration	
				%	g/g uranium	%	g/g uranium
1410	51,25	0,539	$2,77 \cdot 10^{-3}$	(0,32±0,02)	$6,25 \cdot 10^{-3}$	6,17	0,12
1414	44,1	0,4166	$1,83 \cdot 10^{-3}$	(0,38±0,02)	$8,64 \cdot 10^{-3}$	5,05	0,115
1418	58,9	0,569	$3,36 \cdot 10^{-3}$	(0,32±0,02)	$5,34 \cdot 10^{-3}$	6,13	0,104
1402	2,87	0,657	$1,89 \cdot 10^{-4}$	(0,06)	—	—	—
1406	6,4	0,0126	$3,9 \cdot 10^{-4}$	(0,14)	—	1,23	0,192
1422	5,0	0,5098	$2,55 \cdot 10^{-4}$	(0,066)	—	1,33	0,266

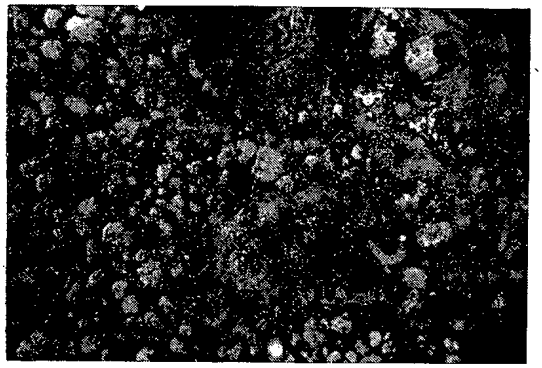

Fig. 4

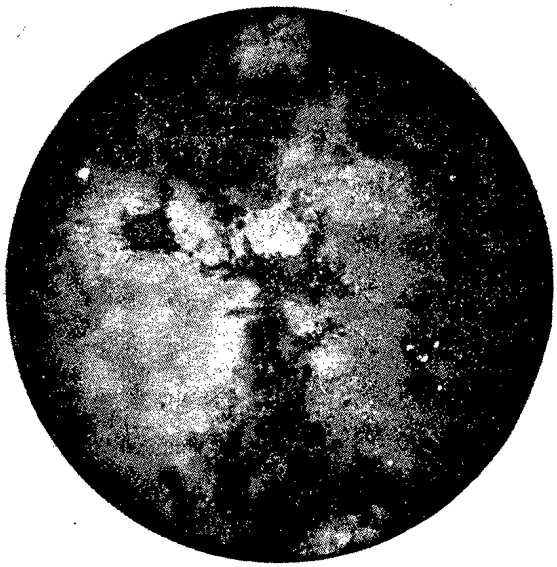

Fig. 5

Fig. 4. Grains of uraninite (bright gray) and nasturan from coffinite (gray) and the argillaceous mass. Polished section, immersed (×2000).

Fig. 5. Coffinite (dark gray) replaces uraninite grains (bright gray and gray phase); the bright dots are galenite grains. Polished section, immersed (×2000).

Unfortunately, radiogenic lead was several times removed while the site existed. Therefore only about one third of the initially accumulated lead was preserved in the samples taken from the reaction zone. The problem can be indirectly solved by comparing the isotope composition of the radiogenic lead determined by mass spectrometry with the calculated composition. The data of the chemical analysis listed in Table 3, the age of 1.7 billion years (accumulation time), and the formulas

$$^{207}Pb = {}^{235}U\,(e^{\lambda_{235}t} - 1);\quad {}^{206}Pb = {}^{238}U\,(e^{\lambda_{238}t} - 1);$$
$$^{208}Pb = {}^{232}Th\,(e^{\lambda_{232}t} - 1).$$

were used for the calculation.

A comparison of the results of an isotope analysis performed on three samples from the reaction zone did not render a clear result. The average concentration of the ^{207}Pb isotope in the samples exceeded the calculated concentration by 5-10%. The excess was about 20% in the zone of contamination. Samples taken from the contaminated zone are distinguished by a rather low ^{235}U concentration (0.6%) and a relatively high uranium concentration (5-10%) and an even higher lead concentration per gram of uranium.

All this may indicate that uranium isotopes migrated several times from the reaction zone into the contaminated zone and in this migration a large deficit of ^{235}U and of radiogenic lead existed. The migration took place to various degrees and in various amounts which cannot be accurately assessed. The

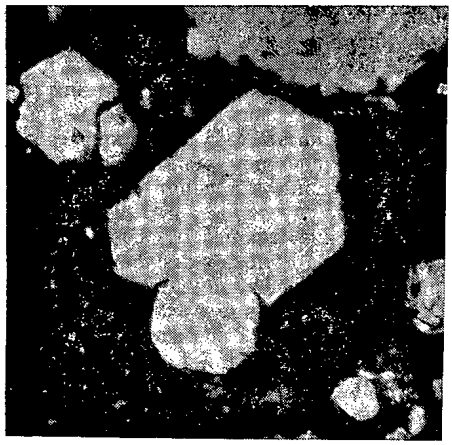

Fig. 6. Uraninite crystals. Polished section, immersed (×2000).

Fig. 7. Block structure of uraninite crystal. Clearly visible are two phases with different reflection (which was enhanced on the print); white corresponds to galenite. Polished section (×1000).

intense migration can be explained by the activity of the natural nuclear reactor.

The results of mineragraphic investigations and x-ray diffraction studies agree with the above data. Three types of ore can be distinguished on the site [13]: bituminous nasturan, uraninitic ore, and uraninitic nasturan ore. Rich uraninitic ore containing about 40-60% uranium (zone of the chain reaction) has the lowest ^{235}U concentration. According to the x-ray diffraction data and the diffractometric measurements, the powders of uraninitic ore from the reaction zone (samples 1410, 1414, and 1418) are composed of uranium oxide with the crystal lattice parameter a_0 = 5.43-5.44 Å; this corresponds to the lattice parameter of typical Oklo uraninite [14].

Mineragraphic investigations were made on nasturan—uraninite ore from the contaminated zone. Monolithic pseudomorphs of uraninite proper to some nonidentified mineral and pseudomorphous aggregates of granular uraninite, nasturan, and coffinite with the outlines of chlorite crystals were found in the ore of the contaminated zone. Veins of separated uraninite crystals in phyllite are strongly developed (Fig. 3); recent nasturan (Fig. 4), which under the electron microscope is determined as pseudomorph of coffinite, and even more recent coffinite (Fig. 5), which, according to the diffraction measurements, conserved its crystal lattice, are present along with uraninite in the veins.

Some small grains of uraninite from the veins or from aggregates of polymineral pseudomorphs have regular crystallographic outlines (Fig. 6) which are close to cubic-octahedral structures. The larger crystals have block structure and have a tendency to splitting and forming spherulites (Fig. 7). Certain phases of different ages can be distinguished with high magnifications on certain complicated uraninite grains which had been etched with acids. Signs of dendritic or spherolithic-crystalline growth were determined for the early phases; indicators pointing to intense recrystallization and to a more recent multiple uraninite ⇌ coffinite replacement were found (see Fig. 5). It was not clearly established whether the ancient uraninite was the primary uranium mineral or whether the uraninite replaced the coffinite.

In x-ray diffraction work on single grains of uranium oxides from the contaminated zone, E. N. Zav'yalov detected up to three cubic UO_{2+x} phases having the following lattice parameters a_0: 5.48-5.49, 5.43-5.45, and 5.39 Å.

Uraninite from pegmatites usually has a greater lattice parameter because thorium is contained in that uraninite. Thorium-free uraninite with the lattice parameter 5.48-5.49 Å is known from a metasomatic ferrouranium site which, like the Oklo site, has an age of $1.8 \cdot 10^9$ years [15]. One might assume that the uranium oxide with a_0 = 5.48-5.49 Å in the samples 1404/2 and 1408/2 belongs to relicts of ancient thorium-free uraninite.

TABLE 4. Results of Radiochemical Investigations

Sample No.	U, %	^{235}U, g/g)	^{230}Th, (Ci/g)	^{226}Ra,(Ci/g)	^{223}Ra,(Ci/g)	$^{230}Th/^{238}U$	$^{226}Ra/^{238}U$	$^{223}Ra/^{235}U$
1402	2,87	$1,89 \cdot 10^{-4}$	$(1,70 \pm 0,05)\ 10^{-8}$	$9,65 \cdot 10^{-9}$	$4,0 \cdot 10^{-10}$	1,74	0,99	0,98
1406	6,4	$3,9 \cdot 10^{-4}$	$(2,23 \pm 0,08)\ 10^{-8}$	$2,84 \cdot 10^{-8}$	$8,6 \cdot 10^{-10}$	1,03	1,31	1,05
1410	51; 25	$2,77 \cdot 10^{-3}$	$(2,05 \pm 0,07)\ 10^{-7}$	$1,65 \cdot 10^{-7}$	$5,35 \cdot 10^{-9}$	1,18	0,95	0,89
1414	44,1	$1,83 \cdot 10^{-3}$	$(1,77 \pm 0,09)\ 10^{-7}$	$1,45 \cdot 10^{-7}$	$3,60 \cdot 10^{-9}$	1,18	0,97	0,92
1418	58,9	$3,36 \cdot 10^{-3}$	$(2,1 \pm 0,1)\ 10^{-7}$	$1,87 \cdot 10^{-7}$	$6,1 \cdot 10^{-9}$	1,05	0,94	0,84
1422	5,0	$2,55 \cdot 10^{-4}$	$(1,76 \pm 0,06)\ 10^{-8}$	$1,87 \cdot 10^{-8}$	$5,15 \cdot 10^{-10}$	1,04	1,10	0,94
1425	2,18	—	$7,9 \cdot 10^{-9}$	$7,15 \cdot 10^{-9}$	—	1,06	0,97	—

Assuming that the lattice parameter of uranium oxide increases in proportion to the incorporation of lead atoms at interstitial sites (with the lead atoms formed in the radioactive decay), uranium oxide with the lattice parameter $a_0 = 5.43$-5.44 Å can be considered younger than the ancient uraninite by at least one order of magnitude. Uranium oxide with the lattice parameter $a_0 = 5.39$ Å is usually created when coffinite decays into the recent stages of mineralization [16].

The oxides are distinguished not only by the time of their formation but also by the mechanism of their formation. The experiments made by A. I. Tugarinov et al. [15] have shown that a uranium oxide with $a_0 = 5.44$ Å is formed when lead is removed from the lattice of ancient uraninite with $a_0 = 5.48$ Å, provided that the uraninite is heated in solution to 600°C. It is possible that the ore of the Oklo site was also liberated from radiogenic lead in the time of the chain reaction. Of particular importance is the fact that oxides with $a_0 = 5.43$-5.44 Å occur mainly in the reaction zone which is also characterized by a sharp deficit of radiogenic lead.

The appearance of coffinite, which, according to our assumptions, was subsequently replaced by nasturan with $a_0 = 5.39$ Å, was preceded by the precipitation of kaolinite or illite (see Fig. 4) which developed in the form of transversely fibrous veins in coarse uraninite grains. The formation of recent uranium minerals, which are associated with the metasomatic replacement of uraninite, could cause a repeated purification of uraninite from several or all preceding generations of radiogenic lead. In any case, galenite accompanies the recent nasturan and coffinite:

$$\underset{a_0=5.48\text{ Å}}{(U, Pb)O_{2+x_1}} \xrightarrow{\nearrow Pb} \underset{a_0=5.44\text{ Å}}{(U, Pb)O_{2+x_2}} \xrightarrow{\nearrow Pb} [USiO_4] \rightarrow \underset{a_0=5.39\text{ Å}}{(U, Pb)O_{2+x_3}} \xrightarrow{\nearrow Pb} USiO_4.$$

Thus, three varieties of uranium oxide were found in the contaminated zone. One variety seems to have developed in the course of the formation of the primary bed; another variety is associated with the response to some recrystallization processes (nuclear chain reaction); and the third variety reflects the recent hydrothermal processes of local redistribution of uranium minerals.

The fact that the recent coffinite is well preserved does not rule out the possibility that this coffinite was formed in the "cementation" zone in the present epoch, particularly since processes of surface migration were recognized: gummite, rutherfordine, and wölsendorfite were established on the site [13, 17].

Table 4 lists the results of radiochemical investigations of the state of the radioactive equilibrium in the decay of ^{238}U and ^{235}U. The results indicate that the ratio of ^{226}Ra to ^{238}U is practically equal to one, whereas the ratio of ^{230}Th to ^{238}U is in some cases substantially greater than one. Specifically, the ^{230}Th activity exceeds the ^{238}U activity by approximately 20% in two samples taken from the zone of the chain reaction. This detail, and the small geochemical mobility of the thorium isotopes relative to uranium, suggest that uranium migrated in the present epoch (the time required for establishing equilibrium between ^{238}U and ^{230}Th amounts to $\sim 10^6$ years). A missing equilibrium between ^{223}Ra and ^{235}U was experimentally established. But in order to explain this phenomenon, one must have information on the concentration of ^{231}Pa and ^{227}Ac in the samples. Work which is done for this purpose is in progress.

Since no lump samples from the zone of the chain reaction nor from the zone of the bituminous nasturan ore are available, it is not possible to completely reconstruct the sequence of geochemical events. But one can tentatively speak of mineral formation in the course of three metallogenetic epochs.

A. Precambrian processes corresponding to an age of $1.8 \cdot 10^9$ years comprise the formation of the primary sediments, evidently glauconites, their conversion into chlorite, the conversion of the chlorites

before, or simultaneous with, the formation of uraninite and, possibly, coffinite, and the replacement of silicates by uranium oxides. One can assume that this epoch is related to nuclear fission processes of ^{235}U and reactions involving neutrons owing to the accumulation of both fission products and ^{232}Th.

B. Events corresponding to an age of several hundred million years: vehement, intense recrystallization and replacement of $(U, Pb)O_{2+x_1}$, accompanied by the separation and migration of lead. The migration of both uranium and radiogenic lead resulted in a zone of blending and mixing.

C. Recent processes, corresponding to an age of dozens of millions of years. These processes encompass the formation of coffinite and its decomposition, the formation of iron sulfides and galenite, the regeneration of coffinite, and more recent supergene processes. The latter processes are related to changes in the radioactive equilibrium between ^{238}U and ^{230}Th, obviously owing to the migration of uranium.

Thus, preliminary investigations of samples from the Oklo site have shown that the uranium minerals from the various sections of the site are characterized by various compositions and ages. A ^{232}Th excess was found in samples from the zone of the chain reaction; the excess is directly related to the degree of the ^{235}U burnup. An excess ^{207}Pb concentration was found in samples from the zone of mixing; this concentration was also increased relative to the equilibrium concentration of ^{230}Th.

The deviations which were observed indicate that the processes causing the disturbances are very complicated and dissimilar and do not always conform to the accepted theories of the ore-formation processes and the laws of radioactive equilibrium. The previously advanced hypotheses only partially explain the deviations.

One must recognize that, in the ore of the Oklo site, there occurred and, possibly, occur to the present time, strong, repeated migration processes involving elements which make it impossible to clearly decide over several problems concerning the mechanism of the isotope replacement. The replacement can originate from ancient nuclear processes, but some of the replacement processes must be ascribed to a more recent time.

LITERATURE CITED

1. R. Bodu et al., Compt. Rend. Acad. Sci., 275, D-1731 (1972).
2. M. Neuilly, Compt. Rend. Acad. Sci., 275, D-1847 (1972).
3. R. Naudet, Bul. Inform. Sci. Techn., 193, 746 (1974).
4. A. P. Vinogradov, Introduction to the Geochemistry of the Ocean [in Russian], Nauka, Moscow (1967).
5. G. V. Gorshkov et al., The Natural Neutron Background of the Atmosphere and the Crust [in Russian], Atomizdat, Moscow (1966).
6. V. V. Cherdyntsev, Geokhimiya, No. 4, 373 (1960).
7. D. Hoffman et al., Nature, 255, 19 (1971).
8. V. V. Cherdyntsev, N. B. Kadyrov, and N. V. Novichkova, Geokhimiya, No. 3, 16 (1970).
9. N. A. Vlasov, Atomnaya Énergiya, 34, No. 5, 395 (1973).
10. R. S. Prasolov, Atomnaya Énergiya, 36, No. 1, 57 (1974).
11. B. G. Dubovskii et al., Critical Parameters of Systems with Fission Substances and Nuclear Safety (Handbook) [in Russian], Atomizdat, Moscow (1966).
12. A. K. Kruglov et al., in: Proc. IAEA Symp. "The Oklo Phenomenon," IAEA, Vienna (1975), p. 303.
13. J. Geffrey, in: Proc. IAEA Symp. "The Oklo Phenomenon," IAEA, Vienna (1975), p. 133.
14. F. Weber and J. Geffrey, in: Proc. IAEA Symp. "The Oklo Phenomenon," IAEA, Vienna (1975), p. 173.
15. A. I. Tugarinov, E. V. Bibikova, and S. I. Zykov, Atomnaya Énergiya, 16, No. 4, 332 (1964).
16. Yu. M. Dymkov, The Nature of Uranium Pitchblende [in Russian], Atomizdat, Moscow (1973).
17. J. Geffrey, Bul. Inform. Sci. Techn., 193, 57 (1974).

STUDYING THE INTERACTION OF MOLTEN FUEL WITH SODIUM IN THE ACTIVE ZONE OF A FAST REACTOR

Yu. K. Buksha, Yu. E. Bagdasarov, and I. A. Kuznetsov

UDC 621.039.58

An important prospective fault process in the operation of fast reactors is the thermal interaction of molton fuel with sodium.

The upper limit of energy accompanying such an interaction can be estimated from the thermodynamic relationships [1]. However, this approach yields very high results for the conversion of thermal energy into mechanical energy, insofar as it assumes an instantaneous transmission of energy from the fuel to the coolant.

The evolution of such a process greatly depends on the rate of heat exchange between fuel and coolant.

Articles [2-6] propose various limitations on the heat exchange, which are determined in the main by the heat resistance of the fuel particles. The approach to the problem of determining the effect of the resultant sodium vapor on the process varies. It is suggested that the vapor envelopes the fuel fully, after which the transmission of heat from the fuel to the coolant can be ignored [2], or that a film of sodium remains on the surface of the fuel particles from which it also evaporates [3-5]. These models describe the boundary cases of the process of heat transmission. Article [6] suggests what appears to be the most realistic model, which takes into account the possibility of the formation of a thin vapor film on the surface of the fuel particles having finite heat resistance. The formation of such a film has been confirmed experimentally [7, 8].

The present article suggests a model which enables us to take into account the condensation of vapor on the cold parts of the channel and the effect of the initial quantity of vapor on the process of interaction. By taking these effects into account, we are able to arrive at a more realistic representation of the interaction of the fuel with sodium. The results are given of a calculation applying to a reactor type BN-600.

Let us consider a certain volume which includes the coolant, its vapor, uncondensed gas, and finely dispersed fuel particles located somewhere within the active zone of a reactor. The process of interaction between the molten fuel and sodium can be described in the following manner.

The variation of the thermodynamic parameters of the coolant, according to the first law of thermodynamics, can be described by the following expressions

$$\frac{di}{dt}=\frac{dQ}{dt}+v_{\mathrm{Na}}\frac{dp}{dt}, \tag{1}$$

where v is the specific density; p is the pressure; Q is the quantity of heat acting on the sodium;

$$i=f(p, v_{\mathrm{Na}}). \tag{2}$$

The quantity of heat Q acting on the sodium can be determined by solving the heat conductivity equation for the fuel particles

$$c_{\mathrm{F}}\rho_{\mathrm{F}}\frac{\partial\theta}{dt}=\lambda_{\mathrm{F}}\Delta\theta+Q_{v}, \tag{3}$$

where c is the specific heat at constant pressure; λ is the heat conductivity; ρ is the density; θ is the temperature of the fuel; Q is the heat generated per unit volume.

Translated from Atomnaya Énergiya, Vol. 41, No. 1, pp. 9-14, July, 1976. Original article submitted May 4, 1975.

The relationship between the volume of uncondensed gases and pressure can be described by the polytropic equation

$$pv_G^n = p_0 v_{G0}^n. \tag{4}$$

Additional ratios between the pressure and the volume of the zone of interaction are determined by the equation of motion of the coolant surrounding the reaction zone

$$p = f\left(V, \frac{dV}{dt}, \frac{d^2V}{dt^2}\right). \tag{5}$$

The process of thermal interaction between the fuel and the coolant can be divided into two phases. In the first phase, the sodium is in the liquid state, while in the second phase the sodium is boiling. Let us consider the first phase. The volume occupied by the zone of interaction can be expressed by the formula

$$V = \frac{M_F}{\rho_F} + \frac{M_{Na}}{\rho_{Na}} + \frac{M_G}{\rho_G}, \tag{6}$$

where M_F, M_{Na}, and M_G represent the weights of fuel, sodium and gas, respectively. We differentiate this equation with respect to time, assuming the density of the fuel to be constant. As shown by calculation, the effect of variations of fuel density on the pressure does not exceed 10%:

$$\frac{dV}{dt} = -\frac{M_{Na}}{\rho_{Na}^2}\frac{d\rho_{Na}}{dt} - \frac{M_G}{\rho_G^2}\frac{d\rho_G}{dt}. \tag{7}$$

By using the equation of state of the gas (4) and of the sodium (2) in the form $\rho = f(p, T)$, we find that

$$\frac{1}{\rho_G^2}\frac{d\rho_G}{dt} = \frac{1}{\theta_{G0} n p_0}\left(\frac{p_0}{p}\right)^{\frac{n+1}{n}}\frac{dp}{dt}; \tag{8}$$

$$\frac{1}{\rho_{Na}^2}\frac{d\rho_{Na}}{dt} = \frac{\beta_F}{\rho_{Na}}\frac{dp}{dt} - \frac{\alpha_p}{\rho_{Na}}\frac{dT}{dt}, \tag{9}$$

where α_p is the coefficient of thermal expansion of sodium; β_F is the coefficient of isothermal compression of sodium. Equation (7) can be written as

$$\frac{dV}{dt} = \left(-\frac{M_G}{\rho_{G0} n p_0}\right)\frac{p_0}{p}^{\frac{n+1}{n}} - \frac{\beta_F M_{Na}}{\rho_{Na}}\Bigg)\frac{dp}{dt} + \frac{\alpha_p M_{Na}}{\rho_{Na}}\frac{dT}{dt}, \tag{10}$$

taking (8) and (9) into account. By using the expression for enthalpy $di = c_{Na}dT + (1/\delta_{Na})dp - (1/\rho_{Na})dpdT$, the equation for the first law of thermodynamics (1) for sodium can be written in the form

$$M_{Na}c_{Na}\frac{dT}{dt} - \frac{M_{Na}\alpha_p}{\rho_{Na}}\frac{dp}{dt} = \frac{dQ}{dt}. \tag{11}$$

Let us consider the equation for the variations of volume and energy in the second phase of the process. In this case, equation of state (2) will take the form $p = p(T)$. Using the expression for enthalpy and the specific density of the coolant in the form*

$$i = xi'' + (1-x)i';$$
$$v_{Na} = xv'' + (1-x)v',$$

and differentiating these with respect to time gives us

$$\frac{di}{dt} = \left[x\frac{di''}{dT} + (1-x)\frac{di'}{dT}\right]\frac{dT}{dt} + (i''-i')\frac{dx}{dt}; \tag{12}$$

$$\frac{dv_{Na}}{dt} = \left[-\frac{x}{\rho''^2}\frac{d\rho''}{dT} - \frac{(1-x)}{\rho'^2}\frac{d\rho'}{dT}\right]\frac{dT}{dt} + \left(\frac{1}{\rho''} - \frac{1}{\rho'}\right)\frac{dx}{dt}. \tag{13}$$

Let us write the energy equation taking (12) into account

$$M_{Na}\left[x\frac{di''}{dT} + (1-x)\frac{di'}{dT} - v_{Na}\frac{dp}{dT}\right]\frac{dT}{dt} + M_{Na}(i''-i')\frac{dx}{dt} = \frac{dQ}{dt}. \tag{14}$$

*One and two apostrophes refer to parameters of sodium and vapor on the saturation line, respectively.

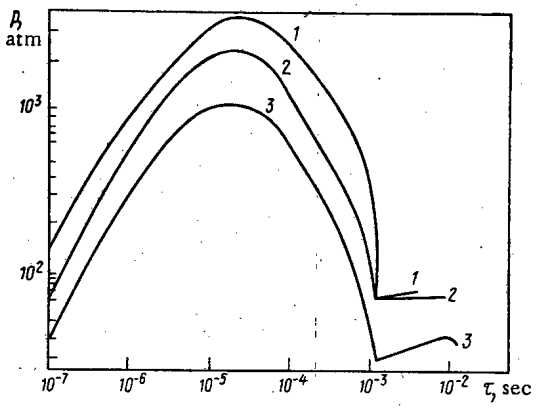

Fig. 1

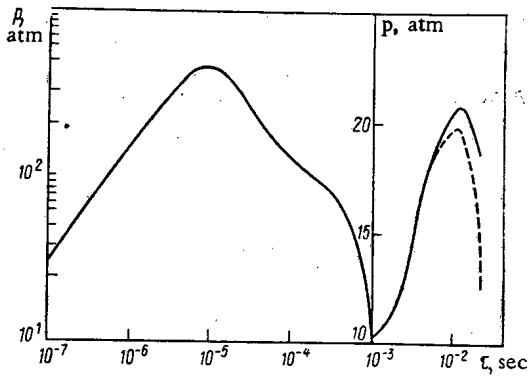

Fig. 2

Fig. 1. Relationship of pressure in interaction zone with respect to time: 1) $z_0 = 10$ cm; R = 0.03 cm; 2) $z_0 = 5$ cm; R = 0.03 cm; 3) $z_0 = 5$ cm; R = 0.06 cm.

Fig. 2. Relationship of pressure in zone of interaction with respect to time for $z_0 = 5$ cm, R = 0.03 cm, and $\varepsilon_F = 3.5$; — — —) and ——) taking into account and ignoring vapor condensation, respectively.

The equation for the variation in volume can be written as

$$\frac{dV}{dt} = M_{Na}\left[\left(-\frac{x}{\rho''^2}\frac{d\rho''}{dT} - \frac{(1-x)}{\rho'^2}\frac{d\rho'}{dT}\right)\frac{dT}{dt} + \left(\frac{1}{\rho''} - \frac{1}{\rho'}\right)\frac{dx}{dt}\right] - \frac{M_G}{n\rho_{G0}p_0}\left(\frac{p_0}{p}\right)^{\frac{n+1}{n}}\frac{dp}{dT}\frac{dT}{dt}, \tag{15}$$

taking (13) into account. To determine the heat flow acting on the sodium, we have to find the temperature field within the fuel particle. The problem can be written in the following system of equations

$$c_F\rho_F\frac{\partial\theta}{\partial t} = \lambda_F\left(\frac{\partial^2\theta}{\partial r^2} + \frac{2}{r}\frac{\partial\theta}{\partial r}\right) + Q_v; \tag{16}$$

$$\left.\frac{\partial\theta}{\partial r}\right|_{r=0} = 0; \tag{17}$$

$$-R\lambda_F\left.\frac{\partial\theta}{\partial r}\right|_{r=R} = \frac{(1+y)\lambda''}{y}(\theta|_{r=R} - T); \tag{18}$$

$$\theta(t=0) = \theta_0, \tag{19}$$

where y is the ratio of the thickness of the film of vapor on the surface of the fuel particles to the radius of these particles; R is the radius of a particle of fuel. When y = 0, we can write $\theta/_{r=R} = T$ in place of (18), as the heat conductivity of sodium is significantly greater than that of the fuel. The heat transmission process is in a large degree defined by the thickness of the vapor film on the surface of the fuel. On the basis of data obtained experimentally, article [6] calculates theoretically the thickness of the vapor film covering the fuel, for conditions in which the weight of the fuel particle is balanced by the hydrodynamic lift caused by the vapor flowing past the particle

$$y = \left(\frac{1.5\mu M_{Na}}{\rho''RgM_F}\frac{dx}{dt}\right)^{1/3}, \tag{20}$$

where μ is the dynamic viscosity of the vapor; q is the acceleration in free fall. The total quantity of heat acting on the coolant per unit time is

$$\frac{dQ}{dt} = -\frac{3M_T}{\rho_F R}\lambda_F\left.\frac{\partial\theta}{\partial r}\right|_{r=R} + \alpha z\pi Dm(T_x - T), \tag{21}$$

where T_x is the temperature of the cold parts of the channel; z is the length of the zone of interaction; D is the diameter of the fuel element; α is the coefficient of heat extraction in the presence of condensation.

Let us consider the equation of motion of the coolant surrounding the zone of interaction. For a melting zone of length z_0 in the individual packets, we assume that the molten fuel mixes with the coolant throughout the entire section of the packet. The walls of the packet are absolutely rigid and the zone of interaction extends only in the axial direction. In the initial stage of the process, we have to take into consideration the compressibility of the sodium. For this, we can employ an acoustic approximation

$$\frac{dz}{dt} = \frac{p(t) - p_0}{\rho_{Na_0} C_0} \quad \text{for} \quad t < t_{ac} = \frac{2l_0}{C_0}, \tag{22}$$

in which C_0 is the speed of sound in sodium; subscript 0 refers to time zero. For times $t > t_{ac}$, we can ignore the compressibility of the sodium and return to the usual expression for the motion of a column of sodium

$$\frac{d^2z}{dt^2} = \frac{p - p_B}{\rho_{Na_0}(l_0 - z - z_0)} - q - \xi\left(\frac{dz}{dt}\right)^2 \frac{1}{D_G}. \tag{23}$$

The initial conditions for equation (23) are

$$\left.\frac{dz}{dt}\right|_{t=t_{ac}} = \int_0^{t_{ac}} \frac{(p - p_0)\,dt}{\rho_{Na_0} l_0}. \tag{24}$$

For the sake of simplicity, let us consider the upwards expansion only; the relationship between the rate of ejection of coolant from the channel and the rate at which the volume of interaction changes can be determined from the expression:

$$\frac{dV}{dt} = \frac{V_0}{z_0}\,\eta\,\frac{dz}{dt}, \tag{25}$$

where l is the height of the sodium column above the zone of interaction; n is the ratio of the cross-sectional area of sodium flow to the cross-sectional area of the zone of interaction.

The mathematical expressions we have given above represent a closed system of control, which fully describes the interaction process of the molten fuel with sodium.

Fig. 1 gives the results of calculation relating to the following parameters: $T_0 = 1110$ K, $\theta_0 = 3100$ K, $\varepsilon_F = 13$, $\varepsilon_G = 0$, $x = 0$; where ε_F is the ratio of the fuel weight to the weight of sodium in the zone of interaction; ε_G is the ratio of the weight of gas to the weight of sodium in the zone of interaction. The ratio of the fuel weight to the sodium weight corresponds to the proportion by volume of these components in the fuel can. The maximum pressure is achieved during the first phase of the process. The rate of rise of pressure in this period is determined by the temperature coefficient of pressure and the rate of heat supply to the sodium, as the expansion of the zone of interaction is insignificant at this stage. The zone of interaction expands depending on the propagation of the disturbance; it then reaches its maximum and starts to fall. When the pressure has fallen to the saturation pressure at the temperature of the sodium, the latter begins to boil and the process advances to the second stage. When $z_0 = 10$ and $R = 0.03$ cm (curve 1), the maximum pressure in the zone of interaction reaches 3150 atm and the fuel packet is free of sodium after $\sim 4.5 \cdot 10^{-3}$ sec. If the zone of interaction is reduced by half, $z_0 = 5$ cm, and at the same fuel particle dimensions, the maximum pressure is reduced to ~2200 atm and this process takes place in $7 \cdot 10^{-3}$ sec (curve 2). By comparing curves 2 and 3, we can see the effect of the heat-transmission surface for a given ratio of fuel and sodium by weight. Curve 3 shows the pressure in the zone of interaction at $z_0 = 5$, $R = 0.06$ cm. Increasing the dimensions of the fuel particles by a factor of two leads to a fall in the maximum pressure, also by a factor of two. This is important, as in all the known experiments, the particle dimensions have been quite small (< 0.1 cm), but the spread of the data has been large. Apparently, the dispersion of the fuel is largely determined by the conditions accompanying the progression of the interaction process. For example, the average particle dimensions were ~0.025 cm in [8], while for the experiments carried out in the loop of reactor TREAT, the dimensions were ~0.05 cm [9]. Further experimental work is needed, under conditions that approximate to the actual conditions existing within a reactor, in order to determine this important parameter.

Figure 2 considers the case of partial melting of fuel and its ejection into the space between the fuel elements when $z_0 = 5$, $R = 0.03$ cm, $\varepsilon_T = 3.5$. Such a fuel—sodium weight ratio corresponds to melting and ejection from the can of 10% of the fuel. A maximum pressure of ~465 atm will be attained.

Figure 2 also shows by means of the dashed line the results of calculations which take condensation of the vapor upon expansion in the cold part of the packet into consideration.

Calculations were also carried out for other weight ratios of fuel and sodium in the zone of interaction; these showed that the effect of condensation depends to a significant extent upon the value of this ratio and the dispersion of the fuel. The smaller the ratio of fuel weight to weight of sodium and the larger

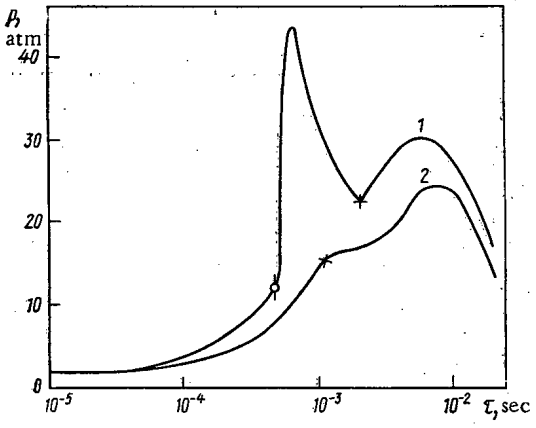

Fig. 3

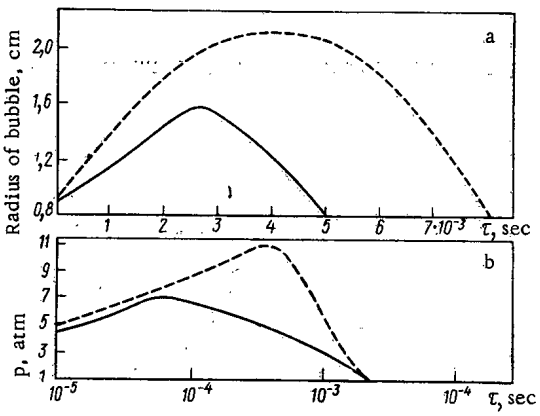

Fig. 4

Fig. 3. Relationship of pressure in interaction zone with respect to time for $z_0 = 5$ cm, R = 0.03 cm: 1) $\varepsilon_F = 3.5$; $\varepsilon_G = 2.5 \cdot 10^{-4}$; x = 0; 2) $\varepsilon_F = 3.5$; $\varepsilon_G = 0$; $x = 10^{-4}$; ○) full condensation; ×) commencement of boiling.

Fig. 4. Local interaction of fuel and sodium with radius of interaction zone (a) and pressure (b) in the zone of interaction: ——) and — — — —) taking into account and ignoring the formation of a vapor film on the surfaces of the fuel particles, respectively.

the fuel particle size, the greater will be the effect of vapor condensation on the pressure. With very large ratios, e.g., in the case of total melting of the fuel, the effect of vapor condensation is practically negligible.

Disruption of the can and ejection of molten fuel will be accompanied by the emission of gaseous fission products. The presence of gas in the zone of interaction can significantly influence the pressure, as the gas will act as a cushion to compensate for variations in the volume of the sodium as it is heated. This can lead to a reduction in pressure during the initial stage of the process.

The results of calculations of the interaction process of molten fuel with sodium in the presence of gas are given in Fig. 3 (curve 1) for the following parameters of the zone of interaction: $z_0 = 5$ cm, R = 0.03 cm, $\varepsilon_F = 3.5$, $\varepsilon_G = 2.5 \cdot 10^{-4}$, x = 0. The ratio of weight of gas to weight of sodium corresponds to 15% of the volume of gas to the total volume of the interaction zone. Let us assume that the gas is under adiabatic conditions (n = 1.4). By comparing the results of calculations that take the gas into account with the result of calculations that ignore the presence of the gas, we are able to draw the following conclusions: If there is gas present in the zone of interaction, then there will be no significant peaks of pressure in the first phase of the process. The nature of the process in the second stage, when the sodium melts, is practically independent of the presence of the gas.

The effect on the interaction of an initial quantity of sodium vapor was studied; this could be formed during the initial stage of the process, when the fuel escapes into the sodium (Fig. 3, curve 2). The calculations were carried out for the following parameters: $z_0 = 5$ cm, R = 0.03 cm, $\varepsilon_F = 3.5$, $\varepsilon_G = 0$, $x = 10^{-4}$.

The heat losses on evaporation, condensation of vapor on the cold parts of the fuel element, and the formation of a vapor film over the surface of the fuel, have a significant effect on the nature of the process. The vapor may not condense at all with large initial formations of vapor or a small scale melting of fuel. The pressure pulses are one or two orders of magnitude less, if we take gas and initial vapor in the zone of interaction into account, than they would be if both vapor and gas were absent (Figs. 1-3). This corresponds more closely with the real picture of the disruption of a fuel element and coincides closely with experimental results [5].

All these calculations are affected by investigations of interactions taking place throughout the whole section of the packet. This same model was used for calculating local interactions between fuel and sodium following the disruption of several fuel elements and the escape of a small quantity of fuel into the sodium. This is the most probable fault situation.

Figure 4 gives the results of calculations of interaction between the fuel and the surrounding sodium when one fuel element melts over a length of 1 cm in the presence of an initial quantity of vapor. The

The calculations were conducted in spherical geometry. The initial radius of the zone of interaction was 1 cm. From Fig. 4 (solid line) we can see that the maximum pressure in the zone of interaction is ~7 atm, the maximum radius of bubble is ~1.6 cm, and the life of the bubble is $\sim 5 \cdot 10^{-3}$ sec. The dashed curve shows the results of calculations for this same interaction process on the assumption of ideal contact between fuel particles and sodium in the zone of interaction (the limiting case of heat transmission), which can be the case in the presence of a film of sodium on the surfaces of the fuel particles [3]. In this case, the maximum pressure in the zone of interaction is ~11 atm, the life of the bubble being $\sim 8 \cdot 10^{-3}$ sec.

From the safety point of view, it is of interest to know how quickly the fault will spread from element to element. Two methods of propagation are possible. In the first, the film of sodium on the surface of the fuel elements dries up and the elements melt. In the second, the pressure generated in the zone of interaction causes mechanical disruption of the fuel elements. The magnitude of the pressure pulse and its duration are insignificant, so that it will not be possible in this case to observe any significant deformation (Fig. 4). As regards the first method of fault propagation; as the life of the bubble is $(5-8)\ 10^{-3}$ sec, whereas the life of the film of sodium on the surfaces of the fuel elements is 0.2-0.3 sec for the parameters of reactor type BN-600, it would not be possible for the film to dry away and for the element to melt and eject fuel into the zone of the bubble.

LITERATURE CITED

1. A. Judd, Trans. Amer. Nucl. Soc., 13, No. 1, 369 (1970).
2. A. Padilla, ibid., p. 375.
3. D. Cho, Trans. Amer. Nucl. Soc., 13, No. 2, 659 (1970).
4. D. Cho, Trans. Amer. Nucl. Soc., 14, No. 1, 290 (1971).
5. A. Cronenberg et al., Nucl. Sci. and Eng., 50, No. 1, 53 (1973).
6. L. Caldarola, Nucl. Eng. and Design, No. 22, 175 (1972).
7. L. Witte, Trans. ASME, Ser. C, 90, No. 1, 9 (1968).
8. M. Farahat, Trans. Amer. Nucl. Soc., 14, No. 1, p. 236.
9. D. Armstrong et al., Trans. Amer. Nucl. Soc., 13, No. 2, p. 660.
10. Y. Marchaterre et al., in: Proc. Symp. IAEA "Eng. of Fast Reactors for Safe and Reliable Operation," Karlsruhe, Oct. 9-13 (1972).

ESTIMATE OF THE CORROSION OF ZIRCONIUM ALLOYS UNDER OPERATING CONDITIONS

V. V. Gerasimov, A. I. Gromova, and V. G. Denisov

UDC 621.039.53

In modern nuclear power generation, zirconium alloys are used widely as materials for the active zone. Soviet reactor construction uses mainly alloys, alloyed with niobium. The most complete investigation of these alloys under static conditions was carried out by A. A. Kiselev et al. [1].

Under operating conditions, the materials of the active zone are subjected to the action of a coolant of a defined chemical composition and temperature, thermal flux and irradiation. Many of these factors require the use of numerical methods for estimating the corrosion stability of the alloy for any specific case.

It is well known that oxidation of zirconium and its alloys takes place by diffusion of anions of oxygen through the oxide film. The protective oxide film formed during corrosion undergoes thinning in consequence of the diffusion of oxygen into the metal and the removal of corrosion products into the water. The solution of

Translated from Atomnaya Énergiya, Vol. 41, No. 1, pp. 14-17, July, 1976. Original article submitted July 10, 1975.

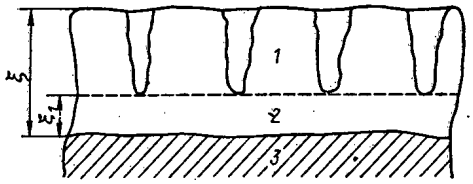

Fig. 1. Structure of the oxide layer of the alloy Zr + 1% Nb: 1) oxide film; 2) barrier layer; 3) metal.

oxygen in the metal exerts a significant effect on the kinetics of corrosion of zirconium and its alloys at a temperature in excess of 400-450°C.

By taking into account the decisive role of diffusion in the process of corrosion, the solution of oxygen in the metal, and the removal of the corrosion products into the water, a differential equation can be compiled

$$\frac{dW}{d\tau} = \frac{K}{W - W_p - S\tau} + K_l, \qquad (1)$$

where K is a parabolic constant of the rate of corrosion $(mg/dm)^2 \cdot h^{-1}$; K_l is a linear constant which takes into account the corrosion by surface defects $(mg/dm)^2 \cdot h^{-1}$; W is the increase in weight of the sample, taking into account the mass of oxygen transferred to the water with the corrosion products, mg/dm^2; W_p is the amount of oxygen dissolved in the metal, mg/dm^2; S is the rate of loss of oxygen from the zirconium corrosion products into the water, $mg/(dm^2 \cdot h)$; τ is the time, h. This equation does not describe corrosion by a cubic law, which for alloys of zirconium with niobium occurs only at the initial instant of oxidation [1].

The first term of Eq. (1) describes quantitatively the process of transfer of oxygen through the entire thickness of the protective film ξ, and the second term can be considered as a quantitative description of the process of the transfer of oxygen by the so-called "short path." This process is shown schematically in Fig. 1. Part of the film during oxidation of the metal can form at a certain thickness ξ_1 a unique barrier layer [2], which is fairly perfect, i.e., it has an insignificant number of defects. A layer of film with a thickness in excess of ξ_1 for a number of reasons has an imperfect structure, i.e., it is porous. Therefore, diffusion of oxygen anions through the thin protective film can emerge as the linear component of the corrosion process for the condition, that the thickness of the barrier layer is not changed significantly.

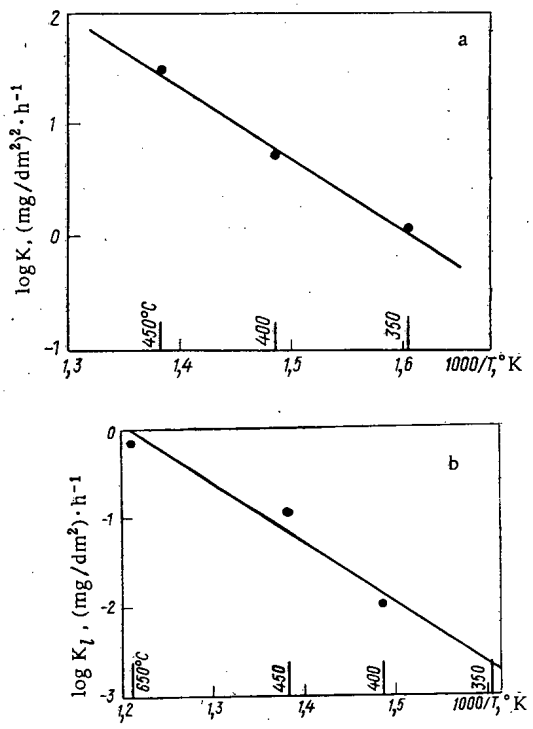

Fig. 2. Dependence of the parabolic (a) and linear (b) corrosion velocity constants on the reciprocal of the temperature, for the alloy Zr + 1% Nb.

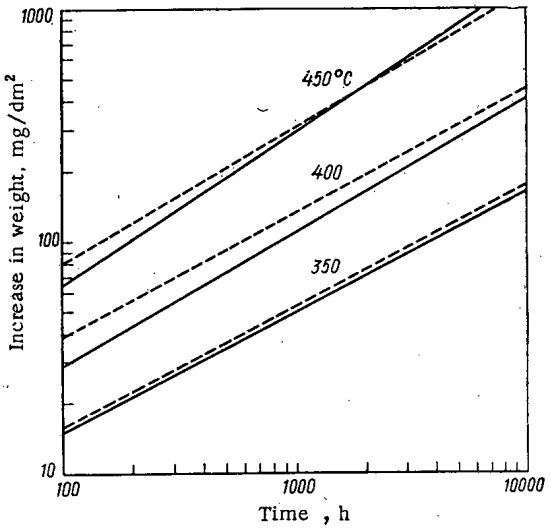

Fig. 3

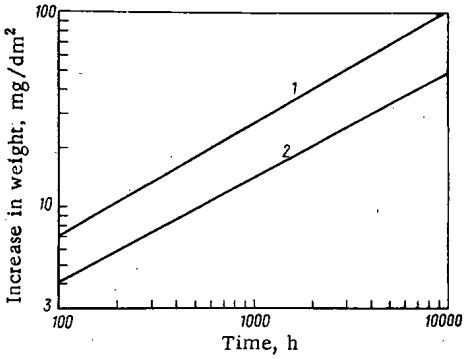

Fig. 4

Fig. 3. Experimental (——) and calculated (— — —) corrosion curves of the alloy Zr + 1% Nb at a different temperature.

Fig. 4. Calculated corrosion curves of the alloy Zr + 1% Nb: 1) with thermal flux and 2) without thermal flux.

Diffusion of oxygen anions through the whole thickness of the film of corrosion products ξ in time will appear as the parabolic component of Eq. (1).

The validity of Eq. (1) can be shown by an example of the corrosion of the alloy Zr + 1% Nb, for which an empirical equation of the type

$$W = a\tau^n \tag{2}$$

was obtained [1], for a series of temperatures. It is necessary to find the values of the constants K and K_l, and also the energy of activation Q. In the case when corrosion of the alloy proceeds according to a parabolic law, i.e., n = 0.5, and the loss of corrosion products into the water can be neglected, it is easy to show that the parabolic constant, taking account of the diffusion of oxygen into the metal, is determined by the equation

$$K = \frac{a\left[a - 2(C_s - C_0)\sqrt{D/\pi}\right]}{2}, \tag{3}$$

where a is the constant in the corrosion equation $W = a\tau^{1/2}$; C_0 is the initial concentration of oxygen in the metal; C_S is the concentration of the saturated solid solution of oxygen in the metal; D is the coefficient of diffusion of oxygen in the metal.

The quantity of oxygen dissolved in the metal is calculated by the formula

$$W_p = 2(C_s - C)\sqrt{(D\tau)/\pi}. \tag{4}$$

Because of the absence of experimental data on the diffusion of oxygen in zirconium alloy Zr + 1% Nb, values for unalloyed zirconium are used [3]

$$D = 9.4\exp\left(-\frac{51780}{RT}\right), \text{ cm}^2/\text{sec}.$$

When corrosion of the alloy proceeds by a paralinear law [4], i.e., n of Eq. (2) is larger than 0.5, the parabolic and linear velocity constants of corrosion can be determined by solving the system

$$\left.\frac{dW}{d\tau}\right|_{\tau_1} = \frac{K}{W_1 - 2(C_s - C_0)\sqrt{(D\tau_1)/\pi} - S\tau_1} + K_l,$$
$$\left.\frac{dW}{d\tau}\right|_{\tau_2} = \frac{K}{W_2 - 2(C_s - C_0)\sqrt{(D\tau_2)/\pi} - S\tau_2} + K_l. \tag{5}$$

The values of $(dW/d\tau)_{\tau_1}$, $(dW/d\tau)_{\tau_2}$, W_1, and W_2, can be found from the empirical Eqs. (2), obtained for several temperatures. The value of S for autoclave conditions can be assumed equal to zero.

Figure 2 shows the dependence of the logarithm of the parabolic and linear velocity constants of corrosion on the reciprocal of the temperature. The value of the linear constant for 650°C is taken from [5].

The energy of activation of the parabolic and linear process amounts to 29.2 and 30.5 kcal/mole, respectively, i.e., the values are quite close. This confirms the opinion stated earlier that the parabolic and linear components of Eq. (1) describe the processes of transport of oxygen anions through the oxide film.

Using the values obtained for the linear corrosion velocity constant, the thickness of the barrier layer ξ_1 can be calculated for the alloy Zr + 1% Nb over the temperature range 400-450°C. If the surface area occupied by defects does not exceed 1% [6] of the total area of the sample, then the thickness of the barrier layer is close to 0.2 μ, which corresponds to an increase in weight of 3.5 mg/dm^2.

The experimental and calculated curves (Fig. 3) coincide satisfactorily, considering the spread of the experimental points [1]. The distribution of the oxygen concentration in the metal was calculated by the equation

$$\frac{C(x)-C_0}{C_s-C_0}=1-\operatorname{erf}\frac{x}{2\sqrt{D\tau}}. \tag{6}$$

At 350, 400, and 450°C, the depth of the diffusion zone amounts to 5-10, 10-15 (after 10,000 h), and 20-25 μ (after 5,000 h), respectively.

Corrosion of zirconium alloys under thermal flux conditions proceeds more intensely than without thermal flux [7]. This is explained by the fact that, in addition to the effect of the drop in temperature around the heat-transferring surface, the temperature of the protective film is being increased continuously, and that of the metal itself in consequence of the high thermal resistance of the zirconium corrosion products. The increase of temperature takes place until a film of constant thickness is formed on the surface of the sample, i.e., dynamic equilibrium is established between the corrosion and the corrosion products carried into the water, and also by the diffusion of the oxygen of the film into the metal.

An increase of the temperature of the oxide leads to an increase of the values of the corrosion velocity constants K and K_l. With increase of the temperature of the metal, the coefficient of diffusion of oxygen in zirconium increases and W_p is increased. The rate of loss of the corrosion products S depends on the temperature of the oxide — medium interface [8].

The values of K, K_l and D can be found from Arrhenius' equations. The value of the temperature occurring in each of these equations can be determined from the thermal conductivity equation. As the thickness of the oxide film is far less than the diameter of the fuel element cladding, the thermal conductivity equation for a plane wall can be used:

$$T=T_0+q\left(\frac{\xi}{\lambda_{ox}}+\frac{\delta(\tau)}{\lambda_{dep}}\right), \tag{7}$$

where T is the temperature of the metal — oxide boundary and the oxide — medium boundary, °K; q is the thermal flux, kcal/(m^2·h); λ_{ox} and λ_{dep} are the coefficients of thermal conductivity of the oxide layer and of the deposits, kcal/(m·h·deg); ξ, $\delta(\tau)$ is the thickness of the oxide layer and of the deposits, m.

$$\xi=(W-W_p-S\tau)\frac{M_{ox}}{M_0\rho}, \tag{8}$$

where M_{ox} and ρ are the relative molecular weight and density of the oxide; M_0 is the mass of oxygen arriving at a single molecule of oxide.

Relations (7) and (8), and also Arrhenius' equation for K, K_l and D allow Eq. (1) to be solved, taking into account the effect of the thermal flux. As an example, Fig. 4 shows the dependence of the rate of corrosion of the zirconium alloy Zr + 1% Nb in water at 285°C, and reflects the effect of a thermal flux of $1\cdot10^6$ kcal/(m^2·h). The rate of loss of corrosion products was assumed to be 0.00234 mg/(dm^2·h) [8]. When estimating the effect of the thermal flux, the formation of deposits on the heat transfer surface was taken into account. This is explained by the fact that the thermal conductivity of these, as a rule, iron oxide deposits approximates to the thermal conductivity of the zirconium corrosion products [9, 10].

As Eq. (4) can be obtained only for a constant diffusion coefficient, and in the actual corrosion process with thermal flux D depends on the temperature, the calculation by Eq. (1) must be carried out for several intervals of time $\Delta\tau$, during which a change of D can be neglected. An estimate of corrosion under heat transfer conditions was carried out on the BÉSM-6 computer by the Runge — Kutta method.

Thus, it was shown that the rate of corrosion of the alloy Zr + 1% Nb in water at a temperature of 285°C and with a thermal flux of $1 \cdot 10^6$ kcal/($m^2 \cdot h$) is higher than without a thermal flux by a factor of two approximately.

LITERATURE CITED

1. A. A. Kiselev et al, in: Proc. IAEA Symp. on "The Corrosion of Reactor Materials," Vol. 2, Salzburg, June (1962), p. 67.
2. D. Douglass, The Metallurgy of Zirconium, IAEA, Vienna (1971).
3. J. Pemsler, Electrochem. Soc., 105, 315 (1958).
4. O. Kubashevskii and B. Hopkins, Oxidation of Metals and Alloys [in Russian], Edition 2, Metallurgiya, Moscow (1965).
5. B. G. Parfenov et al., Corrosion of Zirconium and Its Alloys [in Russian], Atomizdat, Moscow (1967), p. 67.
6. B. Cox, in: Proc. of the Third Intern. Congress on Corrosion of Metals [Russian translation], Vol. 4, Mir, Moscow (1968), p. 347.
7. P. Cohen, Technology of Water for Power Reactors [Russian translation], Atomizdat, Moscow (1973).
8. L. V. Ryabova et al., Teploénergetika, No. 3, 57 (1970).
9. N. G. Rassokhin et al, Teploénergetika, No. 9, 12 (1973).
10. Maki Hideo, J. Nucl. Sci. and Technol., 10, No. 3, 170 (1973).

EFFECT OF THE PRESENCE OF Kh18N10T STEEL ON THE CORROSION STABILITY OF ZIRCONIUM ALLOYS

V. F. Kon'kov, A. N. Sinev, and A. A. Khaikovskii

UDC 621.039.53

It has been noted that during autoclave tests, the rate of corrosion of certain zirconium alloys is considerably higher than at the same temperature under clean conditions: in a quartz facility in a current of superheated steam at atmospheric pressure. Together with other factors, the presence in the medium of stainless steel components may have an effect on the rate of corrosion in the autoclave. This is related also

TABLE 1. Composition of Alloys and Conditions of Preliminary Treatment

Composition of alloy, wt.%	Annealing		Finishing conditions		
	t, °C	time, sec	composition of bath, parts by vol.	t, °C	time, sec
Zr+1Nb	580	3	$40HNO_3$+ +10HF	10—25	10—15
Zr+2,5Nb	550	5	$60HNO_3$+ +20HF+ +$20H_2SO_4$	15—20	5—10
Zr+1Nb— —0,5Fe— —1,2Sn	580	3	$30H_2O$+ +$30HNO_3$+ +$30H_2SO_4$+ +10HF	30	15—20
Zr+1,2Sn+ +0,5Fe	700	1,5	$50H_2O$+ +$35HNO_3$+ +15HF	40	15—20
Zr+0,8Fe+ +0,7Cu	500	4	$40HNO_3$+ +10HF	10—30	10

Translated from Atomnaya Énergiya, Vol. 41, No. 1, pp. 17-22, July, 1976. Original article submitted July 31, 1975.

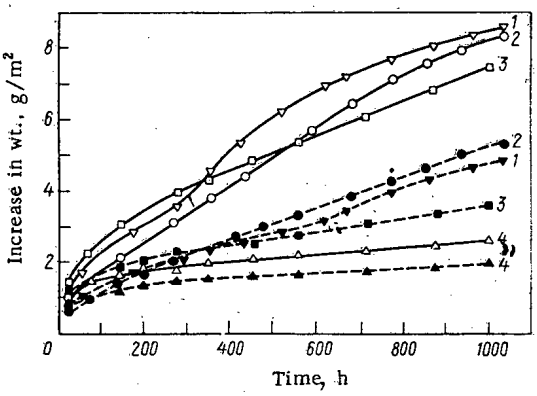

Fig. 1. Corrosion stability of alloys (1-4) tested in water at 350°C in steel (———) and zirconium (— — —) ampoules.

to the behavior of zirconium alloys in reactors. Although in [1] corrosion intensification of the alloy Zircalloy-2, mainly alloyed with tin, was not observed, during tests in stainless steel ampoules it remains unclear to what extent the results can be extended to other zirconium alloys.

EXPERIMENTAL PROCEDURE

Alloys based on zirconium, alloyed with Nb, Fe, Sn, and Cu, were investigated in different combinations (see Table 1). The tests were conducted in two groups of identical ampoules (microautoclaves) with a working volume of 6 cm^3. The ratio of the surface of the samples to the surface of the microautoclave was 1 : 5. One group of ampoules was made from Kh18N10T stainless steel and the other from Zr + 1% Nb.* The tests were conducted over the temperature range 300-450°C in water and in steam. The pressure at 300 and 350°C was equilibrium and at 400 and 450°C it was ~150 atm. In order to avoid an electrochemical effect, the inside surface of the microautoclaves was oxidized beforehand, to create an insulating film. The samples for the corrosion tests (35 × 10 × 1 mm) were chemically finished, recry-

*Later in the text — steel and zirconium ampoules.

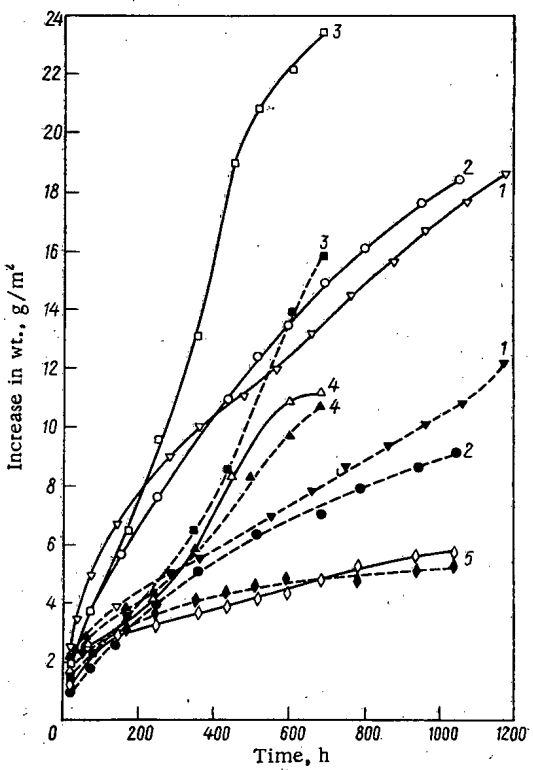

Fig. 2. Corrosion stability of alloys (1-5) tested in steam at 450°C in steel (———) and zirconium (— — —) ampoules.

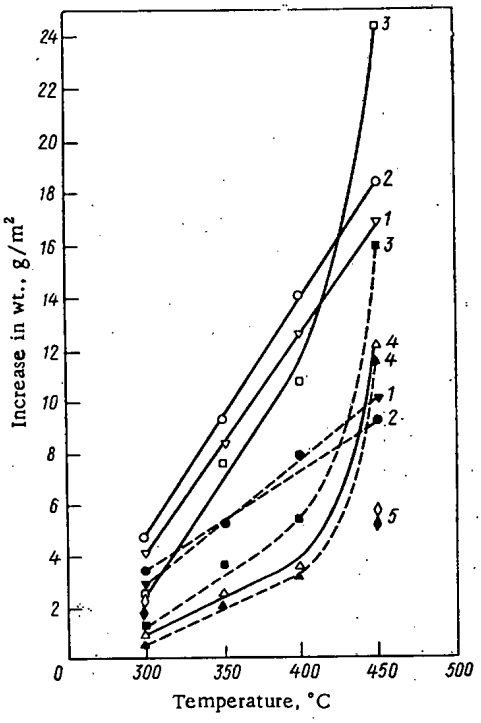

Fig. 3. Effect of temperature on the corrosion stability of zirconium alloys in steel (——) and zirconium (— — —) ampoules.

stallization annealed in vacuo at not less than $5 \cdot 10^{-5}$ mm Hg, and refinished (see Table 1).

The ampoules were cooled after approximately every 100 h in order to weigh and assess the external appearance of the samples. The surface of the samples was rubbed with a wad soaked in alcohol before weighing. In order to assess the corrosion behavior of the alloys, gravimetric, metallographic and micro-x-ray spectral analysis were used. Weighing was carried out on a VLM-20-M analytical balance with a sensitivity of $2 \cdot 10^{-5}$ g. The error in determining the increase of weight of the samples did not exceed 7%. In addition to corrosion, the effect of the presence of steel on the hydrogenation of the samples was studied. The concentration of hydrogen in the alloys was estimated by the method of isotopic equilibrium, with an error of ±10%.

RESULTS OF THE EXPERIMENTS

Corrosion Stability. It can be seen from the arrangement of the curves in the graph (Fig. 1), that in all the tests in water at 300 and 350°C the samples which were placed in steel ampoules showed a higher increase in weight. It was observed that the alloys containing niobium (1, 2, and 3) showed the maximum sensitivity to the presence of stainless steel. After holding for 100 h at 350°C in the steel ampoules, the increase in weight for these alloys was found to be approximately twice as large as for the alloys tested in zirconium ampoules. In the same way, the presence of stainless steel also affected the behavior of samples tested in steam at a temperature of 450 and 400°C (Fig. 2).

Based on the data obtained from the corrosion tests, graphs were constructed of the dependence of the total increase in weight of the samples on the temperature (Fig. 3). The duration of the tests of alloys

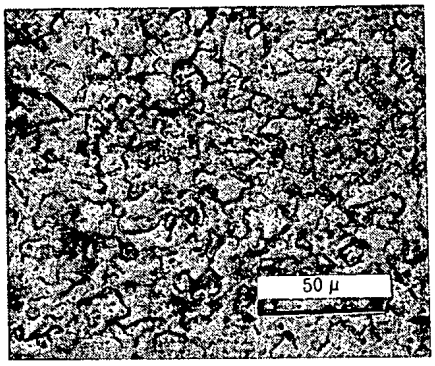

Fig. 4. Surface of oxide film after 1000 h of corrosion of the alloy Zr + 1% Nb in steam, in a zirconium ampoule.

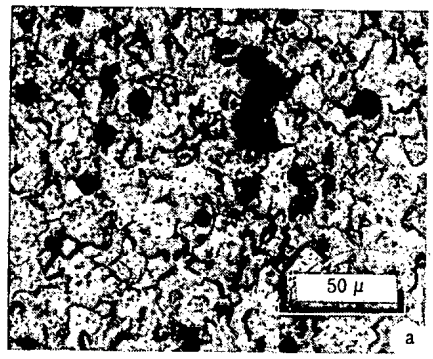

Fig. 5

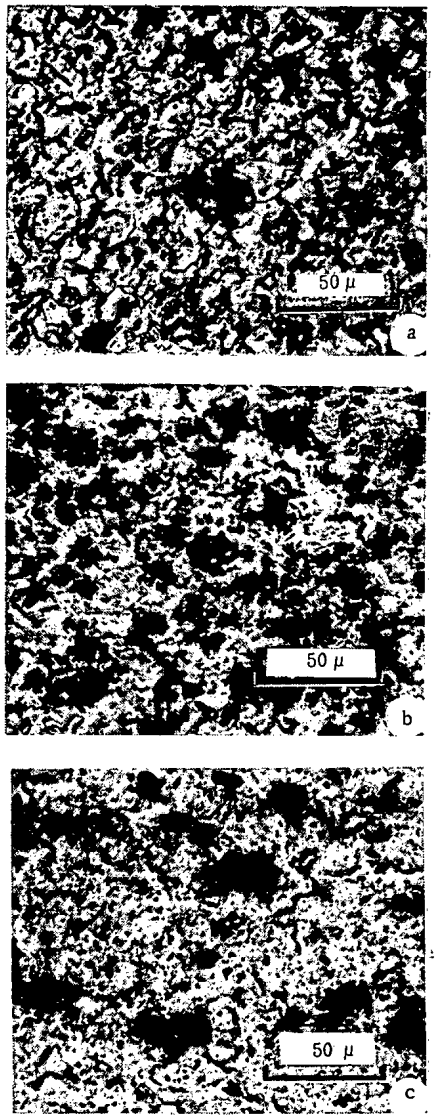

Fig. 6

Fig. 5. Surface of oxide films on zirconium alloys after 1000 h holding in water at 300°C in steel ampoules: a) Zr + 1% Nb; b) Zr + 2.5% Nb; c) Zr + 1% Sn + 0.5% Fe.

Fig. 6. Surface of oxide films on zirconium alloys after 680-1000 h of testing in steam at 450°C in steel ampoules: a) Zr + 1% Nb; b) Zr + 2.5% Nb; c) Zr + 1% Sn + 0.5% Fe.

1, 2, and 5 was 1000 h. Because of severe damage to the samples of alloys 3 and 4 at 450°C, the duration of their tests did not exceed 680 h.

It can be seen from Fig. 3, that with increase of temperature there is a tendency toward intensification of a negative effect of stainless steel on the corrosion stability of niobium-containing alloys (1, 2, and 3), in contrast to alloys which do not contain niobium (4 and 5).

In one of the experiments, the samples during the corrosion tests in steel ampoules at 450°C were not rubbed. Over the lapse of 1000 h their surface was covered with a green deposit, the weight of which was significantly less than the difference of the increase in weight of the samples tested in steel and zirconium ampoules.

Microtopography. The surface of the samples of all the alloys tested in zirconium ampoules, during the entire test in water and steam, was free from any extraneous matter (Fig. 4). The topography of the oxide films on these samples depended only on the composition of the alloy.

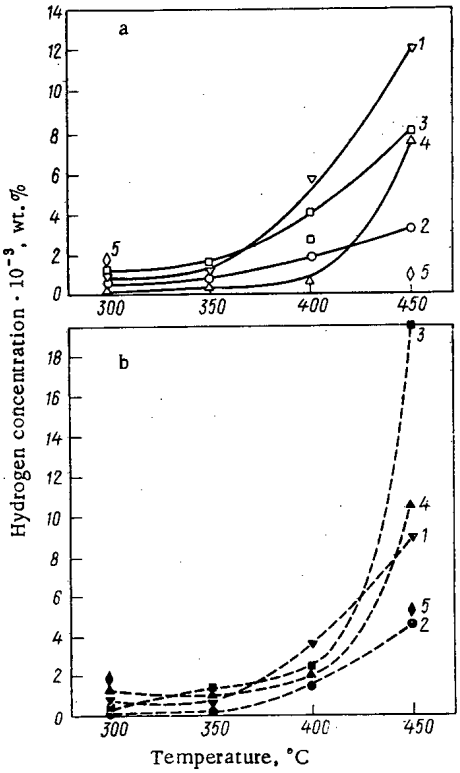

Fig. 7

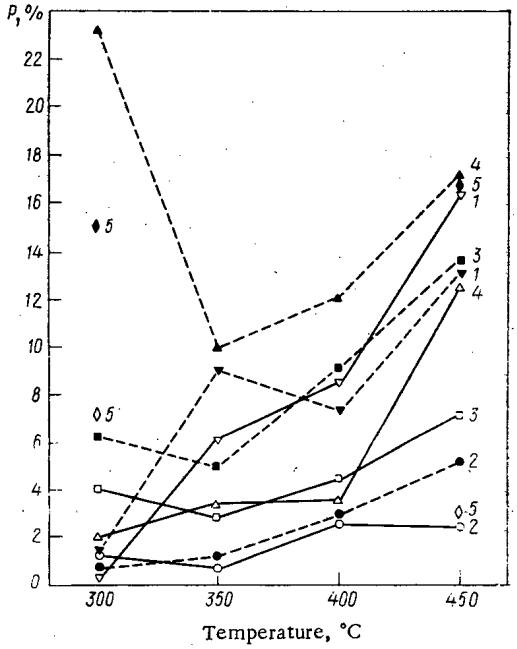

Fig. 8

Fig. 7. Effect of temperature of corrosion tests in water and steam on the hydrogenation of zirconium alloys (1-5) in: a) steel and b) zirconium ampoules.

Fig. 8. Temperature dependence of the ratio P — the quantity of hydrogen absorbed by the alloys — to that theoretically released during corrosion in steel (———) and zirconium (— — —) ampoules.

On the surface of the oxide films of the alloys tested in water in steel ampoules, dark spots appeared (Fig. 5), which became enlarged with increase of the holding time. Micro-x-ray spectral analysis established that chromium and a relatively small quantity of iron was present only in the spots, but nickel or titanium were not detected.

On the surface of samples tested in steam (Fig. 6) during 1000 h in steel ampoules, star-shaped flake formations are encountered on the background of the overall contamination by the mass-transfer products. Many of them contain metallic crystals of regular faceting. Chromium is detected in all the spots. Iron is found in addition to chromium in the particularly black small spots, but these spots are considerably fewer than for the tests in water. Nickel and titanium were absent in the oxide films.

With increase of the temperature and duration of the tests, the clear localization of the regions in which chromium is present rapidly vanishes, especially for the alloys containing niobium.

Thus, it can be stated that during corrosion in water and in steam, mass transfer takes place from the walls of the steel ampoules to the samples of all the alloys. As a result of this, chromium and iron are carried in the water to the surface of the samples, but in steam it is predominantly chromium.

Absorption of Hydrogen. It can be seen from the arrangement of the curves in Fig. 7 that in the corrosion tests during 680-1000 h, absorption of hydrogen by all alloys (with the exception of alloy 5, tested in steel ampoules) is increased with increase of temperature. This effect is expressed the least at a relatively low temperature (300-350°C). An increase of the niobium content from 1 to 2.5% reduces the capability of hydrogen absorption in the tests in steam (400-450°C). For alloys which are alloyed only with niobium (1 and 2), tests in ampoules of different materials did not lead to significant changes of the hydrogen concentration. This confirms also the temperature dependence of the ratio of absorbed hydrogen to that theoretically released during corrosion (Fig. 8).

During the test in zirconium ampoules at 450°C, alloys 3 and 5 displayed a more intense hydrogen absorption, and alloy 4 underwent considerable hydrogenation over the whole temperature range (see Fig.

7). This is true also for the relative hydrogenation of these alloys. It can be seen from the arrangement of the curves in Fig. 8 that alloys 4 and 5 absorbed most intensely the "extraneous" hydrogen (released during corrosion of the walls of the zirconium ampoules). The hydrogen pressure in the medium had relatively less effect on alloy 3.

DISCUSSION OF RESULTS

The data obtained give a basis for concluding that the presence of stainless steel Kh18N10T intensifies the corrosion of alloys containing niobium but has almost no effect on the corrosion of other alloys.

Changes of topography of the oxide films and the results of micro-x-ray spectral analysis show that at all the temperatures of the tests, transfer of the components of stainless steel to the surface of the samples of all alloys is observed. The investigations carried out of the effect of some of the components of Kh18N10T steel on the kinetics of corrosion, and also on the microtopography of the oxide films and the composition of their surface, give the basis for supposing that deterioration of the corrosion stability of alloys containing niobium is caused by deposition on zirconium alloys of compounds of chromium from the stainless steel. As a result of this, the metallic niobium found in the film obviously reduces the chromium compounds to the elementary state. Confirmation of these opinions are the specific changes of topography of the oxide films, depending on the temperature of the medium, the duration of the tests, composition of the alloys, and the appearance in the transfer products of metallic crystals of chromium. Thermodynamic data confirm the possibility of the corresponding reactions proceeding at an increased temperature ($-\Delta F_{Cr_mO_n}$ = 34-78 kcal/g·atom O; and $-\Delta F_{Nb_kO_l}$ = 78-82 kcal/g·atom O) [2]. The surface activity of the oxide film may also promote this process. Zirconium, which just like niobium has a greater affinity for oxygen in comparison with chromium, does not fulfil the reducing function, being bound in ZrO_2. This process can lead to local breakdown of the oxide film structure and a partial loss of the protective properties, so that it is intensified with increase of temperature.

Copper, iron, and tin, which occur in the oxide films of the corresponding alloys, do not interact with chromium compounds, as they possess a lesser affinity toward oxygen ($-\Delta F$ = 24-55 kcal/g·atom O) [2]. This can explain the absence of a mass transfer effect in the corrosion of alloys which do not contain niobium, in particular the alloy Zircalloy-2, which was investigated by Shirvington.

During the tests, not only the samples but also the walls of the microautoclaves were corroded. Consequently, the pressure of molecular hydrogen in the ampoules of the alloy Zr + 1% Nb was higher than in the ampoules of stainless steel. With increase of temperature this pressure increased. As hydrogenation of the alloys containing niobium, after the tests in steel and zirconium ampoules, was almost identical, then it can be supposed that under the given conditions these alloys (in contrast from the alloys not containing niobium), are not disposed toward absorption of associated hydrogen in the molecules.

The relative hydrogenation of alloy 4 in the zirconium ampoules was higher than in the steel ampoules, which may be due to the increased pressure of hydrogen with insufficient protection properties of the oxide film or with an increased affinity of the alloy to hydrogen. The tests at 450°C were an exception, when corrosion of the samples was extremely intense and the hydrogen pressure increased markedly, not only in the zirconium ampoules but also in the stainless steel ampoules.

Comparison of the results of the tests of alloy 5 in steel or zirconium ampoules shows that the relative hydrogenation at 450°C is no higher than at 300°C, which is explained by the excellent protective properties of the oxide film at high temperature and the relatively poor protective properties at low temperature. The relative hydrogenation in zirconium microautoclaves was significantly higher than in steel autoclaves, which indicates the additional absorption of hydrogen at the increased pressure.

Thus, the higher trend to the relative hydrogenation of the alloys which do not contain niobium is probably due to the additional absorption of hydrogen from the medium. Consequently, a reduction of the partial pressure of hydrogen will contribute to a reduction of the absolute absorption of hydrogen by these alloys during corrosion.

LITERATURE CITED

1. P. Shirvington, A. Brandhurst and P. Heuer, J. Nucl. Mater., 44, 79 (1972).
2. K. E. Wieks and F. E. Block, The Thermodynamic Properties of 65 Elements, Their Oxides, Halides, Carbides and Nitrides [Russian translation], Metallurgiya, Moscow (1965).

DETERMINATION OF THE CONTENT OF TRITIUM AND KRYPTON IN VVÉR* FUEL ELEMENTS AND A STUDY OF THEIR DISTRIBUTION IN THE PREPARATORY OPERATIONS OF FUEL ELEMENTS FOR REPROCESSING

A. T. Ageenkov, A. A. Buravtsov,
E. M. Valuev, L. I. Golubev,
Z. V. Ershova, V. V. Kravtsev,
and A. F. Shvoev

UDC 621.039.54

In [1], the composition of the gas collected by puncturing the cladding of irradiated VVÉR fuel elements was studied. In this present paper, the total content of T and Kr-85 is determined in the fuel elements (including the gas phase, cladding and fuel), and also the distribution of T and Kr-85 is studied, with the mechanical cutting of the fuel elements, over the temperature range 50-700°C and by dissolving the fuel in HNO_3. For the investigation, the depleted fuel elements from two fuel assemblies are taken, the characteristics of which are given in Table 1.

The fuel burnup along the fuel elements was nonuniform. The degree of nonuniformity $C = B_{max}/B_{min}$ amounts to 2.5. The minimum burnup is for the fuel located round the ends of the fuel elements. The leak-tightness of the fuel element cladding was checked beforehand; all 14 fuel elements selected for the investigation proved to be leak-tight.

The fuel elements were cut by special hydraulic shears with a leak-tight cutting chamber (Fig. 1). The pitch of the cut was 40 mm. The gas, released by cutting of the fuel elements, was pumped out with a mercury pump through a manganese moisture separator into a calibrated ampoule. The content of T and Kr-85 in the gas was determined on a radiochromatographic apparatus, described in [2]. The results of the experiments are shown in Figs. 2 and 3, where it can be seen that the release of tritium from the sectioned fuel elements

*Water-cooled/water-moderated power reactor.

TABLE 1. Characteristics of the Fuel Elements Being Studied

No. of fuel element assembly	Av. burnup, MW·day/ for U		Spec. thermal power, W/cm	Time of operating period, eff. days	Cooling time, yr	Calculated build-up of GFP,* taking account of decay, Ci/ton U [3]	
	acc. to neutron flux	acc. to Cs-139 content				T	85Kr
1	19 100	20 000	142	502	1	240±20	5300±400
2	7 500	9 000	155	186	2	100±10	2100±200

*Gaseous fission products.

Translated from Atomnaya Énergiya, Vol. 41, No. 1, pp. 23-25, July, 1976. Original article submitted December 1, 1975.

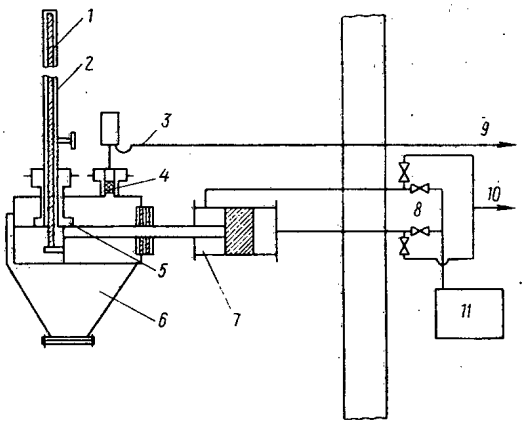

Fig. 1

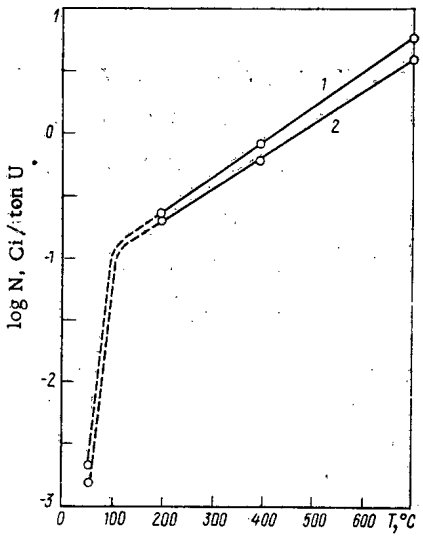

Fig. 2

Fig. 1. Diagram of fuel element cutting equipment: 1) fuel element; 2) guide tube; 3) vacuum communicator; 4) manganese separator; 5) cutting block; 6) bin; 7) hydraulic cylinder; 8) distribution valves; 9) to gas collector; 10) to water drain; 11) hydraulic pump.

Fig. 2. Temperature dependence of release of tritium from the fuel elements of 1) first and 2) second fuel assembly.

at a temperature below 200°C is small and is almost independent of the depth of burnup of the fuel over the approximate range 9000-20,000 MW·day/ton U.

The burnup has a marked effect on the release of tritium at a temperature in excess of 400°C. Thus, at 700°C, 3.5 and 5.4 Ci/ton U of tritium (~9000 and ~20,000 MW·day/ton, respectively) is released from fuel elements with a different burnup.

At 200-700°C, the temperature dependence of tritium release (N, Ci/ton U) is of a logarithmic nature and is expressed by the following empirical formula:

$$\log N = 0.27 \frac{T\,^{\circ}\mathrm{C}}{100} - 0.65. \qquad (1)$$

Between the experimental points of 50 and 200°C there is an inflection (see Fig. 2). The reason for the break in the logarithmic relation over the range 50-200°C is that, at a temperature of 100-200°C desorption of tritiated moisture takes place from the inside surface of the cladding out of the open pores of the fuel.

For Kr-85, a logarithmic dependence of the release of krypton on the temperature is obtained over the whole range investigated, from 50 to 7000°C (Fig. 3), which is described by the following empirical formulas:

$$\lg N = 0.13 \frac{T\,^{\circ}\mathrm{C}}{100} + 0.27 \text{ for a burnup of 9000 MW·day/ton U;} \qquad (2)$$

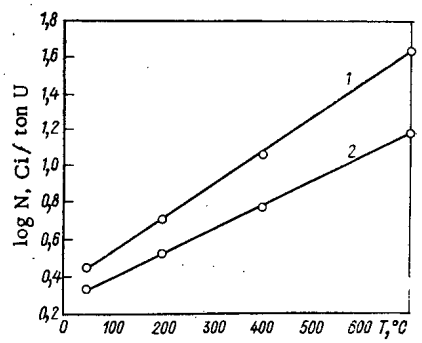

Fig. 3. Temperature dependence of the release of Kr-85 from fuel elements of 1) first and 2) second fuel assemblies.

TABLE 2. Distribution of T and Kr-85 in VVÉR Fuel Elements

Operation	Phase analyzed	Fuel burnup, MW·day/ton U			
		T		^{85}Kr	
		9 000	20 000	9 000	20 000
Cutting (T = 50°C)	Gas	$\frac{1,5\cdot10^{-3}}{0,002}$	$\frac{2,0\cdot10^{-3}}{0,002}$	$\frac{2,0}{0,1}$	$\frac{3,1}{0,1}$
Dissolution of fuel	»	$< \frac{0,1}{0,15}$	$< \frac{0,1}{0,1}$	$\frac{1700\pm500}{99,9}$	$\frac{4900\pm500}{99,9}$
	Solution	$\frac{57\pm8}{85\pm12}$	$\frac{157\pm15}{83\pm8}$	Not determined	Not determined
Content in cladding	Gas	$\frac{10\pm5}{15\pm7}$	$\frac{33\pm10}{17\pm5}$	Not determined	Not determined
Total amount		$\frac{67\pm10}{100}$	$\frac{190\pm20}{100}$	$\frac{1700\pm500}{100}$	$\frac{4900\pm500}{100}$
% of calculated buildup		67±15	79±10	81±29	93±10

Note. Numerator – Ci/ton U; denominator – % of initial amount.

$$\lg N = 0.18\frac{T\,^{\circ}C}{100} + 0,37 \text{ for a burnup of 20,000 MW·day/ton U,} \quad (3)$$

where N is the release of T and Kr, Ci/ton U.

Dissolution of the fuel from the fuel element sections after cutting was accomplished in a leak-tight apparatus with counter-cooling in 9 M HNO_3 at 90-100°C for 2 hours. In this operation, the tritium content was determined in the solution and in the gas phase. The sum of these quantities enabled the initial content of tritium in the fuel to be determined. The Kr-85 content was determined by analysis of the gas.

In the gas phase, collected during dissolution of the fuel, radioactive Kr-85 was identified; elementary tritium was not detected at the sensitivity of the radiochromatograph, $1\cdot10^{-10}$ Ci per sample (on conversion, 0.1 Ci/ton U).

In the liquid phase, purified by double distillation, the content of tritium [4] was determined by a scintillation method (Table 2).

The fuel of the VVÉR fuel elements is enclosed in a cladding of zirconium alloy, which is capable of absorbing hydrogen [5]. The absorption by the cladding material of tritium from the gas phase was verified experimentally. For this, samples were cut out of the fuel element cladding and were washed free of fuel particles in HNO_3 and alcohol. In order to separate the tritium, the samples first of all were saturated with protium at a temperature of 700°C and then dehydrogenized at 900-1000°C in vacuo. The hydrogenation – dehydrogenation operation was carried out twice. The gas liberated was collected and analyzed for tritium. The results of the analysis (see Table 2) confirm the presence in the fuel element cladding of a considerable quantity of tritium. The transfer of tritium to the fuel element cladding, obviously, assists radiolysis of the tritiated moisture under the action of neutron and γ radiations, and also the penetration of recoil atoms as a result of fission.

The experimental data obtained about the content of T and Kr-85 in the gas, in the fuel, and in the claddings, enabled their total content in the VVÉR fuel elements to be determined. The total quantity of Kr-85 in the fuel elements, within the limits of measurement error, corresponds to the calculated content. The total measured quantity of tritium in the fuel elements proved to be somewhat lower than the calculated amount, which may be partially explained by its possible leakage into the coolant through the cladding; however, the deviation from the calculated data obtained is found to be within the limits of spread of the results of analysis.

Thus, the total content of T and Kr-85 in VVÉR fuel elements was determined, and which amounted to 67 ± 10 and 190 ± 20 for tritium; and 2100 ± 500 and 5300 ± 500 Ci/ton U for Kr-85, for fuel elements with burnups of 9000 and 20,000 MW·day/ton U, respectively. By sectioning the fuel elements without heating (50°C), 0.002% of the total T content and 0.1% of the total Kr-85 content is liberated. The release of T and Kr-85 from sectioned fuel elements at a temperature from 50-700°C has been studied. A logarithmic dependence is obtained for the separation of these fission products on the temperature. When the fuel is dissolved in HNO_3, the tritium in the form of oxide is transferred almost completely into the aqueous phase.

LITERATURE CITED

1. A. T. Ageenkov et al., Atomnaya Énergiya, Vol. 40, No. 3, 203 (1976).
2. P. Van Urk and L. Lindner, J. Appl. Rad. Isotopes, Vol. 23, No. 5 (1972).
3. W. A. Haney, Nuclear Safety, Vol. 5, No. 4, 399 (1964).
4. I. M. Lomonosov and L. D. Soshin, Measurement of Tritium [in Russian], Atomizdat, Moscow (1968).
5. A. S. Zaimovskii, V. V. Kalashnikov, and I. S. Golovnin, Nuclear Reactor Fuel Elements [in Russian], Gosatomizdat, Moscow (1962), p. 236.

MATHEMATICAL MODELS OF THE NEUTRON DISTRIBUTION IN A REACTOR

P. T. Potapenko

UDC 621.039.515

The transition from control of the total reactor power to control by the neutron distribution permits an increase in the technical and economic indices of a reactor by optimizing the power distribution.

In designing a system of control by the neutron distribution the problem of choosing and justifying its mathematical model is solved primarily by spatial kinetics methods [1].

Definitions and Mathematical Models. Control is ordinarily accomplished by dividing the core into N cells, each of which has at least one neutron sensor and one control rod for varying the neutron density. The automatic equipment controlling the neutron density in a cell forms the local control LC; means for controlling the total power constitutes the power control PC.

A reactor as a multidimensional control element is described by the transfer matrix H(p). It relates the change in the neutron distribution vector $\delta\Phi$ in the cells to the vector $\delta\mathbf{k}$ describing the change in the neutron multiplication factor (p is the Laplace transform parameter):

$$\delta\Phi(p) = H(p)\,\delta\mathbf{k}(p). \tag{1}$$

According to (1) the neutron flux in the i-th cell is

$$\delta\Phi_i(p) = h_{i1}\delta k_1 + h_{i2}\delta k_2 + \ldots + h_{im}\delta k_m + \ldots + h_{iN}\delta k_N. \tag{2}$$

We expand δk and $\delta\Phi$ in a complete set of orthogonal eigenfunctions — the "harmonics" $f_j(r)$ [1, 2]:

$$\delta\Phi(p, r) = \delta\Phi_0(p) f_0(r) + \sum_{j=1}^{\infty} \delta\Phi_j(p) f_j(r); \tag{3}$$

$$\delta k(p, r) = \delta k_0(p) f_0(r) + \sum_{j=1}^{\infty} \delta k_j(p) f_j(r). \tag{4}$$

Suppose the neutron multiplication factor in the m-th cell changes by δk_m. Then by replacing the spatial coordinate r in Eqs. (3) and (4) by the appropriate subscripts of the cells we find the resulting change in the flux in the i-th cell:

$$\delta\Phi_i(p) = \delta k_{0m}(p) W_0(p) f_{0i} + \sum_{j=1}^{\infty} \delta k_{jm}(p) W_j(p) f_{ji}. \tag{5}$$

Here $W_j(p) = \delta\Phi_j/\bar{\Phi}\delta(kf_0)_{jm}$ is the tranfer function [2] of the j-th harmonic of the reactivity "weighted with f_0" and induced by a local perturbation δk_m (in the form of a delta function) arising from the displacement of a rod in the m-th cell:

Translated from Atomnaya Énergiya, Vol. 41, No. 1, pp. 25-30, July, 1976. Original article submitted September 2, 1975.

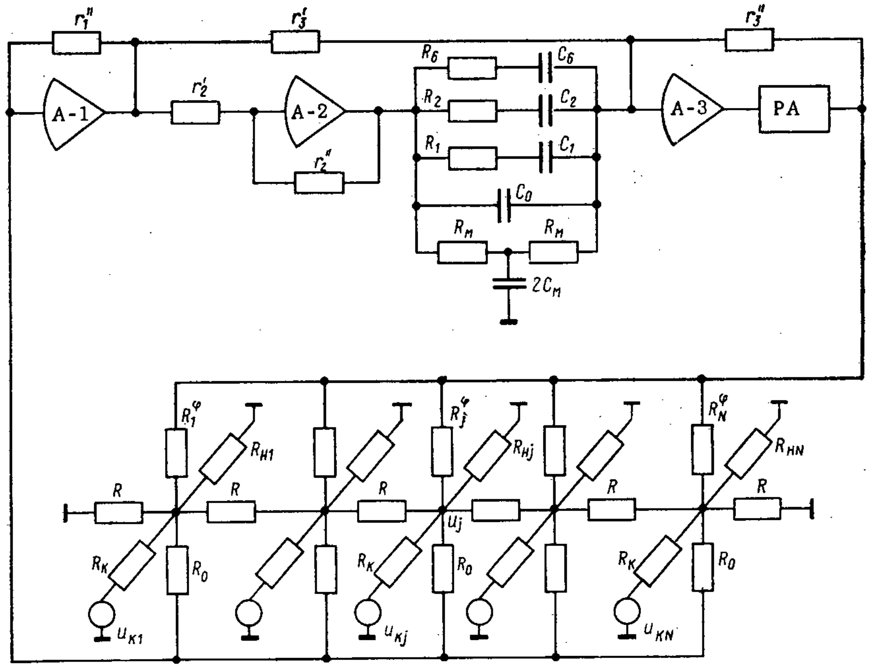

Fig. 1. Analog model of a one-dimensional reactor.

$$\delta(kf_0)_{jm} = \delta k_m(p) f_{jm} f_{0m} V_m, \tag{6}$$

where V_m is the volume of the m-th cell.

Using the fact that the coefficient is proportional to the power $\overline{\Phi} = \Phi^0(r)/f_0(r)$ and taking account of Eqs. (6), (5), and (2), we obtain for the element h_{im} of the matrix H(p)

$$h_{im}\left[W_0(p)\Phi_i^0 f_{0m}^2 + \sum_{j=1}^{\infty} W_j(p)\Phi_{0m} f_{ji} f_{jm}\right] V_m, \tag{7}$$

where Φ_i^0 is the stationary reference neutron distribution in the cells. Thus the reactor transfer matrix can be written as a matrix series

$$H(p) = A_0 W_0(p) + \sum_{j=1}^{\infty} A_j W_j(p). \tag{8}$$

The matrix elements and the scalar coefficients $W_j(p)$ are determined from Eq. (7). When all the sensors and control rods are located in a flat flux $\Phi_i^0 = \Phi^0$ the matrix is symmetric $h_{im} = h_{mi}$ (cf. Eq. (7)).

Using the conclusions of [2] on the nature of the processes of redistribution of the neutron field, we list in order of increasing accuracy the following approximate models of a reactor as a multidimensional control element:

1. The zero adiabatic (point) model

$$H(p) \approx H_0(p) = A_0 W_0(p). \tag{9}$$

Measuring the displacements of the rods in reactivity units $\Delta\rho_m = f_{0m}^2 \Delta k_m V_m$, and the neutron fluxes in the cells relative to the average over the reactor $\Delta\varphi_i = \Delta\Phi_i / (1/N) \sum_{i=1}^{N} \Phi_i^0$, we have from (7) for the elements a_{im} of the i-th row of the power matrix A_0, $a_{im} = \varphi_i = \Phi_i^0/(1/N) \sum_{i=1}^{N} \overline{\Phi_i^0}$. We call φ_i the form factor of the i-th cell. Of course the point model does not take account of changes in the shape of the distribution.

2. The first adiabatic model

$$H(p) \approx H_1(p) = (A_0 + \mathcal{A}) W_0(p) = A W_0(p), \tag{10}$$

where $\mathcal{A} = \sum_{j=1}^{\infty} A_j$ is the distribution matrix and $A = A_0 + \mathcal{A}$ is the reactor matrix.

This model gives an exact description of the steady-state power distribution in a critical reactor. Here the transfer function of the "most heavily weighted" first harmonic is attributed to the change in the neutron distribution.

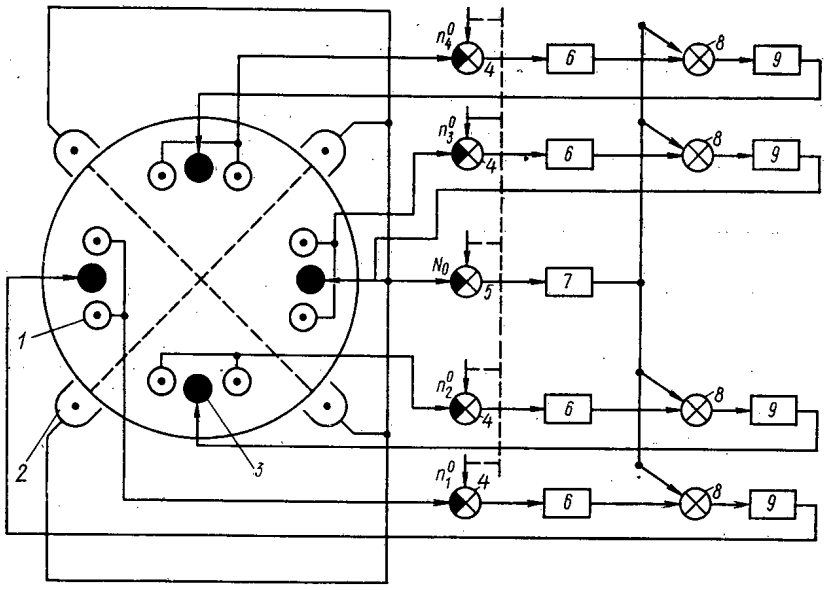

Fig. 2. System for the automatic control of reactor neutron distribution and power: 1) in-pile sensors; 2) PC ionization chambers; 3) LC and PC control rods; 4, 5) LC and PC controllers; 6, 7) LC and PC amplifiers and correcting devices; 8) LC and PC control action integrators; 9) servomotors.

3. The second adiabatic model

$$H(p) \approx H_2(p) \approx A_0 W_0(p) + \mathcal{A}. \tag{11}$$

This model takes account of the fact that the redistribution of power during the motion of control rods occurs practically instantaneously [2] as compared with the control time.

4. The third adiabatic model

$$H(p) \approx H_3(p) = A_0 W_0(p) + \mathcal{A} W_1(p) \tag{12}$$

is used for reactors with an unstable power distribution. $W_1(p)$ is the transfer function of the first unstable subharmonic.

The proposed models have a quite specific physical meaning and can be constructed from experimental and calculated data. The matrix $H_0(p)$ describes the change in total power, and $W_0(p)$ is the point reactor transfer function. All these models are identical in the analysis of changes in the total power. The elements α_{ik} and a_{ik} of the matrices $\mathcal{A}$ and A are defined, respectively, as the reactions of the i-th sensor to a unit displacement of the k-th rod with the power control turned on and turned off. For a reactor with a nonnegative power coefficient of reactivity the reactor matrix is given by the relation $A = A_0 + \mathcal{A}$.

A special analysis shows that the eigenvalues of the positive matrix A are positive, and those of the matrix $\mathcal{A}$ are nonnegative. These properties are important in the analysis of a control system [8].

Application to Digital and Analog Models. The proposed models ensure an acceptable accuracy of the representation of the neutron distribution for systems analysis. Their use sharply reduces the amount of apparatus needed for analog simulation and the amount of machine time for computation. Actually the direct simulation of the diffusion equation by the finite difference approximation [1, 3, 4] requires solving a system of differential equations of total dimensionality $(\nu + 1 + \mu)N$ where ν is the number of groups of delayed neutrons taken into account, μ is the order of the feedback equation, and N is the number of mesh points. For example, the use of the second adiabatic model involves the solution of two sets of algebraic equations, each of degree N, and one system of differential equations of degree $\nu + 1 + \mu$. This takes account of the fact that ordinarily the feedback parameters hardly vary from one reactor zone to another.

We illustrate the above by treating the second adiabatic model by an analog technique [5]. Figure 1 shows a one-dimensional model containing an array of resistors R_0 simulating neutron diffusion. Two- and three-dimensional models require a network and a three-dimensional lattice of resistors, respectively.

The potential of a mesh point U_j simulates the deviation of the neutron field from its reference value Φ_j^0 in the j-th cell. The reference distribution $\Phi_0(r)$ corresponds to zero potentials at all mesh points. The assembly of A-1 and A-3 amplifiers simulates point kinetics $W_0(p)$ and supplies the network, through the resistors R_j, a voltage proportional to the total power.

Since the current through the resistors R_j^{φ} simulates the multiplication of neutrons in cells with various fluxes and is due to the total voltage from the output of the power amplifier PA, the quantity R_j^{φ} is chosen in accord with the form factor φ_j.

The one-dimensional reactor statics equation is [4]:

$$[\delta\Phi_{j-1}+\delta\Phi_{j+1}-2\delta\Phi_j]+h^2\Delta k_j\Phi_j^0+h^2\delta\Phi_j[k_{0j}-1+K_M\Phi_j^0]=0, \tag{13}$$

where h is the step between cells in migration lengths, and K_M is the power feedback factor.

The statics equation of the proposed circuit (Fig. 1) for $K_M = 0$ is:

$$[U_{j-1}+U_{j+1}-2U_j]+U_j\left[\frac{R}{R_j^{\varphi}}\frac{K_{13}-\varphi_j}{\varphi_j}-\frac{R}{R_0}-\frac{R}{R_k}\right]+\frac{U_{hj}R}{R_k}=0, \tag{14}$$

where $K_{13} = K_1K_3$ is the amplification factor of the A-1 and A-3 amplifiers. We introduce scales for the neutron density and the multiplication factor

$$U_j=M_{\varphi}\delta\Phi_j;\quad U_{kj}=M_k\Delta k_j. \tag{15}$$

Then Eq. (14) can be written in the form

$$[U_{j-1}+U_{j+1}-2U_j]+\frac{R\delta\Phi_j}{\varphi_jR_j^{\varphi}}\left[K_{13}-\varphi_j\left(1+\frac{R_j^{\varphi}}{R_0}+\frac{R_j^{\varphi}}{R_k}+\frac{R_j^{\varphi}}{R_{Hj}}\right)\right]+\frac{M_k}{M_{\varphi}}\Delta k_j\frac{R}{R_k}=0. \tag{16}$$

The working equations for determining the nominal values of the circuit parameters are determined from the similarity of Eqs. (13) and (16)

$$h^2=\frac{R}{\varphi_jR_j^{\varphi}};\quad k_{0j}-1=K_{13}-\varphi_j\left(1+\frac{R_j^{\varphi}}{R_0}+\frac{R_j^{\varphi}}{R_k}+\frac{R_j^{\varphi}}{R_{Hj}}\right); \tag{17}$$

$$\Phi_j^0=\frac{M_k}{M_{\varphi}}\frac{R}{R_k}.$$

Similarly by comparing the reactor dynamics equations [4] with those for the proposed circuit, specifying, e.g., $K_1 = 1$ (in this case the A-1 amplifier output simulates the total reactor power) we obtain the working equations for the amplifier circuits:

$$r_1''=\frac{R_0}{M};\quad K_2=\frac{r_2''}{r_2'};\quad K_3=\frac{r_3''}{r_3'};\quad \beta_i=\frac{r_3''K_2}{R_i};$$
$$K_M\Phi_j^0=\frac{r_3''K_2}{2R_M};\quad l=K_2r_3''C_0;\quad T_M=R_MC_M; \tag{18}$$
$$\lambda_i^{-1}=R_iC_i,$$

where T_M is the feedback time constant, β_i and λ_i are, respectively, the partial yield and the decay constant of the i-th group of delayed neutrons, l is the neutron lifetime, and M is the number of cells used in calculating the average flux ($M \leq N$).

An amplidyne supplied by an A-3 operational amplifier can be used, e.g., as a power amplifier. These amplifiers have a large negative feedback.

The number of working equations shown is smaller than the number of nominal circuit parameters determined by them. This makes it possible to optimize the circuit parameters to minimize the modeling error.

A model of a one-dimensional reactor with N = 25, h = 1, $K_M\Phi^0 = -\beta$ was constructed in accord with the circuit proposed. The circuit parameters were optimized by computer calculations. The modeling error was determined by a comparison with accurate computer calculations. The error in simulating the deviations of the neutron field at the mesh points from the reference distribution Φ_j^0 did not exceed 10% which for the scales chosen corresponds to an error of 1% in determining the absolute values of the neutron flux.

To simulate an unstable neutron distribution in a one-dimensional (two-dimensional) reactor by this

method it is necessary to provide at least two (four) identical amplifier assemblies (Fig. 1), one for each half (quadrant) of the reactor. In simulating processes over a large range of powers the change in the neutron multiplication factor is simulated by a change in the resistance of the resistors R_k.

For the third adiabatic model the circuit shown in Fig. 1 must be supplemented by an assembly of amplifiers and inverters simulating the transfer function W_1; its input is determined by the power misalignment over half the reactor, and its output introduces currents of opposite sign at appropriate mesh points through the extra resistors.

Application to the Analysis of Control Systems. We illustrate the methods of analysis using the proposed models by the example of the most typical system (Fig. 2) [6]. The power of each cell (quadrant) is measured by the in-pile sensors, and the total power is determined by four practically inertialess ionization chambers 2. The system has an LC and a PC connected to the LC rod servomotors.

Since the number and velocity of the control system rods are limited, this circuit permits an increase in the accuracy of the control of the distribution by an increase in the number of LC. The large inertia and small range of the in-pile LC sensors are appropriate for the circuit shown. As a rule the use of only LC cannot ensure the required fast action, range, and reliability of the control of the total power. Therefore a special PC circuit is necessary.

A local perturbation of the reactivity is first compensated by a simultaneous synchronous displacement of all the control rods of the system in response to the PC signal. Then the LC begins to act. After the transient processes are damped out the perturbations is compensated by the rods closest to the place where the perturbation was introduced.

We first analyze the stability of the system with the PC disconnected. As a first approximation we neglect the interference between the first and higher harmonics [7] and take account of the fact that the fundamental is the most unstable (of the transfer functions $W_j(p)$ the most unfavorable for stability is the function $W_0(p)$); we find that in the stability analysis all the adiabatic models reduce to the zero (point) model. In this case all the LC turn out to be connected in parallel with the element with the transfer function $W_0(p)$, and stability is determined for an equivalent system with the transfer function in the disconnected state

$$W_{\text{equiv}}(p) = W_0(p) \sum_{i=1}^{N} \varphi_i W_{pi}(p), \tag{19}$$

where the transfer function $W_{pi}(p)$ of the i-th LC includes the transfer functions of the sensor, controller, amplifier, and servomotor. If the output signal of the i-th LC is considered as the linear displacement of a rod rather than the reactivity ρ_i (proportional to φ_i^2) as in Eq. (19), it turns out that in the transition to an equivalent system the LC transfer functions are summed with a weighting factor proportional to the cube of the neutron flux at the LC rod location. This conclusion is important for the analysis.

The proposed estimate of the stability generalizes the procedure of [8] to the case of nonidentical LC placed in regions with different neutron fluxes, and for a reactor with any (e.g., nonnegative) power feedback factor. According to [8] the stability of a system of identical LC is determined for the equivalent system

$$W_{\text{equiv}}(p) = W_0(p)\lambda_{\max} W_p(p), \tag{20}$$

where $\lambda_{\max}$ is the largest eigenvalue of matrix A. If the LC rods are located in cells with the same neutron flux, the sum of the elements of any row (column) of matrix A is the same, and by a familiar theorem [9] taking account of the fact that $\sum_{k=1}^{N} \alpha_{ik} = 0$ we have

$$\lambda_{\max} = \sum_{k=1}^{N} a_{ik} = \sum_{k=1}^{N} (a_0 + \alpha_{ik}) = N a_0 = N\varphi, \tag{21}$$

where φ is the form factor for the LC rods.

Thus the results (20) and (19) agree. It is important to emphasize that Eq. (21) is Gershgorin's upper estimate [9] for $\nu_{\max}$ in the general case, and therefore the stability analysis using the point model ensures an estimate with a certain stability margin.

If the total power is stabilized by turning on the PC, the stability of the system (Fig. 2) is analyzed in two steps using higher adiabatic models. First the stability is analyzed "at high frequencies" of the

equivalent system

$$W'_{\text{equiv}}(p) = W_0(p)\,[W_{\text{PC}}(p)\,\varphi_{\text{PC}} + \sum_{i=1}^{N} \varphi_i W_{pi}(p)], \tag{22}$$

where W_{PC} and φ_{PC} are the PC transfer function and form factor. If this system is stable the second part of the investigation consists in the analysis of a multidimensional system at "lower frequencies and higher harmonics," e.g., by the method of [8]. The second part of the analysis is necessary in at least two cases: Without the LC system the power distribution is unstable (in the analysis the element is described by the transfer matrix $\mathcal{A}\,W_1(p)$); the speed of response of the LC is an order of magnitude or more lower than that of the PC (the element must be described by the matrices $\mathcal{A}$ or $\mathcal{A}\,W_1(p)$).

By harmonic linearization [10] the proposed procedure is extended to an analysis of on—off control systems. The satisfactory agreement (within 20%) of the values of threshold parameters of the control adjustments, estimated by the method presented, with the values obtained by accurate methods such as computer calculations or direct analog simulation with network models [4, 8] permits the use of the procedure in designing similar systems.

Thus our proposed approximate mathematical models of a reactor require much less apparatus and machine time than previous models for analog and digital simulation and facilitate the design of control systems.

The author thanks Ya. V. Shevelev for a discussion.

LITERATURE CITED

1. A. B. Fokin and P. T. Potapenko, Atomnaya Tekhnika za Rubezhom, No. 12, 3 (1974).
2. P. T. Potapenko, in: Control of Nuclear Power Plants [in Russian], Vol. 4, Atomizdat, Moscow (1970), p. 5.
3. B. N. Seliverstov et al., At. Énerg., 39, No. 5, 324 (1975).
4. P. T. Potapenko, I. G. Vintizenko, and A. N. Kosilov, in: Analog and Analog-Digital Computational Techniques [in Russian], Vol. 6, Sovetskoe Radio, Moscow (1973), p. 102.
5. E. V. Filipchuk, P. T. Potapenko, and A. A. Kucherenko, Byul. Izobr., No. 26, 132 (1975).
6. E. V. Filipchuk, P. T. Potapenko, and A. N. Kosilov, Inventor's Certificate No. 453120, Byul. Izobr., No. 45 (1974).
7. J. Miida et al., Paper P/848, Third Geneva Conference, Vol. 3 (1964), p. 151.
8. E. V. Filipchuk, P. T. Potapenko, and A. N. Kosilov, At. Énerg., 35, No. 5, 317 (1973).
9. F. R. Gantmacher, The Theory of Matrices, Chelsea, New York (1959).
10. E. P. Popov, Applied Theory of Control Processes in Nonlinear Systems [in Russian], Nauka, Moscow (1973).

THE DISTRIBUTION OF MOVING HOLES IN A MATERIAL WITH SOURCES OF GAS ATOMS

V. V. Slezov and V. I. Ryabukhin

UDC 548.4

In the present work a closed system of equations is derived which describes the diffusion processes in a material being irradiated. The system consists of three equations of continuity, in the dimension space with sources, for the distribution functions of prismatic interstices, vacancy loops, and moving gas-filled holes, and three equations of balance for the point defects (vacancies, interstices, and gas atoms). The expressions for the rate of growth for macrodefects that occur in this system are determined. It is shown that for sufficiently large samples the gas is removed from them in two stages: At first it flows into the holes and then it is removed together with the holes to the surface. The limiting cases of "small" and "large" holes are investigated; the dimensions of these holes satisfy the relations

$$R \gg R^*,\ R \ll R^*,\ R^* = \frac{D^* \gamma a^3}{kTD^g \delta},$$

where D^* is the self-diffusion coefficient of the internode atoms, D^g is the diffusion coefficient of the gas atoms, kT is the temperature, a is the lattice constant, δ is the solubility of the gas, and γ is surface energy. The formulas for the rate of growth of the macrodefects are obtained.

The stationary solution of the system of equations is obtained in an explicit form for a material in the form of a plane-parallel plate in which a small temperature gradient is maintained along the x axis. The size distribution of the dislocation loops is uniform right up to their maximum radius in the given crystal. This radius is determined by the dimension of the crystal if the elastic interaction between the dislocations can be neglected, or by the supersaturation of the point defects and the elastic characteristics of the crystal if the interaction between the dislocations is significant. The graph of the size distribution of the dislocation loops is of a step form and does not depend on the point where the loops are observed, whereas the rate of generation and growth of the loops is a function of the coordinates, since it is determined by the effective supersaturation at a given point.

Because of the presence of the temperature gradient, the distribution of the moving holes is directly proportional to the radius but the size of the holes at a given point has an upper limit. The maximum radius depends on x and is determined by the size of the holes which were generated near the boundary of the samples and moved to the given point.

The effective super-saturation of the point defects and the density of the gas atoms in the crystal were obtained taking into account the elastic interaction of the dislocation loops and the absence of this interaction. These quantities are determined by the crystal and the irradiation characteristics. Their dependence on x is of the form $(1 - (x/d))^N$, where d is the thickness of the plate in the x direction; N is determined by the interaction of the loops and the mechanism of motion of the holes under the action of the temperature gradient. For the gas density, the power index is positive while for supersaturation it is negative.

Original article submitted May 27, 1975.
Revision submitted January 12, 1976.

Translated from Atomnaya Énergiya, Vol. 41, No. 1, pp. 31-34, July, 1976.

EFFECT OF THE DISTRIBUTION OF NEUTRON FLUX IN THE ACTIVE ZONE ON IRRADIATION INTENSITY OF URANIUM RADIATION CONTOUR

A. V. Putilov, M. A. Markina,
N. A. Robakidze, V. A. Rudoi,
E. S. Stariznyi, and N. P. Syrkus

UDC 621.039.551

The method of computing γ-intensity of the irradiator of a uranium radiation contour (URC) from the average neutron flux in the active zone (AZ) of a nuclear reactor (NR) has been published in the work of A. Kh. Breger and E. S. Stariznyi (Dokl. AN SSSR, Vol. 195, No. 6, 1385 (1970)). Since the density distribution of the neutron flux (R) in the AZ is nonuniform, a need arose for studying the effect of the distribution on the output characteristics of the URC. In order to determine the effect of R on the γ-intensity of the irradiator, a mathematical model of the URC was developed, which forms the basis of Cycle-1 and Quant programs. Using these programs, the radiation characteristics of the irradiator were computed for the two types of circulation regimes: For the "direct" regime R increases during the period of the stay of the fuel in AZ; for the "reverse" regime it decreases according to the same law.

In the present work the effect of step, exponential, and cosine density distribution function of neutrons on the γ intensity derived from the active zone is investigated, since the distributions encountered in practice can be represented by the superposition of already investigated functions. The total number of fissions in both types of regimes remained constant while the ratio W_1/W_2 of the total intensity of irradiation (in all 12 energy groups of γ quantas) for "direct" (W_1) and "reverse" (W_2) regimes serve as an indicator of the influence of function R. The results of the computations were verified experimentally on the reactor VVR-Ts. A hermetically packed (in order to avoid leakage of gaseous fission products) uranium sample was irradiated in the AZ by the flux of thermal neutrons with given R for a period t_p. The absolute value of the thermal neutron flux at the point of irradiation of the uranium sample was measured by the method of activation of gold foils in a cadmium sheet and without it. After irradiation the intensity of the γ radiation of the fission products of the nuclear fuel was measured as a function of the time of exposure. A comparison of the computed and experimental results (Fig. 1) showed a good agreement between the two.

It is found that the effect of function R on the γ intensity of the irradiator can be significant: For the exponential distribution $R = \exp(\pm\lambda t)$, e.g., $\lambda = 0.245$ min^{-1}, the ratio of the γ intensity of the irradiator of a URC operating stationarily in "direct" and "reverse" regimes comprises 1.5 for a cycle period of ~1 h.

It is shown that for the cosine distribution of the neutron flux density which is characteristic for real NR, the γ intensity of the fission products staggered into the irradiator practically coincides with the γ intensity for the uniform distribution (R = const) and the estimates of the characteristics of the URC [1] remain unchanged.

The nonuniformity of the neutron flux, which is characteristic for high-temperature nuclear reactors

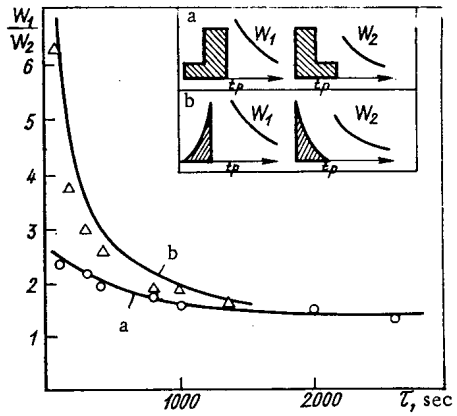

Fig. 1. The dependence of the ratio of total γ intensity for "direct" and "reverse" regimes on the period of the stay of the fuel outside the active zone for: a) step and b) exponential variable neutron flux in the active zone.

with spherical fuel elements, can increase the γ intensity (compared to R = const) by a few percent.

It is concluded that in constructing a nuclear reactor with URC it is necessary to strive for displacing the maximum of the neutron flux density towards the point of exit of the nuclear fuel from the active zone which increases the γ intensity of the irradiator.

Original article submitted July 4, 1975.

DEACTIVATION OF WEAKLY ACTIVE DISCHARGE WATERS BY FIBROUS IONITES

G. L. Popova, R. I. Radyuk, A. S. Syltanov, and B. É. Geller

UDC 621.039.714.066

In the present work the possibility of using fibrous ionites for extracting genetically hazardous isotopes ^{60}Co and ^{134}Cs from solutions is investigated. The investigation of sorption of these isotopes was conducted in static and dynamic conditions. The fibrous ionite has a sodium exchange capacity of 2.3 ± 0.2 mg·eq/g.

The absorption of cobalt and cesium depends on the pH value of the solution. The maximum sorption of cobalt (98%) is observed for pH = 4.3. For pH > 7.0 the sorption of cobalt falls off sharply; this is apparently related to the formation of its hydrolyzed forms having worse affinity to ionite. The sorption of cesium is maximum (86%) in the pH range of 3-10. For the concentration of ^{60}Co and ^{134}Cs equal to $1 \cdot 10^{-5}$ g·eq/liter the maximum sorption is attained when 2 g of ionite/liter of the solution is used. An increase of the concentration of radioactive cobalt and cesium by two orders of magnitude does not lower the sorption of these elements for one and the same suspension. The degree of purity of real sewage waters reaches 82%.

The results show the feasibility of using an ion exchange fiber for extracting these investigated isotopes from weakly active discharge waters by the method of filtration.

Original article submitted July 22, 1975.

ERRORS OF A FLUCTUATION-TYPE REACTOR POWER AND PERIOD METER

A. I. Sapozhnikov and V. I. Kazachkov

UDC 621.039.564.2

Much interest has recently been shown [1] in reactor power monitoring on the basis of statistical γ-ray background discrimination. It is important to know the instrumental and statistical errors in neutron-flux and reactor-period measurement in operating monitoring, control, and protection equipment. Formulas are derived for the error of measurement in monitoring neutron flux by reference to the second moment of the signal distribution for the neutron detector.

The following working characteristics of a fluctuation-type meter may be defined on the basis of the errors in measuring the neutron flux and reactor period, especially by comparison with pulse-counting and analog monitoring systems with logarithmic diodes in the input circuit [2]:

1. The relative statistical errors are determined by the relation between the time constants of the load circuit of the fission chamber, the preamplifier, and the smoothing filter.

2. The relative statistical error in neutron-flux measurement on a linear scale is independent of the flux itself.

3. The relative statistical error in neutron flux measurement on a logarithmic scale increases with the flux.

4. The relative statistical error in reactor-period measurement is less at low flux levels than at high ones; the main contribution to the error in the period comes from the error in the approximation to a logarithmic response, another important contribution being dependent on the relation between the reactor period and the time constant of the differentiating amplifer.

Error calculations from these formulas agree with measurements made in tests on AMBM and IRT-2000 systems [3], and the formulas can be used in designing wide-range monitoring and control equipment in which fission chambers are used in the pulse mode [1].

LITERATURE CITED

1. A. I. Mogil'ner and S. A. Morozov, At. Énerg., 26, No. 6, 491 (1969).
2. R. Stanfield, IRE Trans. Nucl. Sci., NS-8, No. 3, 22 (1961).
3. A. I. Sapozhnikov and V. I. Kazachkov, At. Énerg., 36, No. 3, 215 (1974).

Original article submitted July 31, 1975.

THERMODYNAMIC PROPERTIES OF LIQUID ALLOYS OF ACTINIDES AND LANTHANIDES

V. A. Lebedev

UDC 669.825+669.85/865

The article presents in systematic fashion the data of 18 studies devoted to the investigation of the thermodynamic properties of liquid alloys of 4f and 5f elements. It is established that the partial enthalpies of solid actinides and lanthanides in liquid metals Me_2 with a specified atomic radius r_2 and in compounds which are in equilibrium with saturated solutions (i.e., $\Delta\bar{H}^*$ and $\Delta\bar{H}$, respectively) vary linearly with the difference in the electronegativity of the components $\Delta\varkappa$ (see Fig. 1 and Table 2). The values of the electronegativities of the elements are shown in Table 1.

The deviations of the experimental measurements of $\Delta\bar{H}$ and $\Delta\bar{H}^*$ from the values calculated from the equations using the electronegativity values of Table 1 are ±(2-3) kcal/mole. The equation for Al satisfactorily describes $\Delta\bar{H}$ for silicides and sulfides, the equation for Ga describes $\Delta\bar{H}$ for tribromides, and the equation for Cd, In, Sn, Sb describe $\Delta\bar{H}$ for the triiodides of uranium, thorium, lanthanum, and cerium.

The enthalpies of the 4f and 5f elements in all liquid metals (excluding Al) and in compounds in equilibrium with solutions (except aluminides and zincides) can be evaluated from the relations

$$\Delta\bar{H},\ \text{kcal/g}\cdot\text{atom} = -135.6+94.3r_2-105\Delta\varkappa \pm 5.7;$$
$$\Delta H^*,\ \text{kcal/g}\cdot\text{atom} = -136.0+108.3r_2-112\Delta\varkappa \pm 5.2.$$

There is a direct proportionality between the thermodynamic characteristics of the solutions and those of the compounds in equilibrium with saturated solutions (Table 3).

The equations of Table 3 enable us, if we know the characteristics of the compounds, to evaluate the characteristics of the solutions and the solubility of Me_1 in Me_2. The deviation of the experimental values of $\Delta\bar{H}^*$ and $\Delta\bar{S}^*$ from the approximating equations is close to the error in the measurement of

TABLE 1. Values of Electronegativity of the Elements

Me	×[1]	Me	×[1]	Me	×[2]	Me	×[2]
Zn	1,6	Bi	1,9	La	1,1	Dy	1,2
Cd	1,7	S	2,5	Ce	1,1	Ho	1,2
Al	1,5	Br	2,8	Pr	1,1	Er	1,3
Ga	1,6	I	2,5	Nd	1,1	Tu	1,3
In	1,7	U	1,4	Pm	1,2	Yb	1,2
Tl	1,8	Th	1,3	Sm	1,2	Lu	1,3
Sn	1,8	Y	1,2	Eu	1,1	Pu	1,2
Pb	1,9	Sc	1,3	Gd	1,2	Np	1,2
Sb	1,9	Si	1,8	Tb	1,2	Zr	1,3

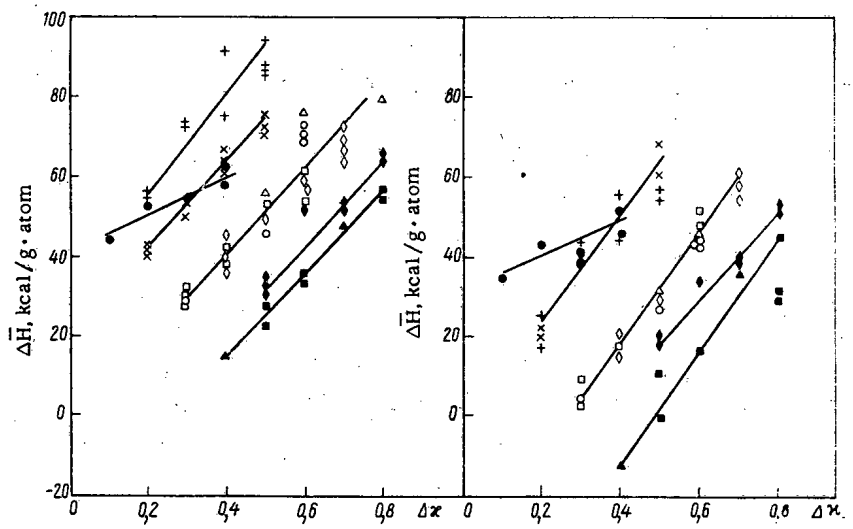

Fig. 1. ΔH and $\Delta\bar{H}^*$ as functions of the difference in electronegativity of the alloy components: +) Zn; •) Al; ×) Ga; □) In; ○) Cd; ◇) Sn; △) Sb; ◆) Bi; ▲) Tl; ■) Pb.

TABLE 2. Coefficients of the Equations $\Delta\bar{H}(\Delta\bar{H}^*) = a + b\Delta x$

Me_2	$\Delta\bar{H} = a + b\Delta x$		$\Delta\bar{H}^* = a + b\Delta x$		r_2, Å
	a, kcal/mole	b, kcal/mole	a, kcal/mole	b, kcal/mole	
Zn	35,6	112	2,1	114,3	1,33
Al, Si	41,7	45,6	30,8	42,6	1,43, 1,18
Ga	21,3	105,7	2,1	114,3	1,22
Cd, In, Sn, Sb	—0,4	105,3	—33,8	130,1	1,49—1,50
Tl, Pb	—26,5	104,3	—52,1	112,1	1,41, 1,45 1,71, 1,75
Bi	—17,5	103,4	—26,8	96,7	1,56

TABLE 3. Coefficients of the Equations $\Delta\bar{b}^* = a + b\Delta\bar{b}$.

Me_2	$\Delta\bar{H}^* = a + b\Delta\bar{H}$		$\Delta\bar{S}^* = a + b\Delta\bar{S}$		$\Delta\bar{G}^*_{1000\ K} a + b\Delta\bar{G}_{1000\ K}$	
	a, kcal/mole	b	a, electronic units/g·atom	b	a, kcal/mole	b
Al, Bi	9,43	0,934	5,13	0,955	6,96	1,009
Ga, In, Tl	30,0	1,303	11,3	1,286	16,2	1,236
Zn, Cd, Sb, Pb	15,2	0,803	4,9	0,573	—	—
Zn, Sb	—	—	—	—	9,83	0,974
Sn	66,8	1,973	—	—	21,1	1,286

these quantities. In those cases in which the coefficients b differ considerably from unity, it is possible to evaluate the thermodynamic characteristics of the solutions and compounds from the coefficients of the equation specifying variation as a function of temperature and from the solubility values.

LITERATURE CITED

1. L. Pauling, General Chemistry (3rd edition), W. H. Freeman, San Francisco, Ca. (1970).
2. S. S. Batsanov, Zh. Strukt. Khim., 5, 293 (1964).

Original article submitted August 6, 1975.

LETTERS

NUMERICAL BUILDUP FACTORS AND AVERAGE γ-SPECTRUM ENERGY BEHIND SCATTERING MEDIA

A. A. Gusev

UDC 621.039.84

As is well known, in passing through matter the discrete spectrum of primary quanta changes into a continuous spectrum. Such a spectrum contains all energies from the minimum (cutoff) energy E_c to the initial energy E_0. The role of scattered photons is accounted for by buildup factors. Many data have been published on energy B_e and dose B_d factors and on absorbed-energy buildup factors B_a [1-4]. On the other hand information concerning the quanta buildup factors B_N is scant. It consists merely of a few graphs and several indirect tables [2].

Any continuous spectrum can be described by some average energy $\bar{E}$. This energy is determined on the basis of spectral distributions which is quite complicated. Certain $\bar{E}$ values can be also found from the distributions cited in [1-3] and others. However, these values do not include many of the frequently encountered combinations of E_0, $\mu\rho x$, and geometry (where μ, ρ, and x are, respectively, the mass absorption coefficient, density, and thickness).

B_N and $\bar{E}$ are needed, in particular, in the design of instruments whose operation is based on the irradiation of substances by a broad γ-radiation beam, such as level, density, and thickness gauges, etc.

The author and colleagues have developed a method for finding $\bar{E}$ without the need for spectral distributions of gamma spectra [6]. Our method is based on the fact that within a certain photon energy range the ratio of efficiencies of gas-discharge counters with cathodes made of materials with different atomic numbers is a unique function of E. For example, for the pair tungsten—graphite E = 0.08 — 1.5 MeV. The correctness of the method has been confirmed by experiments with monochromatic emitters (^{141}Ce, ^{203}Hg, ^{137}Cs, ^{85}Kr), spectrometric experiments, and Monte Carlo calculations. Considerably simplifying the measurement of $\bar{E}$ and B_N, the method can be used in investigations of the γ field in barrier geometry when $\mu\rho x < 3.5 - 4$. Such conditions prevail in most applications of instruments based on γ irradiation.

By this method, and also with the aid of scintillation spectroscopy and Monte Carlo calculations, we have measured $\bar{E}$ and B_N for limited-barrier geometry, frequently encountered in practice, and analyzed their dependence on certain controlling parameters.

TABLE 1. Sample Values of λ, a, and b

E_0, MeV	Substance	$\mu\rho x$	λ	a	b
0,66	Iron	$\leq 4,5$	0,28	0,76	0,07
	Marble	≤ 4	0,23	0,57	0,36
	Light materials*	≤ 4	0,23	0,86	0,42
1,25	Iron	$\leq 4,5$	0,46	0,90	0,13
	Aluminum	≤ 3	0,37	1,90	0,018
	Light materials*	≤ 3	0,37	1,1	0,26

* Water, fiberboard, dry plaster, etc.

Translated from Atomnaya Énergiya, Vol. 41, No. 1, pp. 35-36, July, 1976. Original article submitted November 19, 1974.

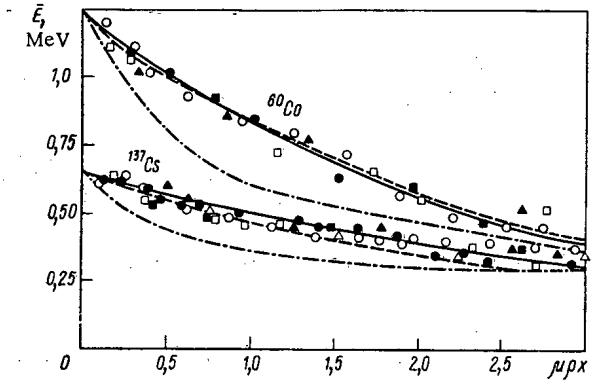

Fig. 1

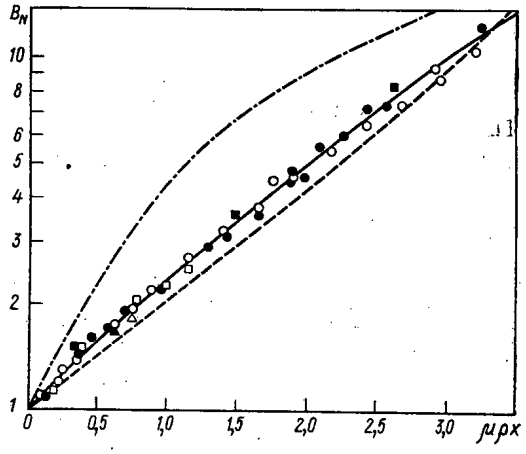

Fig. 2

Fig. 1. The function $\bar{E} = E(\mu\rho x)$ for water (○), fiberboard (●), aluminum (□), dry plaster (■), marble (▲), and fiberglass (△): ——) experiment, —·—·—) theoretical curve [2], — — — —) theoretical graph [5].

Fig. 2. The function $B_N = B(\mu\rho x)$. Notation the same as in Fig. 1.

For the studied thickness ($\mu\rho x < 4.5$), and L = 10-90 cm and l = 5-45 cm, no marked effect of L and l on $\bar{E}$ and B_N has been observed (where L is the distance from source to detector, and l is the distance from source to barrier). Source collimation has little effect on $\bar{E}$ and B_N provided the aperture angle of the gamma quanta beam exceeds 37-40°. As collimation increases, $\bar{E}$ approaches E_0 and B_N unity, which is explained by a reduction of the fraction of scattered photons entering the detector. Thus, it can be assumed that under the above conditions, $\bar{E}$ and B_N are functions of only the surface density of the material, its atomic number Z, and energy E_0. This made it possible to average B_N and $\bar{E}$ corresponding to these conditions.

The function $\bar{E} = E(\mu\rho x)$ is illustrated in Fig. 1. Experimental points fit quite well the curve described by

$$\bar{E} = E_0 \exp(-\lambda\mu\rho x), \tag{1}$$

where λ is a function of E_0 and Z (see Table 1).

Figure 2 shows an example of the function $B_N = B(\mu\rho x)$. This function can be approximated by the Berger — Chilton [4] expression:

$$B_N = 1 + a\mu\rho x \exp(b\mu\rho x), \tag{2}$$

where a and b are functions of E_0 and Z (see Table 1).

Figures 1 and 2 show data for the plane-parallel quantum beam of [5]. These data are in good agreement with those found by the author for a point source, at least up to $\mu\rho x$ = 3-3.5. This also agrees with the conclusion [7] about the validity of describing B_N of a point source by the graphs [5]. The same figures also show data obtained from spectral distributions for an infinite medium [2]. It is well known that $B_N < B_\infty$ and $\bar{E} > E_\infty$. The same conclusion follows from Figs. 1 and 2. All this confirms the validity of the discussed data.

Applying the principle resembling the "analytic extension" used in protection calculations in [4], $\bar{B}_N$ and $\bar{E}$ of heterogeneous systems of j layers can be written as

$$\bar{B}_N = \prod_{i=1}^{j} B_{Ni}(\mu_i\rho_i x_i'); \quad \bar{E}_j = E_0 \exp\left(-\sum_{i=1}^{j} \lambda_i\mu_i\rho_i x_i'\right), \tag{3}$$

where

$$x_i' = x_i \exp\left[-\sum_{k=1}^{i-1} (1+\lambda_k)\,\mu_k\rho_k x_k'\right]. \tag{4}$$

The expressions are valid for systems with a total thickness of 3-3.5 mean free paths of γ quanta when the system is completed by a heavy medium (the layers are counted beginning with the source). Experimental and theoretical values of $\bar{E}$ and $\bar{B}_N$ are usually in agreement to within experimental accuracy.

LITERATURE CITED

1. O. I. Leipunskii et al., Propagation of γ Quanta in Matter [in Russian], Fizmatgiz, Moscow (1960).
2. H. Goldstein and J. Wilkins, in: Protection of Transport Plants with Nuclear Engines [Russian translation], IL, Moscow (1961), p. 212.
3. N. G. Gusev et al., Protection from Ionizing Radiation [in Russian], Vol. 1, Atomizdat, Moscow (1969).
4. Handbook of Radiation Protection for Engineers [in Russian], Vol. 1, Atomizdat, Moscow (1972).
5. G. Peebles, J. Appl. Phys., 24, No. 10, 1272 (1953).
6. A. A. Gusev et al., in: Physics. Proc. of the 28th Scientific Conference of the Leningrad Construction Engineering Institute [in Russian], Izd. LISI, Leningrad (1970), p. 26.
7. K. Eife, Die Bestimmung des Raumgewichtes von Böden und Gesteinen durch γ Strahlen. Freiberger Forschungshefte, No. C61, Academie Verlag, Berlin (1959).

QUANTITATIVE RELATIONSHIPS OF TANTALUM, RADIOACTIVE ELEMENTS, AND ZIRCONIUM IN RARE-METAL ORES

G. N. Kotel'nikov

UDC 550.835.553.064

Small-scale mapping and prospecting have led to the discovery of a large number of radioactive segments with complex radioactivity of a uranium — thorium type. Anomalies in granitoids and acid orthogneisses with low-intensity γ radiation and a predominance of thorium (Th : U > 1) are usually classified as rock anomalies and are discounted while the investigation is still at the prospecting stage.

Among such anomalies, investigators have found some promising rare-metal ore manifestations localized in endo — exocontacts of Devonian granitoid intrusions appearing in metamorphic schists of the Proterozoic and Lower Paleozoic. Visual diagnosis of the rare-metal mineralization is difficult because of the small dimensions of the columbite — tantalite and pyrochlore crystals (0.08-0.1 mm) [1], but in the study of the mineralization it has been possible to establish quantitative relationships between tantalum — niobium, radioactive elements, and zirconium, which made it possible to check out a method for the preliminary field evaluation of such manifestations by means of a spectrometric survey before the laboratory analyses for tantalum are received.

The rare-metal tantalum — niobium manifestations are characterized by paragenetic bonds with radioactive minerals: thorite, orangite, and uranothorite. In addition, uranium and thorium are found in the crystal lattice of some rare-metal minerals — djalmaite, pyrochlore, hatchettolite, betafite, mendeleyevite, columbite, and others [2]. Consequently, high radioactivity in the ores of rare-metal deposits is not a special but a constant phenomenon, reflecting the mineral composition of the ore bodies, which makes it possible to use radiometric methods at the prospecting stage.

The quantitative relationships between tantalum, uranium, thorium, and zirconium, found from the processing of several thousand samples from six rare-metal ore manifestations and dozens of radiometric anomalies, are shown in Table 1. From these data it follows that the tantalum — niobium ore manifestations of the apogranitic type are characterized by rigorously defined parameters: a total γ activity >200 μR/h, uranium — thorium ratios ranging from 1 : 1 to 1 : 3, ZrO_2 content values > 0.2% (as high as several percent in lumpy ores). The uranium content and thorium content are approximately equal.

Thorium and uranium ore manifestations with similar γ-ray activity and radioactive-element ratios outside the range of 1 : 1 to 1 : 3 do not contain high concentrations of zirconium and contain no tantalum.

Translated from Atomnaya Énergiya, Vol. 41, No. 1, pp. 36-37, July, 1976. Original article submitted April 1, 1975.

TABLE 1. Nature of the Relationships between Elements in Various Types of Ore Manifestations

Type of rock	γ-ray intensity, μR/h	Uranium content, n · 10^{-3} %	Thorium–uranium ratio, Th:U	ZrO_2 content, %	Ta_2O_5 content, n · 10^{-3} %	Nb_2O_5:Ta_2O_5 ratio	U:Ta ratio
Granites of the parent massif	25—35	0,7	3,0	0,02	0,7	11	1
Modified granites on the fringes of the ore field	50—80	2	1,5	0,04	4,0	10	0,5
Granitoids of the ore field		5	3,0	0,05—0,2	7,0	10—30	1
Ore metasomatites with columbite	200—500	10—20	1,0—3,0	0,2—0,5	10—40	10—30	1—0,5
Rich lumpy tantalum ores	500—1200	50—100	3,0	0,5—0,8	50—230	4—8	1—0,5
Complex thorium–uranium ore manifestations	500—1500	50—150	10,0	0,01	5,0	2	10
Uranium ore manifestations	200—1500	20—150	0,05	0,02	1,0	10	100

Zirconium content, in addition to approximate visual estimates (counting of those zircon crystals in the ore samples which have well-marked pleochroic haloes), can be rapidly and cheaply determined at the nearest spectrometric laboratory, whereas expensive analyses for tantalum (6-9 rubles) take weeks and are carried out by specialized laboratories far from the work site.

Prospecting and survey parties usually do not have the Bars-2 or Mineral-3 field x-ray spectral instrument for rapid analyses for tantalum, except in the case of specialized rare-metal parties. They are well equipped with radiometric apparatus, including the SP-3 mass-produced spectrometers, are trained in the method of spectrometric surveys in the field, and can make use of established patterns for the incidental estimate of radiometric anomalies in distinguishing rare-metal ore manifestations and reduce the number of expensive tantalum analyses to a fraction of the number otherwise necessary.

In the estimating studies on rare-metal ore manifestations the potassium channel of the spectrometer was also used.

Rare-metal granites contain approximately 7.5-8.0% of the alkalis $Na_2O + K_2O$, with equal amounts of sodium and potassium (Na : K = 0.92). In the ore field the rare-metal mineralization is localized in albitized zones, from which potassium is almost completely absent, being replaced by sodium; the "negative" anomalies of a spectrometric survey with respect to potassium are usually found in zones of ore-bearing albitized metasomatites, which can be used for primary testing and detection.

A check of ores and concentrates of some rare-metal deposits in other areas has shown that in those areas too there are high concentrations of zirconium and that the uranium — thorium ratios are always constant and are often close to the values given in the tables of [3]. Accordingly, the method under consideration can be recommended for use even outside the region investigated, with the necessary area correction for the quantitative ratios.

It may be of practical interest to review the operating logs of spectrometric laboratories which do not normally work on rare-metal ore: Any detected samples containing more than 0.2-0.5% ZrO_2 should be analyzed for tantalum.

LITERATURE CITED

1. M. V. Kuz'menko and E. M. Es'kova, Tantalum and Niobium [in Russian], Nauka, Moscow (1968).
2. A. I. Ginzburg, Problems of Rare-Earth Granites [in Russian], Nedra, Moscow (1972).
3. F. A. Letnikov, in: Characteristics of the Formation of Columbite-Bearing Granitoids of the Kokchetav Block [in Russian], Nauka, Moscow (1972).

ANALYSIS OF THE SPECTRAL COMPOSITION OF X-RAY SIGNALS BACKSCATTERED FROM VARIOUS SURFACES

F. L. Gerchikov

UDC 539.121.72:539.122

Data on the spectral distribution of ionizing radiation backscattered from various media usually refer to monochromatic γ radiation with energies higher than a hundred keV [1, 2]. In many practical problems, however, one has to deal with bremsstrahlung x-ray radiation with energies $E_\gamma \leq 100$ keV [3].

Problem Formulation. In the general case it is necessary to determine the distortion of x-ray signal spectra backscattered from various semi-infinite reflectors (concrete, water, iron). The distance between the radiation source and the reflecting surface H = 10, 30, and 60 m. The analysis deals with bremsstrahlung x-ray radiation sources.

The spectrogram of the probing x-ray signal of the two sources, experimentally plotted with the aid of a PD-2 threshold discriminator and a PP-9 scaler, occupies the regions 10-110 keV and 10-75 keV, and has an intensity peak at about 50 and 40 keV, respectively, for x-ray sources with anode voltages U_a = 110 and 75 keV.

Calculation Algorithm. Let N_0 denote the quantum flux at the x-ray source output. Considering that we discuss a narrow parallel x-ray beam ("good geometry" conditions), the number of quanta reaching the reflecting surface at a distance H from the source is

$$N_{in} = N_0 \exp(-\mu_1 H), \tag{1}$$

where μ_1 is the attenuation of x-ray radiation at the source – reflector path.

This assumption is valid since, firstly, the geometry of such a parallel beam is the most general problem on backscattering. It is known that a radiator of any configuration can be represented by a superposition of thin parallel beams [1]. Secondly, an analysis of the spectral pattern under "good geometry" conditions does not affect the qualitative aspects of the involved processes which, in the final analysis, are the decisive factors in the design of instruments.

In the general case of backscattering, the energy of incident quanta E_i changes into E_S in accordance with

$$E_S = E_i [1 + \alpha_i (1 - \cos\theta_S)]^{-1}, \tag{2}$$

where $\alpha_i = E_i (m_0 c^2)^{-1}$, θ_S is the x-ray radiation scattering angle, and $m_0 c^2$ is the electron rest energy.

Considering the energy albedo A_E of the reflecting surface, the backscattered x-ray flux is

$$N_S = N_0 \exp(-\mu_1 H) A_E E_i E_S^{-1}. \tag{3}$$

If μ_2 is the x-ray attenuation factor on the semi-infinite reflector – detector path, then considering Eqs. (2) and (3), the backscattered x-ray flux at the detector input is given by

$$N_{ref}^H = N_0 A_E [\exp -(\mu_1 + \mu_2) H] [1 + \alpha_i (1 - \cos\theta_S)]. \tag{4}$$

The energy albedo of the reflecting surface is

$$A_E = \frac{C_1 (d\sigma/d\Omega)\, 10^{26} + C_2}{1 + \cos\Psi \sec\theta_S}, \tag{5}$$

Translated from Atomnaya Énergiya, Vol. 41, No. 1, pp. 38-39, July, 1976. Original article submitted May 21, 1975.

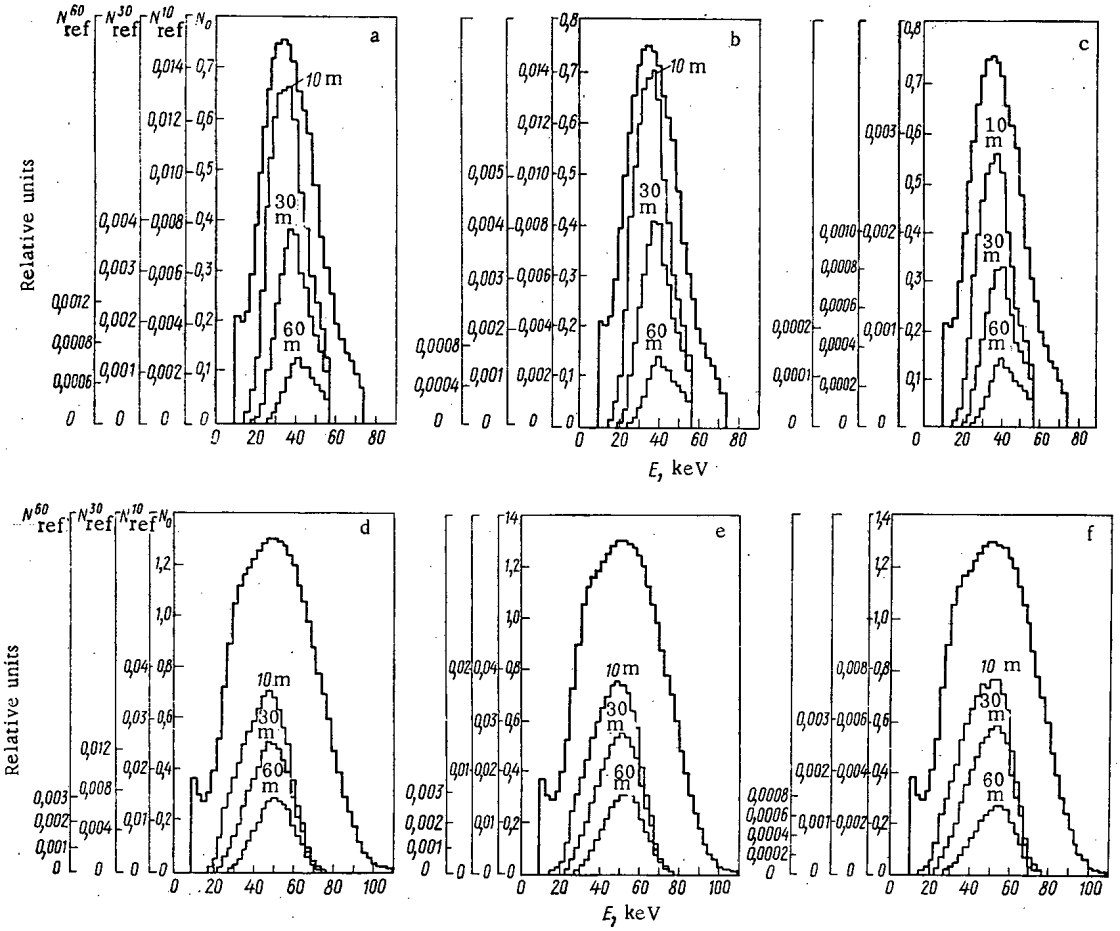

Fig. 1. Spectral composition of probing and backscattered from concrete, water, and iron x-ray signal for U_a = 75 keV (a, b, c) and 110 keV (d, e, f).

where C_1 and C_2 are tabulated constants, $d\sigma(d\Omega)^{-1}$ is the Compton interaction cross section [1], and Ψ is the radiation source collimation angle.

After simple transformations of $d\sigma/d\Omega$, and assuming that the radiation source and detector are at the same point, we have $d\sigma(d\Omega)^{-1} = (B + 2\alpha_i^2)B^{-4}$, where $B = 1 + 2\alpha_i$, so that Eq. (5) becomes

$$A_E = \frac{C_1 (B+2\alpha_i^2) B^{-4} + C_2}{2}.$$

Thus, knowing the spectral composition of the probing signal, the factors μ_1, μ_2, C_1, and C_2, it is possible to determine the spectral composition of the backscattered signal. For this purpose we have compiled a program which implements an algorithm for computing Eq. (4) on a BÉSM-4 computer. Taking into account multiple scattering does not substantially change the overall pattern of the reflected-signal spectral distribution introducing only a small distortion on the low-energy side.

Discussion of Results. The spectral composition of the backscattered x-ray signal differs little from the probing signal spectrum for all types of reflecting surfaces. The peak spectral density of scattered radiation corresponds to quanta with an energy of about 50 and 40 keV for x-ray source with U_a = 110 and 75 keV, respectively.

As the distance between the source and reflecting surface changes, the integral energy of the backscattered signal varies (see Fig. 1), and at the same time the probing signal spectrum on the low-energy quanta shifts to the right as a result of filtration by the air layer between the source — detector and the reflecting surface. As result of Compton interaction of the probing beam quanta with reflecting surface material, the backscattered radiation spectrum is shifted to the left at the high-energy side.

For fixed radiation source — detector distances, only the integral energy of the backscattered signal depends on the kind of the reflecting surface. The spectrum proper remains undistorted.

In conclusion the author thanks N. F. Andryushin and V. N. Barkovskii for critical remarks in reviewing the paper.

LITERATURE CITED

1. O. I. Leipunskii et al., Propagation of γ Quanta in Matter [in Russian], Fizmatgiz, Moscow (1960).
2. N. G. Gusev et al., Physical Principles of Radiation Protection [in Russian], Atomizdat, Moscow (1969).
3. B. P. Bulatov et al., Backscattered γ Radiation in Radiation Engineering [in Russian], Atomizdat, Moscow (1971).

ESTIMATING THE NUCLEAR SAFETY OF SYSTEMS OF SUBCRITICAL ASSEMBLIES BY THE INTERACTION-PARAMETER METHOD

V. D. Laptsev and Yu. I. Chernukhin

UDC 621.039.58

Finding the maximum allowable number of assemblies in a group and the multiplication factor M_A of the entire system is very important in the group storage of subcritical assemblies with a multiplication factor $Q_b > 1$ for the neutrons from an external source.

In calculating M_A for a system of identical assemblies we often make use of the interaction-parameter method [1]

$$M_A = \frac{Q_b - \lambda_{max}}{1 - \lambda_{max}}. \quad (1)$$

Here λ_{max} is the maximum eigenvalue of the symmetric positive matrix of interaction Q, whose elements are the interaction parameters $q_{ij} \geq 0$. For a subcritical system of identical assemblies, $\lambda_{max} < 1$ can be found by solving the system of equations

$$\lambda F_i = \sum_{j=1}^{N} q_{ij} F_j, \quad i = 1, 2, \ldots, N, \quad (2)$$

where N is the number of assemblies in the system and F_i is the neutron yield from the i-th assembly.

Equation (1) determines the multiplication factor of systems of identical assemblies with respect to neutrons from an external source with a distribution $S_i = F_i (\sum_{i=1}^{N} F_i)^{-1}$, where S_i is the fraction of neutrons from the source that hits the i-th assembly.

An exact solution of the system (2) for a large number of interacting assemblies N is difficult to obtain. However, for the purposes of nuclear safety it is often sufficient to know an upper bound for M_A or λ_{max}.

By Frobenius's theorem, for nonnegative matrices Q we can write [2]

$$r \leqslant \lambda_{max} \leqslant R; \quad (3)$$

$$r = \min_{1 \leqslant i \leqslant N} \sum_{j=1}^{N} q_{ij}; \quad R = \max_{1 \leqslant i \leqslant N} \sum_{j=1}^{N} q_{ij}, \quad (4)$$

where r, R are the minimum and maximum total parameters of interaction of an individual assembly of the system with all the others.

Translated from Atomnaya Énergiya, Vol. 41, No. 1, pp. 39-41, July, 1976. Original article submitted May 21, 1975.

The specific properties of the interaction matrix Q and the distribution of the neutron yields F_i from the assemblies in the system make it possible to narrow the range of λ_{max} values somewhat by obtaining a more precise lower bound for the inequality (3).

According to Eq. (2) and the proportionality property of the functions $r_j = \sum_{i=1}^{N} q_{ij}$, F_j, we can obtain

$$\lambda_{\max} \sum_{i=1}^{N} F_i = \sum_{i,\,j=1}^{N} q_{ij} F_j \geqslant \frac{1}{N} \sum_{i,\,j=1}^{N} q_{ij} \sum_{i=1}^{N} F_i,$$

from which it follows that

$$\lambda_{\max} \geqslant \bar{r} = \frac{1}{N} \sum_{i,\,j=1}^{N} q_{ij}, \tag{5}$$

where $\bar{r}$ is the average total parameter of interaction of an individual assembly with all the others.

In deriving Eq. (5) we made use of the Chebyshev inequality

$$\int_a^b f(x)\,\varphi(x)\,dx \geqslant \frac{1}{b-a} \int_a^b f(x)\,dx \int_a^b \varphi(x)\,dx,$$

which holds for arbitrary functions if they are simultaneously monotone increasing or monotone decreasing in the interval [a, b].

Thus, according to Eqs. (1), (3), and (5), we obtain for M_A the inequalities

$$\frac{Q_b - \bar{r}}{1-\bar{r}} \leqslant M_A \leqslant \frac{Q_b - R}{1-R}, \tag{6}$$

which can serve as the basis for estimates used in assessing the nuclear safety of complex systems of subcritical assemblies.

The values of $\bar{r}$ and R are determined to a large extent by the arrangement of the assemblies in the system. For a periodic rectangular lattice the expressions for $\bar{r}$ and R have the following form:

$$\bar{r} = \left(\sum_{p=1}^{k} + \sum_{p=2}^{k}\right)\left(\sum_{j=1}^{m} + \sum_{j=2}^{m}\right)\left(\sum_{i=1}^{n} + \sum_{i=2}^{n}\right) \frac{(k-p+1)(m-j+1)(n-i+1)}{mnk}\, q_{ij}^{p};$$

$$R = \left(\sum_{p=1}^{k'} + \sum_{p=2}^{k''}\right)\left(\sum_{j=1}^{m'} + \sum_{j=2}^{m''}\right)\left(\sum_{i=1}^{n'} + \sum_{i=2}^{n''}\right) q_{ij}^{p};$$

$$k' = \left[\frac{k+1}{2}\right],\quad m' = \left[\frac{m+1}{2}\right],\quad n = \left[\frac{n+1}{2}\right]; \tag{7}$$

$$k'' = \left[\frac{k+2}{2}\right],\quad m'' = \left[\frac{m+2}{2}\right],\quad n'' = \left[\frac{n+2}{2}\right],$$

where k, m, and n are the numbers of assemblies arranged in a row along each of the three directions of the coordinate basis for a three-dimensional rectangular lattice; q_{ij}^{p} ($1 \leq i \leq n$, $1 \leq j \leq m$, $1 \leq p \leq k$) is the parameter of interaction between the first element of the first row of the first plane and the i-th element of the j-th row of the p-th plane of the lattice [the numbering of the assemblies with the indices i, j, and p is carried out from the corner assembly of the lattice in three mutually perpendicular directions ($q_{11}^{1} = 0$)]. The total number of assemblies in the system is N = mnk.

The symbolic representation of Eqs. (7) means that the summation sign should be used as an operator. For example, for an arbitrary matrix a_{ij}

$$\left(\sum_{j=1}^{m} + \sum_{j=2}^{m}\right)\left(\sum_{i=1}^{n} + \sum_{i=2}^{n}\right) a_{ij} = \sum_{j=1}^{m}\sum_{i=1}^{n} a_{ij} + \sum_{j=1}^{m}\sum_{i=2}^{n} a_{ij} + \sum_{j=2}^{m}\sum_{i=1}^{n} a_{ij} + \sum_{j=2}^{m}\sum_{i=2}^{n} a_{ij}.$$

When we pass to the formulas for $\bar{r}$ and R of the two-dimensional and one-dimensional lattices, in Eqs. (7) we should set k = 1 and k = m = 1, respectively.

Results of Calculations. We shall make use of the formulas obtained above for certain special cases of the calculation of the critical number of assemblies in the lattice ($M_A \to \infty$) under a number of different assumptions.

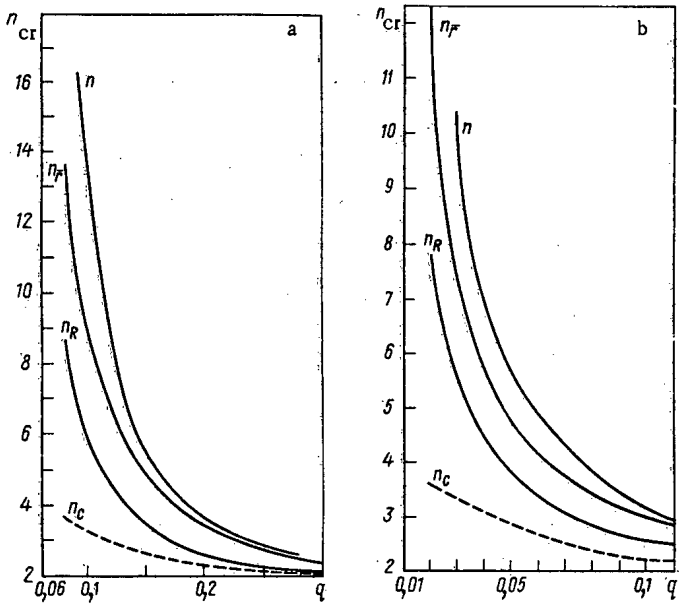

Fig. 1. Critical number of assemblies in: a) a square lattice and b) a cubic lattice as a function of the interaction parameter.

The "Strong Interaction" Approximation. This approximation is characterized by the condition $q^p_{ij} = q_{max}$; $q_{max} = \max\{q^p_{ij}\}$, for which Eqs. (7) take the form

$$\bar{r} = R = q_{max}(N-1). \tag{8}$$

According to Eqs. (6) and (8) the critical number of assemblies in the lattice will be equal to

$$N_c = \frac{1+q_{max}}{q_{max}}. \tag{9}$$

Total Shielding of Assemblies in a One-Dimensional Lattice. Here we assume that what is essential is only the interaction between adjacent assemblies, i.e.,

$$q_2 \neq 0; \quad q_i = 0; \quad i \neq 2. \tag{10}$$

Making use of (10), according to Eq. (7), for m = k = 1 (N = n), we obtain

$$\bar{r} = 2q_2\left(1-\frac{1}{n}\right); \qquad R = \begin{cases} 2q_2, & n>2; \\ q_2, & n=2. \end{cases} \tag{11}$$

Consequently, for n > 2 the criticality of such a system with respect to the upper limit does not depend on the number of assemblies in the system and is determined only by the interaction between two assemblies ($M_A \to \infty$ as $q_2 \to 1/2$).

Regular Cubic (Square) Lattice of Subcritical Assemblies ($N = n^3$, $N = n^2$) Disregarding Shielding. In this case the interaction parameter q^p_{ij} has the form

$$q^p_{ij} = \begin{cases} \dfrac{q}{(i-1)^2+(j-1)^2+(p-1)^2}, & i^2+j^2+p^2>3, \\ 0, & i=j=p=1, \end{cases} \tag{12}$$

where q is the parameter of interaction between two assemblies separated by a distance equal to the pitch of the lattice.

Substituting Eq. (12) into Eq. (7) and setting k = m = n, we can estimate the critical value $n_{cr}(q)$ as follows:

$$n_R(q) \leqslant n_{cr}(q) \leqslant n_{\bar{r}}(q), \tag{13}$$

where $n_R(q)$, $n_{\bar{r}}(q)$ are the roots of the equations R = 1 and $\bar{r} = 1$ in the variable n for a given parameter q. By numerical solution of these equations we have obtained the functions $n_R(q)$ and $n_{\bar{r}}(q)$ for a square lattice (Fig. 1a) and a cubic lattice (Fig. 1b).

For comparison, we also show in Fig. 1 the results of corresponding calculations performed in a numerical solution of the system of Eqs. (2) in [3], from which it follows that the estimates found for n_{cr} differ from their more exact values [3] only in the direction of increased nuclear safety.

Thus, the resulting expressions for $\bar{r}$ and R considerably simplify the calculation procedure for estimating the nuclear safety of systems of subcritical assemblies by the interaction-parameter method.

LITERATURE CITED

1. B. G. Dubovskii et al., Critical Parameters of Systems with Fissionable Substances and Nuclear Safety [in Russian], Atomizdat, Moscow (1966).
2. M. Marcus and H. Mink, Survey of the Theory of Matrices and Matrix Inequalities [Russian translation], Nauka, Moscow (1972).
3. D. C. Dowson, React. Sci, Techn., 17, No. 1, 1 (1963).

TEXTURE IN OXIDE FILMS ON ZIRCONIUM AND BINARY ZIRCONIUM — TIN AND ZIRCONIUM — TITANIUM ALLOY SINGLE CRYSTALS

F. P. Butra and A. A. Khaikovskii

UDC 54.31.162

The structure of the oxide films on zirconium and zirconium alloys has attracted a great deal of attention in connection with a study of the mechanism underlying the corrosion of these materials, which are widely employed in reactor building.

Published papers indicate a considerable anisotropy of the corrosion on crystal faces of different orientations; at the same time there is no single opinion as regards the epitaxial relationships existing between the film and the substrate in such cases [1-3]. Even very thin films exhibit structural inhomogeneity [4], while thicker films have a columnar structure (texture), the perfection of the texture increasing with increasing stress at the metal — oxide boundary [3, 5]. We accordingly decided to study the structure of oxide films of various thicknesses on single-crystal and polycrystalline zirconium and zirconium alloy samples subject to corrosion tests in air, under autoclave conditions, and in water vapor at 1 atm.

TABLE 1. Conditions of Corrosion Tests Carried Out on Zirconium and Its Alloys

Mode of testing	Medium	Single crystal		Polycrys. aggreg.	
		material	max. duration of tests, h	material	film thickness, μ
400° C, 100 atm, Kh18N10T stainless steel autoc.	Water vapor	Zr	286	Zr	30
500° C, 100 atm, Kh18N10T stainless steel autoc.	The same	—	—	Zr	60
				Zr+Nb	5
				Zr+Nb	28
500° C, 1 atm, quartz apparatus	» »	Zr	267	Zr+Sn	45
		Zr+Sn	267		
		Zr+Ti	36	Zr+Ti	70
500° C, 1 atm	Oxygen	—	—	Zr+Al	70
500° C, 1 atm	Air	Zr	267	—	—
		Zr+Sn	267		
		Zr+Ti	36		

Translated from Atomnaya Énergiya, Vol. 41, No. 1, pp. 42-44, July, 1976. Original article submitted October 23, 1975.

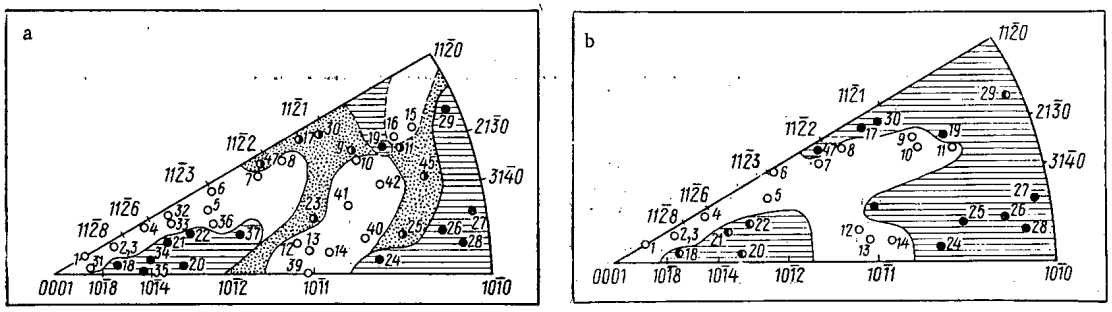

Fig. 1. Influence of the crystallographic orientation of the surfaces of zirconium single crystals on the color (a) and microtopography (b) of oxide films formed in water vapor (500°C, 1 atm, 267 h): a) black (○), gray (●), and grayish (◑) films; b) even (○), undulating (●), and hilly (◐) films.

Materials and Method of Investigation. The samples examined were plates (35 × 8 × 1 mm) of zirconium prepared by the iodide method, and binary zirconium alloys containing 1 at. % of tin, titanium, niobium, or aluminum. In the zirconium, Zr — Sn, and Zr — Ti plates, single-crystal grains with surface areas of 25-150 mm^2 suitable for examination were obtained. After cold working, the polycrystalline samples were subjected to recrystallization annealing at 700°C.

The corrosion tests (Table 1) were periodically interrupted in order to estimate the external form of the oxide films; the topography of the surface was also studied under the microscope, and the samples were subjected to x-ray diffraction analysis.

The crystallographic orientation and the structural perfection of each single crystal were judged by reference to back-reflection Laue photographs. The thickness of the oxide film was estimated from the weakening of the Laue spots produced by the single crystal. The texture in the oxide film was determined qualitatively from x-ray diffraction photographs taken at an angle of 16-20° to the primary beam on a cylindrical photographic film. In order to make a detailed study of the texture, the oxide films were subjected to transmission-type x-ray diffraction analysis in the mixed x radiation of an x-ray tube containing a copper anode. For this purpose the thin, dark, pretransitional [6] oxide films were separated from the substrate by the chemical dissolution of the latter. The thick, bright, posttransitional films were freely separated by a mechanical procedure.

Results of the Experiments. X-ray structural analysis showed that, quite independently of color or microtopography (Fig. 1), oxide films more than 0.5 μ thick grown on single crystals of any crystallographic orientations had the structure of monoclinic ZrO_2 with a polycrystalline constitution; the films were also textured. Microscope examination showed that the corrosion of the surfaces on single crystals of any crystallographic orientation started from a multitude of individual centers, with the subsequent formation of a continuous film.

The texture of the oxide film at the onset of corrosion depends in a complicated manner on the substrate orientation. Figure 2 shows the x-ray diffraction patterns of single crystals with different orientations, containing the Laue spots of the single crystals and the texture maxima of the oxide film. No specific laws governing the orientational relationships between the substrate and the film are revealed by calculations based on such x-ray diffraction patterns. With increasing thickness of the oxide film, the texture maxima first become considerably sharper, then some of them gradually weaken, while others merge to form Debye lines. The formation of the texture in the thin oxide films and its development as the films become thicker follow exactly the same laws in zirconium, Zr — Sn, and Zr — Ti alloys under the corrosion test conditions specified. Internal stresses develop in the crystal layer immediately under the film, and these cause severe diffuse scattering of the x radiation; this appears especially clearly in the crystals tested at 500°C (Fig. 2).

The transmission x-ray diffraction photographs of both the thin oxide films and the thicker, bright corrosion products exhibit a regular disposition of the texture maxima (Fig. 3). The $11\bar{1}$, 111, 002, and 200 maxima formed by the characteristic Cu K_α radiation are arranged in groups separated by azimuthal angles of about 60°, while the 110 maxima lie between these groups (Fig. 3a). For thin films we may choose a direction of the primary x-ray beam such that the foregoing texture maxima form a configuration closely resembling a system of six-fold symmetry.

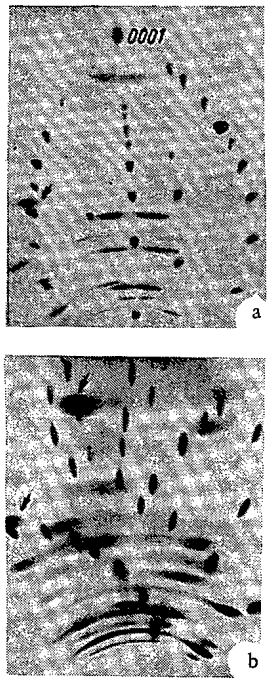

Fig. 2

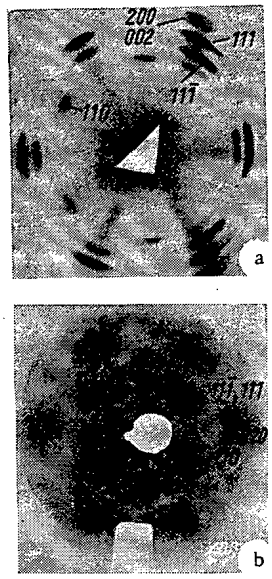

Fig. 3

Fig. 2. X-ray diffraction patterns of variously-oriented zirconium single crystals bearing thin oxide films, recorded at an angle of 16° on a cylindrical film (the arrows indicate the diffuse scattering maxima).

Fig. 3. Transmission-type x-ray diffraction patterns of oxide films taken from single-crystal surfaces: a) black film 6 μ thick; b) white film over 70 μ thick.

On subjecting thick (70-150 μ) peeling oxide films to x-ray diffraction analysis in the transmission mode, the primary x-ray beam being incident in a perpendicular direction, the characteristic radiation of copper is almost completely absorbed, and strong diffuse maxima appear; these are due to the reflection of the harder white radiation from the $\{11\bar{1}\}$, $\{111\}$, $\{110\}$ and $\{220\}$ planes (Fig. 3b). The maxima on the x-ray diffraction pattern exhibit a well-defined six-fold symmetry. The contrast is intensified by the selective absorption of some of the white radiation by the zirconium (absorption edge $\lambda = 0.687$ Å) and also by the bromine in the emulsion of the x-ray film (absorption edge $\lambda = 0.918$ Å). Thus the transmission-type x-ray diffraction photographs (Fig. 3) reflect the peculiar texture of the oxide film on the zirconium and Zr — Sn and Zr — Ti alloy single crystals.

We also applied x-ray diffraction analysis in the transmission mode to the oxide films formed on polycrystalline samples of zirconium and its binary alloys. On the x-ray diffraction patterns of thin films (up to 10 μ thick) obtained with the primary x-ray beam perpendicular to the surface, the $(11\bar{1})$ line was severely weakened in comparison with the (111) line, which corresponds to a texture having a preferential disposition of the $(10\bar{1})$ planes parallel to the sample surface. With increasing film thickness the intensity of the $(11\bar{1})$ line increases, but never reaches that of the (111) line; at the same time the diffuse ring formed by the reflection of some of the white radiation spectrum from the $\{11\bar{1}\}$ and $\{111\}$ planes is intensified, which corresponds to the formation of a texture with a preferential dispostion of the $\{11\bar{1}\}$ planes parallel to the sample surface (Fig. 4). In the x-ray diffraction patterns of ZrO_2 without any texture, the $(11\bar{1})$ line is stronger than the (111). The texture in the oxide films formed on the zirconium and alloy polycrystalline aggregates indicated is exactly the same for all forms of corrosion tests.

Discussion of Results. The oxide films formed on zirconium and zirconium alloys grow as a result of the diffusion of oxygen into the metal [6]; the texture in the thick films is a growth texture. Even in thin films (0.5-3.0 μ) a fibrous texture is created; the initial directions of the fibers depends on the structure of the substrate and the mutual relationship between the intergrowing sections of the film formed at the many corrosion centers on the oxidizing surface.

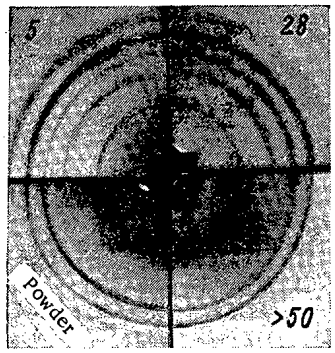

Fig. 4. Transmission-type x-ray diffraction patterns of oxide films taken from polycrystalline samples (film thickness in μ).

As the continuous film grows, compressive stresses develop in the film and at the boundary with the metal. In this case the oriented growth of the inner layer of the film becomes energetically favorable, the unit cell of the monoclinic ZrO_2 being arranged with its greatest dimension perpendicular to the surface undergoing oxidation, i.e., normal to the $(11\bar{1})$ plane.

In the x-ray diffraction patterns of the type shown in Fig. 3a, the texture maxima from the $(11\bar{1})$, (111), (002) and (200) planes are arranged in groups, and the 111 maxima are stronger than the $11\bar{1}$, whereas in the untextured material $J_{11\bar{1}} : J_{111} = 5 : 4$ [7]. This arrangement of the texture maxima and the intensity ratio between them characterizes a fibrous texture, with a relative crystallographic rotation of the fibers around their axes equal to a multiple of 60°, the $\{11\bar{1}\}$ planes being disposed perpendicularly to the axes of the fibers (Fig. 3a). With increasing thickness of the oxide film, the fiber axes tend to become perpendicular to the oxidized surface. The planes (101), $(1\bar{1}0)$ and (011) are parallel to the fiber axes and have a similar disposition of their zirconium and oxygen atoms; this gives rise to an ordered intergrowth of the fibers, with a mutual transition of one plane into the other. In this way a perfect axial texture is created, having its axis in the direction of the normal to the $(11\bar{1})$ plane, as observed experimentally in posttransitional oxide films on single crystals, independently of their crystallographic orientation, composition, and test conditions (Fig. 3b). As a result of this, the texture development bears the same character in the oxide films formed on polycrystalline aggregates of zirconium and its alloys; hence in the posttransitional films the same axial texture is obtained (Fig. 4). The grain in the oxide films is extremely fine; a qualitative estimate gives a grain size of 0.1 μ. The diameter of the fibers is of a similar order.

Thus as thickness increases the texture in the oxide films on zirconium and its alloys develops by the rotation of the fibers, their direction approaching that of the normal to the sample surface. This process is accompanied by the loss of the protective properties formerly characterizing the films. The interfiber boundaries containing the greatest number of crystal-lattice defects constitute easier paths for the diffusion of oxygen.

LITERATURE CITED

1. A. Bibb and J. Faschia, Trans. Soc. AIME, 230, No. 3, 415 (1964).
2. F. Vahldick, J. Less-Common Met., 12, No. 1, 19 (1967).
3. C. David, R. Geschier, and C. Roy, J. Nucl. Mater., 38, 329 (1971).
4. D. Douglass and J. Van Landuyt, Acta Met., 13, No. 10, 1069 (1965).
5. C. Roy and C. David, J. Nucl. Mater., 37, 71 (1970).
6. V. G. Parfenov, V. V. Gerasimov, and G. I. Venediktova, Corrosion of Zirconium and Its Alloys [in Russian], Atomizdat, Moscow (1967).
7. A. I. Kitaigorodskii, X-Ray Structural Analysis of Fine-Crystalline and Amorphous Solids [in Russian], Gostekhteorizdat, Moscow — Leningrad (1952).

RELATIVE YIELDS OF XENON ISOTOPES IN THE PHOTOFISSION OF ^{237}Np AND ^{235}U

K. A. Petrzhak, E. V. Platygina,
Yu. A. Solov'ev, and V. F. Teplykh

UDC 539.173.3:546.791.3

The xenon isotopes with A = 131-136 occur in that part of the mass spectrum of fission fragments in which the finest structure of the yields is observed in the fission of several atomic nuclei [1-5]. The absolute and relative yield values of fission fragments were obtained with highest accuracy with mass spectrometry from the fission of the isotopes of thorium, uranium, plutonium, and other heavy nuclei by thermal and fast neutrons. Research on the yield in the photofission made use of the less accurate radiochemical method, because the amounts of fission fragments which are to be investigated and accumulated under the usual irradiation conditions do not suffice for an analysis by mass spectrometry.

In the present work a mass spectrometer of high sensitivity was used to measure the relative yields of the xenon isotopes with A = 131-136 obtained from the fission of ^{237}Np and ^{235}U by bremsstrahlung. The B-30 betatron of the Leningrad Technological Institute was used for the irradiation. Targets made from neptunium dioxide and uranous uranic oxide in the form of pressed tablets with a mass of 1 g were inserted near the orbit of the accelerated electrons in order to increase the absorbed dose; the device described in [6] was used. After an irradiation time of 40-50 h, the total amount of xenon which had been formed by fission reached about 10^{-9} cm^3. After an exposure of 2 months, the noble gases were thermally extracted from the target in a vacuum system of quartz. The gases were purified with the generally adopted method of [7].

The measured spectra of the xenon fragments resulting from the photofission of ^{237}Np and ^{235}U are listed in Table 1. The data indicate that a fine structure of the yield curve of the fission fragments exists and that a peak occurs at the mass 134. An energy dependence can also be noted in the case of the ^{237}Np fission. Thus, the yield of the fragments with A = 134 decreases, whereas the yield of the fragments with A = 131 increases when the energy of excitation of the nucleus undergoing fission increases.

TABLE 1. Relative Yields of Xe Isotopes in the Photofission of ^{237}Np and ^{235}U

Fission nucleus	Max. energy (MeV) of the bremsstrahlung	Isotope composition (%)			
		^{131}Xe	^{132}Xe	^{134}Xe	^{136}Xe
^{237}Np	20	21,50±0,60	23,00±0,70	29,10±0,50	26,40±0,40
^{237}Np	15	19,70±1,20	21,40±1,50	31,80±1,10	27,10±0,90
^{235}U	20	20,00±0,20	24,20±0,30	28,50±0,20	27,30±0,20

LITERATURE CITED

1. R. Wanles and H. Thode, Canad. J. Phys., 33, 541 (1955).
2. D. Wiles, J. Petruska, and R. Tomlinson, Canad. J. Chem., 34, 227 (1956).
3. K. A. Petrzhak et al., Yadernaya Fizika, 14, 950 (1971).
4. I. Meason and R. Kuroda, Phys. Rev., 142, 691 (1966).
5. H. Richter and C. Koryel, Phys. Rev., 95, 1550 (1954).
6. M. Ya. Kondrat'ko, O. P. Nikotin, and K. A. Petrzhak, Atomnaya Énergiya, 27, No. 6, 544 (1969).
7. K. A. Petrzhak, V. F. Teplykh, and M. G. Pan'yan, Yadernaya Fizika, 11, 1178 (1970).

Translated from Atomnaya Énergiya, Vol. 41, No. 1, pp. 44-45, July, 1976. Original article submitted October 28, 1975.

MEASUREMENT OF $\alpha(E) = \sigma_c(E)/\sigma_f(E)$ OF ^{239}Pu FOR 0.007-eV-12-keV NEUTRONS

Yu. V. Ryabov

UDC 539.173.4

Detailed information on the energy dependence of α, the ratio of the radiative capture and fission cross sections, over a wide range of energies is of great interest for reactor physics.

We have performed relative measurements of $\alpha(E)$ for ^{239}Pu in the 0.007-eV-12-keV range.

Fissions and radiative captures were detected by a stillbene crystal 70 mm in diameter and height, and an FÉU-82. Prompt fission neutrons (f channel) were recorded by proton recoils with discrimination against the γ background by luminescence time [1]. The energy threshold for recording neutrons was ~0.9 MeV for a γ-ray suppression of $\sim 3 \cdot 10^{-4}$. The threshold for recording fission and radiative capture γ rays (γ channel) was set at ~0.5 MeV. The detector was in a B_4C and Pb shield 15 cm thick. The entrance window of the crystal was shielded against resonance neutrons scattered from the beam by a 2.5-cm-thick ^{10}B filter, and against the natural γ activity of the sample and γ rays from the capture of scattered neutrons in boron by 0.5 cm of lead. A metallic sample of ^{239}Pu containing 1.75% ^{240}Pu was placed at an angle of 45° with a well-collimated neutron beam. The surface density of the sample was $2.13 \cdot 10^{21}$ nuclei/cm^2. In order to make time-of-flight measurements in a single experiment over such a broad range of neutron energies using a flight path L = 251.6 m the OIYaI fast reactor was pulsed once every 3.8 sec at an average power of 10 kW. The information was accumulated in two 4096 channel analyzers with channel widths of 16 (first thousand) and 64 μsec. The nominal resolution was 230 nsec/m. The use of a small volume scintillation detector with widely spaced powerful neutron pulses enabled measurements to be made with a constant background which was very low for the method chosen (<1% of the counts per channel in both spectra for E_n = 0.0253 eV) which in practice was determined solely by spontaneous fission in the sample. The background of fast neutrons and γ rays from the reactor became important for energies >100 eV, and was determined by the method of "black" filters [2]. In the fission and capture channels it was equal to 0.8 and 5.2% (100-200 eV); 3.8 and 20% (1-1.5 keV), and 14 and 56% (10-12 keV) of the total counts, respectively.

TABLE 1. Average Values $\langle\alpha(E)\rangle$ in the 0.007-100-eV Range.

ΔE, eV	⟨α(E)⟩		ΔE, eV	⟨α(E)⟩		
	this work	[6]		this work	[6]	[8]
0,007—0,008	0,332±0,036	—	0,5—0,6	0,446±0,055	0,46±0,05	—
0,008—0,009	0,335±0,036	—	0,6—0,7	0,394±0,048	0,38±0,081	—
0,009—0,010	0,338±0,036	—	0,7—0,8	0,363±0,046	0,31±0,11	—
0,010—0,015	0,346±0,038	—	0,8—0,9	0,348±0,046	0,31±0,14	—
0,015—0,020	0,350±0,039	—	1,5—2,0	0,218±0,096	—	—
0,02—0,03	0,357±0,041	0,37±0,03	2,0—3,0	0,221±0,107	—	—
0,03—0,04	0,368±0,042	0,38±0,03	3,0—4,0	0,231±0,085	—	—
0,04—0,05	0,386±0,044	0,40±0,03	4,0—5,0	0,233±0,078	—	—
0,05—0,06	0,414±0,044	0,42±0,03	5,0—10,0	0,482±0,067	—	0,64±0,07
0,06—0,07	0,439±0,045	0,44±0,03	10,0—20,0	0,579±0,069	—	0,52±0,06
0,07—0,08	0,451±0,046	0,46±0,03	20,0—30,0	0,787±0,089	—	0,61±0,07
0,08—0,09	0,465±0,046	0,48±0,03	30,0—40,0	0,840±0,093	—	0,40±0,04
0,09—0,10	0,485±0,049	0,50±0,03	40,0—50,0	3,261±0,192	—	1,40±0,15
0,10—0,15	0,538±0,054	0,61±0,04	50,0—60,0	1,082±0,087	—	0,74±0,08
0,15—0,20	0,636±0,059		60,0—70,0	0,398±0,058	—	0,47±0,06
0,2—0,3	0,675±0,065	0,69±0,04	70,0—80,0	0,412±0,061	—	0,47±0,09
0,3—0,4	0,637±0,058	0,66±0,04	80,0—90,0	0,237±0,047	—	0,23±0,03
0,4—0,5	0,534±0,056	0,56±0,03	90,0—100,0	0,682±0,076	—	1,16±0,12

Translated from Atomnaya Énergiya, Vol. 41, No. 1, pp. 45-48, July, 1976. Original article submitted October 28, 1975.

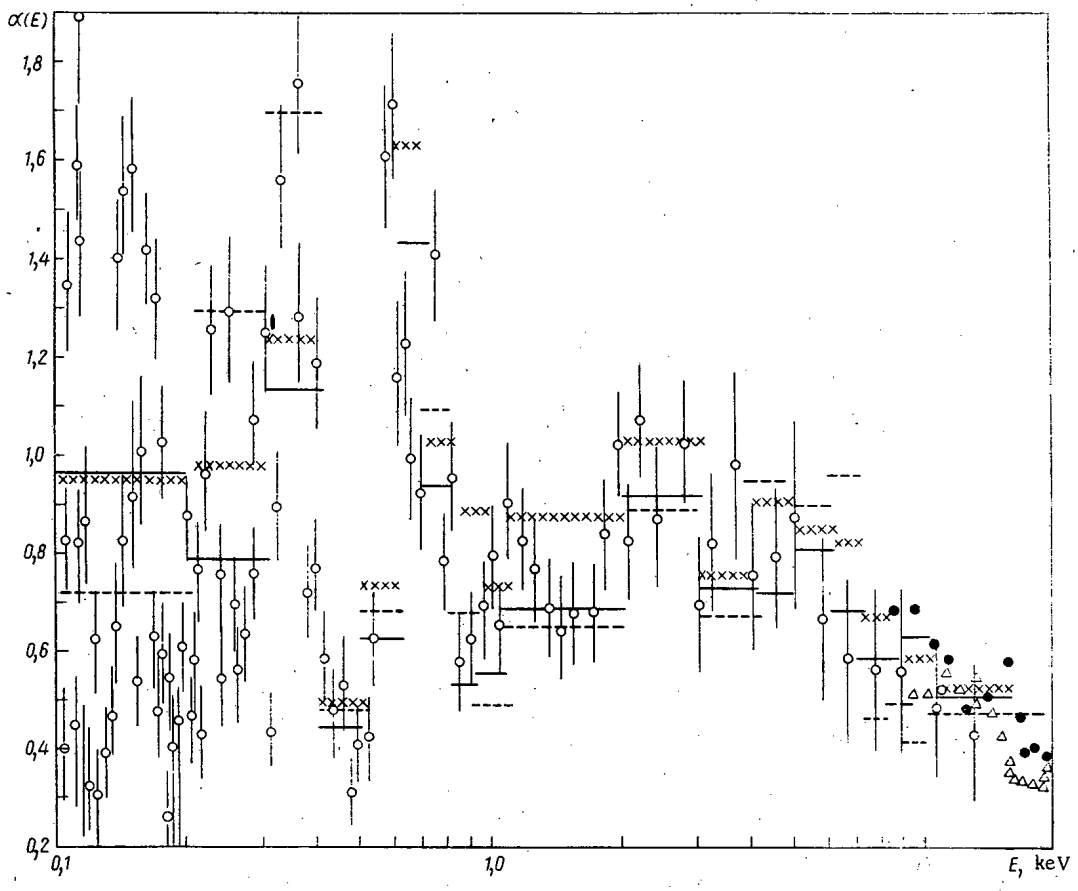

Fig. 1. Measured values of α(E) from 0.1-20 keV: ○) this work; — — —) [2]; ———) [3]; ×××) [6]; △, ●) data obtained with electrostatic generators [7, 9].

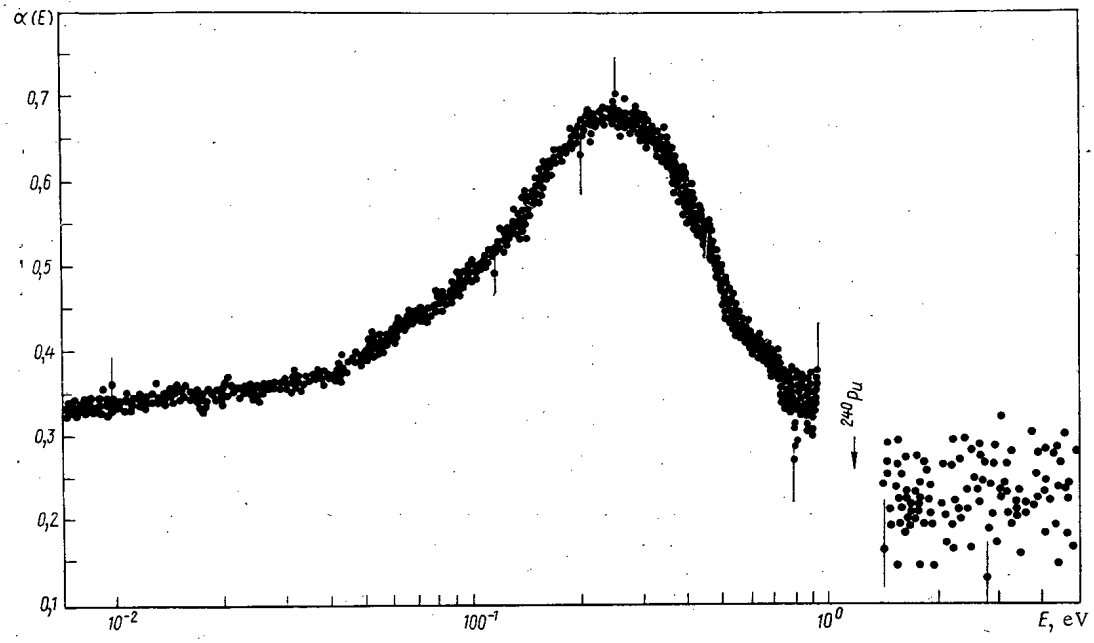

Fig. 2. Measured values of α(E) in the 0.007-5-eV range.

The value of α(E) was computed from the relation [3]

$$\alpha(E)=\frac{A\frac{N_\gamma(E)}{N_f(E)}-1}{B-C\frac{N_\gamma(E)}{N_f(E)}},$$

where N_γ is the counting rate in the γ channel; $N_f(E)$ is the rate of counting fission neutrons in the f channel; A, B, and C are the ratios of the counting efficiencies in the respective channels of fission neutrons and fission γ rays, capture and fission γ rays, capture γ rays in the f channel and fission γ rays, respectively. The values of the constants A, B, and C determined by normalizing to known values of α_0 for low energy resonances [2] and correcting for the energy dependence of the average number of prompt neutrons [4] were A = 0.26, B = 0.66, C = 0.0054.

The experimental errors $\Delta\alpha(E)$ depend [5] on the accuracy of the background counts, the normalization, and to a lesser degree on the statistical accuracy. In Fig. 1 our measured values of $\alpha(E)$ in the 100-eV-12-keV range are compared with results obtained by various methods with higher energy resolution. The agreement with [3] is best. Our results and [2] do not confirm the existence of a pronounced structure in the average values of $\alpha(E)$ below 1 keV. The increase in the error in $\alpha(E)$ above 3 keV is related to the fact that the last value of the energy at which the background is determined is $E_n = 2.85$ keV (Na resonance) and the fitting of the background curve [2] is more uncertain here than in the region below 3 keV. The values of $\alpha(E)$ for the 0.007-5-eV range are shown in Fig. 2 for the first time, and Table 1 gives the average values $\overline{\alpha(E)}$ in energy ranges up to 100 eV where the energy resolution still permits the use of an averaging procedure. In this energy region our results are in basic agreement with those of [6, 8].

We note that in obtaining the values of $\alpha(E)$ corrections for radiative capture in ^{240}Pu were not introduced since the systematic errors characteristic of the method of measurement used and the normalization are much larger than this correction.

The author thanks A. A. Omel'yanenko for help with the measurements.

LITERATURE CITED

1. Zen Chang Bom et al., Yad. Fiz., 18, 34 (1973).
2. M. A. Kurov et al., At. Énerg., 30, No. 4, 258 (1971).
3. M. G. Shomberg, in: Proc. IAEA Symp. on Nuclear Data for Reactors, Vol. 1, Helsinki (1970), p. 315.
4. J. Trochon et al., J. Phys. 34, 131 (1973).
5. Yu. V. Ryabov, Report IAEA 71-2101 (1971).
6. R. Gwin et al., Nucl. Sci. and Eng., 45, No. 1, 47 (1971).
7. V. N. Kononov, in: Proc. of Conf. on Neutron Physics [in Russian], Vol. 1, Naukova Dumka, Kiev (1972).
8. Yu. V. Ryabov et al., At. Énerg., 24, No. 4, 351 (1968).
9. R. Bandl et al., in: Proc. Third Conf. on Neutron Cross Sections and Technology, Knoxville, Vol. 1, March 15-17 (1971), p. 273.

YIELDS OF ^{73}As AND ^{74}As IN NUCLEAR REACTIONS WITH PROTONS, DEUTERONS, AND α PARTICLES

P. P. Dmitriev and G. A. Molin

UDC 621.039.8.002

The isotopes ^{73}As and ^{74}As are widely used in applied research problems. These isotopes can be obtained in appreciable amounts only in charged-particle reactions, and therefore they are classed as cyclotron nuclides.

The decay schemes of ^{73}As and ^{74}As given in [1, 2] are shown in Fig. 1 ([1] is a compilation of original papers).

It can be seen from Fig. 1 that ^{73}As is transformed by electron capture into ^{73m}Ge ($T_{1/2} = 0.53$ sec). There is a high-resolution Mössbauer resonance for the 13.26-keV γ transition of ^{73m}Ge [3].

Translated from Atomnaya Énergiya, Vol. 41, No. 1, pp. 48-51, July, 1976. Original article submitted November 4, 1975.

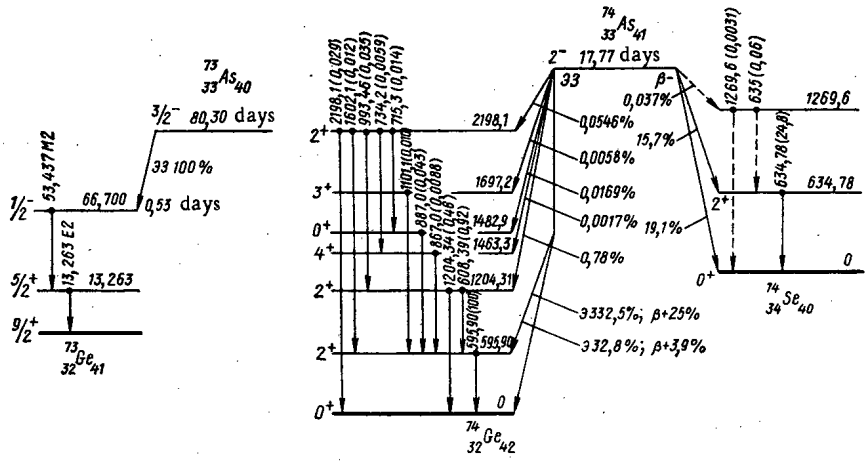

Fig. 1. Decay schemes of ^{73}As and ^{74}As. Transition energies for γ rays are given in keV. The relative intensities of the γ transitions for ^{74}As are shown in parentheses.

Both γ transitions of ^{73}As are strongly converted, and therefore it is necessary to know their total internal conversion coefficients in order to calculate the absolute quantum yields of the 53.437- and 13.263-keV γ rays. An important component of the quantum emission of ^{73}As are Kx rays arising from the decay of ^{73}As by K capture and in the conversion of γ transitions to the K shell. Table 1 gives the absolute quantum yields of the ^{73}As γ and Kx rays, the total internal conversion coefficients α_n, and the K internal conversion coefficients α_k. The value $\alpha_k = 7.4$ is the average of three values of α_k given in [1]. The value $\alpha_n = 8.4$ was obtained for K/LM = 7.1 [1].

The values of α_k and α_n for 13.26-keV γ radiation were obtained in a similar way using K/LM = 0.36 [1].

The values of the average K x-ray energies and the energies of the K_α and K_β components and their relative intensities are taken from [4]. The quantum yield of K x rays was obtained from the intensity ratio $I(Kx)/I(\gamma^{53.4}) = 8.95$ given in [1], from which $n_{KX} = 10.6\% \cdot 8.95 = 95\%$. Nearly the same value of n_{KX} is calculated by using the values of n_γ and α_k from Table 1, the probability of K capture ($\varepsilon_k/\varepsilon_n = 0.875$ from [1]), and the fluorescence yield $\omega_k = 0.49$.

According to the scheme shown in Fig. 1, ^{74}As decays by electron capture (36.3%), β^+ decay (28.9%) and β^- decay (34.8%); the β^+-decay percentage is taken from [4]. The ^{74}As γ-transition conversion can be neglected, and therefore the γ-transition probabilities are practically equal to the absolute γ-ray yields. From the probabilities of ^{74}As decay to the 595.90- and 634.78-keV levels and the γ-transition balances, the weighted mean value of the scale factor to convert the relative intensities of the γ transitions given in parentheses in Fig. 1 to quantum yields in percent is 0.592. Table 2 gives the quantum yields of the two most intense gamma transitions and the annihilation and K x radiations. The yield of K x radiation was calculated using $\varepsilon_k/\varepsilon_n = 0.88$; then $n_{KX} = 36.3\% \cdot 0.88 \cdot 0.49 = 15.7\%$. The quantum yield of any of the remaining 12 weak ^{74}As γ lines can be obtained by multiplying its relative intensity by 0.592.

We have measured the ^{73}As and ^{74}As yields as functions of the incident particle energy by bombarding thick targets of metallic germanium with protons, deuterons, and α particles, and metallic gallium with α particles; also the yield of ^{74}As by bombarding arsenic with maximum energy protons, deuterons, and α particles.

TABLE 1. Energy and Quantum Yield of ^{73}As γ and K X Radiation

Energy of radiation, keV	Transition probability, %	α_k	α_n	No. of quanta per decay, %
53,437	100	7,4	8,4	10,6
13,263	100	347	1310	0,076
10,01 $\overline{KX}$	194	—	—	95
(9,88 K_α)	(172)	—	—	(84)
(11,10 K_β)	(22)	—	—	(11)

TABLE 2. Energies and Quantum Yields of Main γ and K X-Ray Lines of ^{74}As

Energy of radiation, keV	No. of quanta per decay, %	Energy of radiation, keV	No. of quanta per decay, %
634,78	14,7	10,01 $\overline{KX}$	15,7
595,90	59,2	(9,88 K_α)	(13,9)
511,0±	57,8	(11,10 K_β)	(1,8)

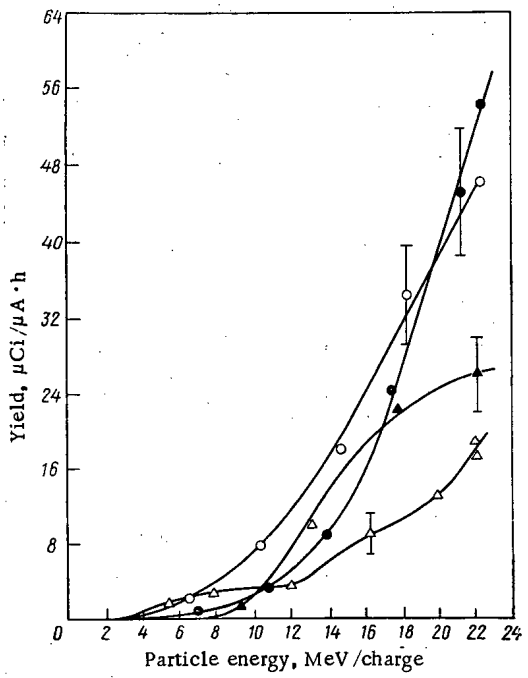

Fig. 2

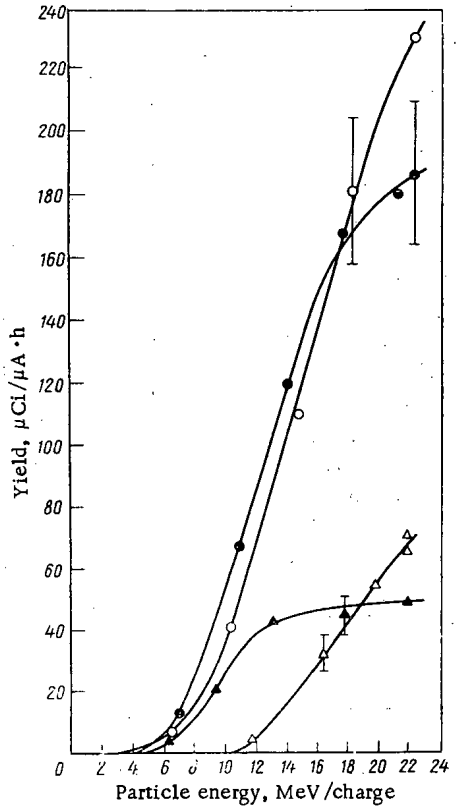

Fig. 3

Fig. 2. ^{73}As yields as functions of the energy of the bombarding particles for the irradiation of thick germanium targets with protons, deuterons, and α particles, and gallium with α particles. •) Ge + p; ○) Ge + d; △) Ge + α (×2); ▲) Ga + α (×2).

Fig. 3. ^{74}As yields as functions of the energy of the bombarding particles for the irradiation of thick germanium targets with protons, deuterons, and α particles, and gallium with α particles. •) Ge + p; ○) Ge + d; △) Ge + α (×4); ▲) Ga + α (×4).

The extracted beam of the 1.5-meter FÉI cyclotron at Obninsk was used. The technique of irradiating the samples and measuring their activities was similar to that described in [5]. The energy of the bombarding particles was varied by copper retarding foils. The ^{73}As activity was determined from the photopeak of the 53.437-keV γ line, and the ^{74}As activity from the total photopeak of the 595.90- and the 634.78-keV lines. Values of the quantum yields were taken from Tables 1 and 2. The ^{73}As activity was measured approximately five months after irradiation, and that of ^{74}As after approximately a one-month decay of ^{71}As ($T_{1/2}$ = 62 h), ^{72}As ($T_{1/2}$ = 26.0 h), and ^{76}As ($T_{1/2}$ = 26.3 h).

^{73}As was separated radiochemically from samples of Ge and Ga, and the aliquot of the solution was measured with a well-type NaI(Tl) crystal.

The integrated irradiation current to the samples was measured with copper monitor foils. The ^{65}Zn activity was measured in 18-mg/cm^2-thick monitor foils and the integrated current was calculated using cross sections from experimental excitation functions of the appropriate nuclear reactions: ^{65}Cu(pn)^{65}Zn [6], ^{65}Cu(d, 2n) ^{65}Zn [7], ^{63}Cu(α, pn + 2n) ^{65}Zn [8]. Our measured values of the ^{63}Cu excitation function are in good agreement with data from [8].

The experimental curves for the yields of ^{73}As and ^{74}As are shown in Figs. 2 and 3. The error in the measurement of the yields is ±13% and is due mainly to systematic errors in measuring the activities of the nuclides and the integrated irradiation current. Table 3 gives the nuclear reactions in which ^{73}As and ^{74}As are formed, the yields for bombarding particles of maximum energy, and data from other papers. It is clear from Table 3 that the few published values are appreciably smaller than the physical yields we measured. In [9-12] the yields of ^{73}As and ^{74}As were measured with commercial targets and the lower yields observed might be due to the following:

TABLE 3. Yields of ^{73}As and ^{74}As

Production reaction	Energy threshold of reaction, MeV	Content of nuclide in natural mixture, %	Data on yields: particle energy, MeV	Data on yields: yield, μCi/μA·h	References
$^{73}Ge(pn)^{73}As$	1,16	7,84	22,2±0,3	54,6±7,1	This work
$^{74}Ge(p2n)^{73}As$	11,4	36,40	22	8	[9]
$^{72}Ge(dn)^{73}As$	—	27,43	22,2±0,3	46,4±6,0	This work
$^{73}Ge(d2n)^{73}As$	3,47	7,84			
$^{74}Ge(d3n)^{73}As$	13,9	36,40			
$^{70}Ge(\alpha n)^{73}Se\rightarrow$	8,34	20,60	44,0±0,6	9,0±1,2	" "
$^{70}Ge(\alpha p)^{73}As$	4,63	20,62			
$^{72}Ge(\alpha 3n)^{73}Se\rightarrow$	27,9	27,43			
$^{72}Ge(\alpha p2n)^{73}As$	24,2	27,43			
$^{73}Ge(\alpha 4n)^{73}Se\rightarrow$	34,8	7,84			
$^{71}Ga(\alpha 2n)^{73}As$	13,4	39,9	44,1±0,6	13±1,7	" "
$^{74}Ge(pn)^{74}As$	3,38	36,40	22,2±0,3	187±24	" "
$^{76}Ge(p3n)^{74}As$	19,5	7,73	22	50	[9]
$^{73}Ge(dn)^{74}As$	—	7,84	22,2±0,3	231±30	This work
			30	80	[10]
$^{74}Ge(d2n)^{74}As$	5,72	36,40	15	31±10	[11]
			10,8	25±4	[12]
$^{72}Ge(\alpha pn)^{74}As$	15,8	27,43	44,0±0,6	17±2,2	This work
$^{73}Ge(\alpha p2n)^{74}As$	22,7	7,84			
$^{71}Ga(\alpha n)^{74}As$	5,04	39,9	44,1±0,6	12,5±1,6	" "
$^{75}As(ppn)^{74}As$	10,4	100	21,8±0,3	95±12	" "
			22,5±0,3	30±4	" "
$^{75}As(dt)^{74}As$	4,1	100	15,2	3,5	[13]
$^{75}As(\alpha\alpha n)^{74}As$	10,8	100	43,0±0,6	20±2,6	This work

a) loss of a nuclide in irradiation as a result of evaporation of the nuclide and target material;

b) part of the beam being recorded irradiates structural components of the target;

c) loss of the nuclide in the radiochemical separation. Therefore the yields measured in [9-12] are technological yields. In [13] the ^{74}As yield was obtained by integrating the experimental excitation function of the reaction.

The data in Figs. 1 and 2 show that the most efficient way to obtain ^{73}As is to bombard germanium with protons having energies $\geq$22 MeV. In obtaining ^{74}As it is important to decrease the admixture of ^{73}As, and for the FÉI cyclotron the irradiation of germanium by 11-MeV protons is recommended. Intense proton beams of this energy are easy to obtain by accelerating molecular hydrogen under conditions for accelerating deuterons. In view of the low cross section of the $^{75}As(pt)^{73}As$ reaction ^{74}As can be obtained with a negligible admixture of ^{73}As, but "with carrier" by bombarding arsenic with protons having $E_p \leq 18.5$ MeV, which is below the threshold of the $^{75}As(p, p2n)^{73}As$ reaction.

The authors thank G. N. Grinenko and Z. P. Dmitriev for help with the work.

LITERATURE CITED

1. K. Alvar, Nucl. Data Sheets, 13, No. 3,305 (1974).
2. J. Van Hise and C. Paperiello, Nucl. Phys., A188, 148 (1972).
3. R. Raghavan and L. Pfeiffer, Phys. Rev. Lett., 32, 512 (1974).
4. C. Lederer et al., Table of Isotopes, Wiley, New York (1967).
5. P. P. Dmitriev et al., At. Énerg., 31, No. 2, 157 (1971); 32, No. 5, 426 (1972).
6. P. P. Dmitriev et al., At. Énerg., 24, No. 3, 279 (1968).
7. P. P. Dmitriev and N. N. Krasnov, At. Énerg., 18, No. 2, 184 (1965).
8. N. Porile and D. Morrison, Phys. Rev., 116, 1193 (1959).

9. J. Martin et al., Nucleonics, 13, 28 (1955).
10. A. Aten and J. Halberstadt, Philips Tech. Rev., 16, 1 (1954).
11. I. Gruwerman and P. Kruger, J. Appl. Rad. and Isotopes, 5, 21 (1959).
12. A. I. Guldamashvili et al., At. Energ., 5, No. 6, 660 (1958).
13. L. Bowen and J. Irvine, Phys. Rev., 127, 1698 (1921).

NONDESTRUCTIVE ANALYSIS OF THIN SURFACE LAYERS OF MATERIALS FOR HYDROGEN CONTENT

I. P. Chernov, V. V. Kozyr',
and V. A. Matusevich

UDC 539.106:543.843

It is known that the hydrogen content of metals, alloys, and semiconductors to a large extent determines their electrophysical properties. The presence of even a small amount of hydrogen in metals leads to a worsening of plastic properties (hydrogen embrittlement), an increase in electrical resistance, a decrease in magnetic permeability, etc. Therefore, monitoring for hydrogen content is very important. Among other known methods is the nuclear physics method of hydrogen determination based on the characteristics of the scattering of equal-mass particles [1, 2]. The main shortcoming of this method of hydrogen analysis is that it is restricted to films up to 10 μ in thickness. We propose a method for determining the hydrogen content of surface layers of samples of arbitrary thickness based on the recording of hydrogen nuclei ejected from the surface of the sample by accelerated ions.

To understand the essence of the method, let us consider the special features of the elastic scattering of heavy by light nuclei. Suppose accelerated ions of mass M_1 are incident on a thick sample containing nuclei of mass M_2 ($M_2 < M_1$) in its surface layer. There is a certain probability that an incident ion will encounter a nucleus of mass M_2 and be scattered by it. Recoil nuclei of mass M_2 will be emitted at any angle in the forward hemisphere while the bombarding ions are scattered into a cone of apex angle $\theta_{1\,max} = \sin^{-1}(M_2/M_1)$. For the scattering of ^{4}He and ^{12}C ions by hydrogen the apex angle is 14.5 and 4.75°. Therefore the scattered ions lose all their energy in a thick sample and remain in it. For an appropriate angle of inclination of the sample to the incident beam ($\theta < 90°$) the recoil nuclei emerge from the target and can be recorded. The energy E_2 of the recoil nuclei for a given recording angle θ_2 is given by the relation

$$E_2 = \frac{4M_1M_2}{(M_1+M_2)}\cos^2(\theta_2)\,E_1. \qquad (1)$$

The content of the lightest nuclei can be determined by using particles of the same sort as the impurity of interest. In this case, however, it is necessary to separate the recoil nuclei from an intense background of particles scattered by nuclei of the matrix, which makes the problem impracticable. In the method we propose the background which interferes with the extraction of useful information found in the samples exceed by 10- scattered by matrix nuclei, and light particles from nuclear reactions induced in matrix and impurity nuclei by ions. The first component of the background can be eliminated by identifying the type of charged particles. For matrices of intermediate and large atomic numbers the second component can be eliminated by choosing the bombarding energies below the Coulomb barrier.

When 12-MeV α particles and 20-MeV carbon ions are used for the analysis the sensitivity of the method is $4 \cdot 10^{12}$ and 10^{12} nuclei/cm^2, respectively. In this case the ion current is 0.1 μA, the analysis time is 1 h, and the solid angle of the telescope is 10^{-2} sr.

The possibilities of the method were investigated by using 18-MeV α particles for hydrogen determination. The α particles were obtained from the Tomsk Polytechnic Institute cyclotron. The accelerated ions

Translated from Atomnaya Énergiya, Vol. 41, No. 1, pp. 51-53, July, 1976. Original article submitted November 4, 1975.

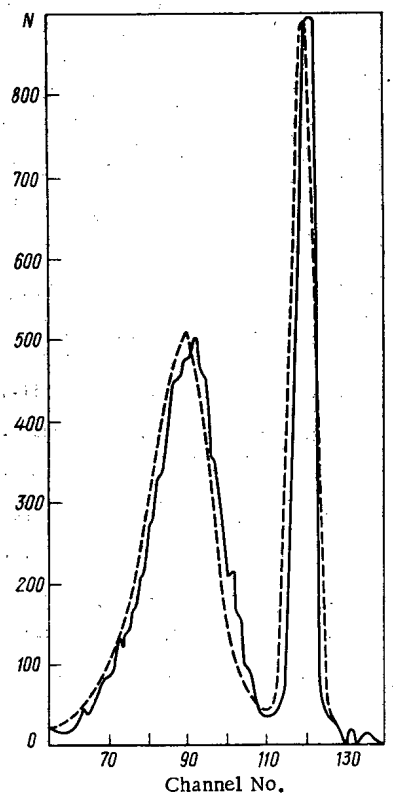

Fig. 1

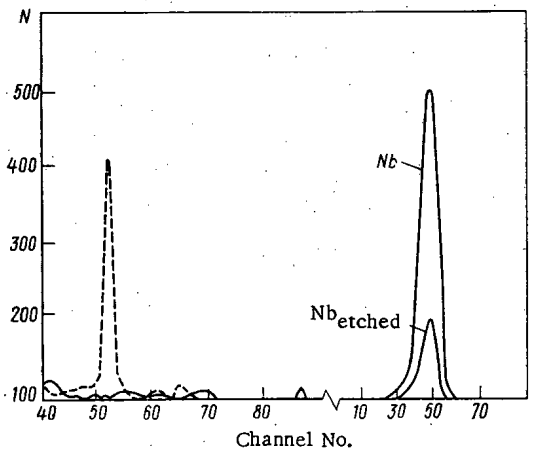

Fig. 2

Fig. 1. Energy spectra of hydrogen recoil nuclei resulting from elastic collisions with 18-MeV α particles at $\Theta_{lab} = 45°$: — — —) from a target consisting of two layers of dacron (each 0.324 mg/cm^2) and a layer of aluminum (2.7 mg/cm^2); ———) from a target deposited on a plate of gallium arsenide.

Fig. 2. Energy spectra of hydrogen recoil nuclei emitted: ———) from a surface layer of gallium arsenide and niobium; — — —) from gallium arsenide annealed in a hydrogen atmosphere.

were led from the accelerator chamber through an ion guide, where they were focused and collimated, onto the sample at the center of the scattering chamber. The plane of the surface layer of the sample was set at an angle of 30° with the incident beam. The diameter of the beam of accelerated particles at the sample was 2.5 mm. The particles emerging from the samples were recorded by a telescope consisting of a "thin" ΔE and a "thick" E semiconductor detector. The energy resolution of the spectrometer was 60 keV. The incident α particles were monitored by a semiconductor spectrometer recording the α particles scattered by a thin film placed in front of the sample.

The first stage of the investigation was devoted to a study of the possibility of using the method to measure the hydrogen concentration profile (Fig. 1).

Two peaks are observed: The first is narrow and the second is broadened as a result of the spread of ionization losses of hydrogen recoil nuclei. There is practically no background from the (α, p) reaction in oxygen, carbon, and matrix nuclei. The presence of a thick plate does not change the shape of the proton spectra significantly.

During the next stage the method was used to perform analyses. The hydrogen content of a sample was determined by comparison with a standard dacron film 0.324 mg/cm^2 thick. The hydrogen content was determined in a surface film of gallium arsenide which was first annealed in a hydrogen atmosphere. Its hydrogen content was $9.7 \cdot 10^{17}$ nuclei/cm^2 (Fig. 2). The figure also shows the spectrum of hydrogen nuclei ejected by ^{4}He ions from the surface of a plate which was annealed in air. Its hydrogen content was at the sensitivity level of the method ($\sim 4 \cdot 10^{12}$ nuclei/cm^2). The energy spectrum of hydrogen nuclei from niobium plates is shown. One of these plates was in air for a long time and the other was etched before analysis. In the first plate the hydrogen content was $1.5 \cdot 10^{16}$ nuclei/cm^2, and in the second it was an order of magnitude smaller. It should be noted that the method described can be used to determine the content of heavy hydrogen isotopes and helium.

The authors thank V. V. Sokhorev for help in preparing the targets and A. A. Yatisa for a discussion of the results.

LITERATURE CITED

1. K. P. Artemov et al., At. Énerg., 34, No. 4, 265 (1973).
2. B. Cohen, C. Fink, and J. Degnan, J. Appl. Phys., 43, No. 1, 19 (1972).

ANOMALOUS ISOTOPE COMPOSITION OF XENON AND KRYPTON IN MINERALS OF THE NATURAL NUCLEAR REACTOR

Yu. A. Shukolyukov, G. Sh. Ashkinadze, and A. B. Verkhovskii

UDC 539.175.2

A natural nuclear reactor functioned in the Oklo uranium deposit (Gabon, Africa) $1.8 \cdot 10^9$ years ago [1].

Five samples of uranium ore of this deposit (borehole SC20) have now been studied: One sample is from the zone of the chain reaction proper, whereas the four other samples were picked at increasing distances from that zone (see Table 1). The uranium concentration was determined (with an error of ±5% at low concentrations) on an MI-1311 mass spectrometer with the isotope dilution technique.

The same instrument was used to determine the ^{235}U concentration in a mixture of uranium isotopes; the error of the determination of the isotope composition was ±(1.0-1.5)%.

An MV-2302 mass spectrometer with a resolution of 4000 and an electron multiplier at the output was used for the isotope analysis of xenon and krypton (error in the measurement of the isotope ratios ±(0.5-2.0)%, depending upon the isotope) and the determination of their amounts (error ±(10-15)%) according to the previously described method of [2]. The measurements were made in a static vacuum; the sensitivity to xenon and krypton was $4 \cdot 10^{-12}$ and $11 \cdot 10^{-12}$ $cm^3 \cdot mV^{-1}$, respectively; the background resulting from the instrument was 10^{-12} and 10^{-11} cm^3, respectively; the amount of gas measured was 10^{-9}-10^{-7} cm^3.

An uranium sample was irradiated in a reactor (Karlsruhe, Federal Republic of Germany) for a precise

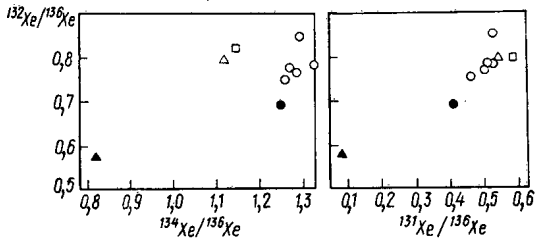

Fig. 1. Isotope ratios of xenon in: ○) the natural nuclear reactor, ●) in the fission of ^{235}U, □) in the fission of ^{239}Pu by thermal neutrons, Δ) in the fission of ^{238}U by fast neutrons, and ▲) in the spontaneous fission of ^{238}U.

Translated from Atomnaya Énergiya, Vol. 41, No. 1, pp. 53-55, July, 1976. Original article submitted January 13, 1976.

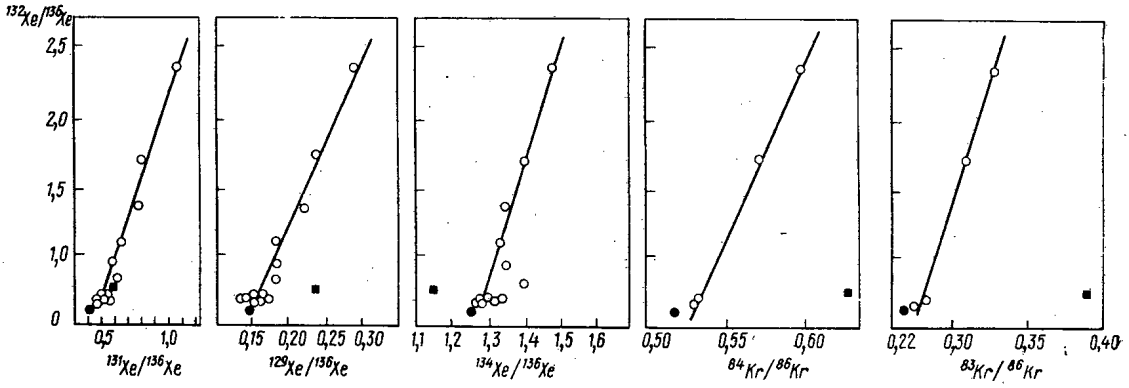

Fig. 2. Isotope correlations of xenon and krypton in the thermal annealing of sample 1348 (*a* and b): ○) denotes minerals of the natural nuclear reactor; ●) and ■) denote the fission of ^{235}U and ^{239}Pu in the laboratory irradiation by thermal neutrons and fast neutrons, respectively.

determination of the isotope composition of the gases which are generated in the fission of ^{235}U by slow neutrons. The fraction of superthermal neutrons in the neutron spectrum was less than 0.1% during the irradiation.

The xenon quantities found in the samples exceed by 10- 5000 times the possible amount of xenon and krypton produced by the spontaneous fission of ^{238}U. In accordance with earlier data [1, 2], the isotope composition of the xenon of the samples investigated resembles that of the xenon formed in the fission of ^{235}U by slow neutrons or the fission of ^{238}U with fission neutrons; the isotope composition differs substantially from that of the xenon obtained by spontaneous fission of ^{238}U [3] (Fig. 1). However, the differences between the xenon liberated from the natural nuclear reactor and the xenon from the neutron-induced fission of ^{235}U and ^{238}U are still rather large. The strongest anomalies were observed in the xenon which had been taken from the reaction zone proper (sample 1348).

TABLE 1. Isotope Composition of the Xenon and the Krypton from the Natural Nuclear Reactor

Sample No.; temperature (°C) of annealing	Distance (m) from the reaction zone	Amount (%)		Flux ($\cdot 10^{20}$ neutrons/cm^2) calculated from burnup of ^{235}U	Amount (10^{-9} cm^3/g) of ^{136}Xe	Isotope composition of Xe and Kr								
		uranium	^{235}U in isotope mixture			136	134	132	131	130	129	86	84	83
1348 *a*;	0 (reaction	26,85	0,557	~ 4										
400					334	1,00	1,44	2,21	1,04	0,014	0,260	1,00	0,602	0,331
750					1000	1,00	1,36	1,69	0,760	⩽0,0014	0,219	1,00	0,568	0,304
1000					—	—	—	—	—	—	—	1,00	0,526	0,268
1150					2979	1,00	1,28	0,725	0,448	0,0014	0,130	1,00	0,532	0,280
1350	zone)				6786	1,00	1,24	0,685	0,418	0,0009	0,119	1,00	0,531	0,272
1348 b;	0 (reaction	26,85	0,557	~ 4										
300					243	1,00	1,28	0,922	0,528	0,0022	0,157	—	—	—
500					473	1,00	1,27	1,375	0,702	0,0037	0,228	—	—	—
800					1027	1,00	1,31	1,06	0,598	0,0047	0,186	—	—	—
1065					3920	1,00	1,24	0,701	0,462	0,0011	0,127	—	—	—
1160	zone)				4135	1,00	1,25	0,708	0,428	0,0009	0,122	—	—	—
1361; 1350	0,85	0,050	0,609	~ 2,5	224	1,00	1,24	0,722	0,453	0,0035	0,131	—	—	—
1364; 1350	1,35	0,00082	—	—	98	1,00	1,26	0,736	0,460	0,0016	0,126	—	—	—
1368; 1350	2,0	0,0026	0,740	—	26	1,00	1,23	0,704	0,453	0,0009	0,114	—	—	—
1371; 1350	2,5	0,00048	—	—	19	1,00	1,23	0,698	0,449	0,0035	0,126	—	—	—
$^{235}U + n_{ther}$	—	100	—	—	—	1,00	1,25	0,689	0,410	—	0,11	1,00	0,517	0,279
$^{238}U + n_{spont.}$	—	100	—	—	—	1,00	0,82	0,579	0,082	—	0,002	1,00	0,140	0,0034
$^{239}Pu + n_{ther}$	—	—	—	—	—	1,00	1,15	0,808	0,578	—	0,232	1,00	0,633	0,390
Atmosphere	—	—	—	—	—	1,00	1,18	3,03	2,39	0,460	2,98	1,00	3,28	0,665

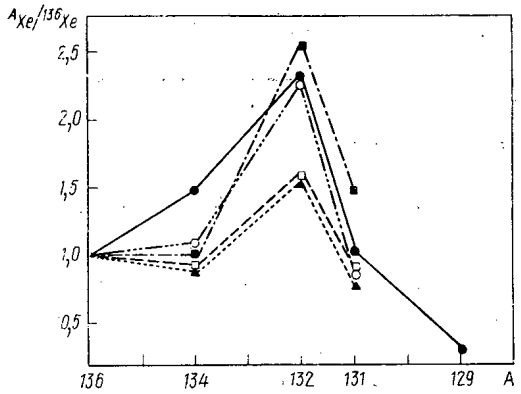

Fig. 3. Isotope ratios in xenon of various sources: ●) refers to the natural nuclear reactor (sample 1348 *a*, 400°C); "fission xenon" in the terrestrial atmosphere, with various models of the primary xenon: ○) from the Fayetville meteorite [9]; ▲) from lunar soil [6]; □) "fission xenon" in a deep gas well [7]; ■) excess xenon in ancient anorthosite [8] (A denotes the mass number of the isotope).

In order to determine the reasons for the differences, two portions of sample 1348 (portion *a* and portion b; 3 and 15 mg, respectively) were subjected to a stepwise thermal annealing, and the isotope composition of xenon and krypton was analyzed in each fraction of the gas. The low-temperature fraction contained (see Table 1) xenon with an isotope composition which is unusual for fission processes: the ratios of $^{131}Xe/^{136}Xe$, $^{132}Xe/^{136}Xe$, and $^{129}Xe/^{136}Xe$ were 2-3 times greater, and the ratios of $^{134}Xe/^{136}Xe$, $^{84}Kr/^{86}Kr$, and $^{83}Kr/^{86}Kr$ were 1.1-1.2 times greater than in the xenon and krypton obtained under laboratory conditions from the fission of ^{235}U by slow neutrons.

The position of the experimental points on a single straight line in the $^{i}Xe/^{136}Xe - ^{j}Xe/^{136}Xe$ coordinate system (i = 132 and j = 131, 134, 129; Fig. 2) can point to a two-component composition of the xenon (the same conclusion applies to krypton). One of these components is certainly the xenon from the ^{235}U fission by slow neutrons, but the isotope composition of the second component is unknown. One can determine only a "limit" isotope composition of this component in the fraction with the isotope ratios of strongest anomalies (sample 1348a, 400°C): $^{136}Xe = 1.00$; $^{134}Xe = 1.47$; $^{132}Xe = 2.32$; $^{131}Xe = 1.03$; and $^{129}Xe = 0.303$. Thus a pronounced fine structure is observed at ^{132}Xe.

An abnormally high yield of ^{131}Xe, ^{132}Xe, and ^{134}Xe relative to ^{136}Xe was earlier observed when UO_2 which had been irradiated in a reactor with thermal neutrons was annealed [4]. It was concluded that iodine and tellurium atoms, which are the predecessors of xenon in the radioactive series, have time to diffuse to the grain boundaries before these atoms decay. The probability of this diffusion increases with increasing lifetime of the radioactive predecessors of xenon. Accordingly [4], the amount of the corresponding xenon isotope increases in the low-temperature fraction of the gas which was liberated from the intercrystalline space.

However, in our experiments the anomaly at ^{129}Xe (^{129}I half-life = $1.7 \cdot 10^7$ years) did not noticeably exceed the anomalies at ^{131}Xe and ^{132}Xe (^{131}I and ^{132}Te half-lives = 8.06 days and 77.7 h, respectively) nor even the anomaly at ^{134}Xe (^{134}I half-life = 52 min). The anomaly which we found seems to be associated with another effect which exists in addition to the separation of the isotopes during the migration of the β-active parent atoms.

The nuclear origin of this anomaly cannot be ruled out. The following coincidences deserve particular attention. A special component, the "fission xenon" [5], was long ago detected in the terrestrial atmosphere. Compared with the primitive lunar xenon [6], the heavy xenon isotopes are present in excess in the terrestrial atmosphere and have a fine structure at ^{132}Xe (Fig. 3). In some natural gases which stem from a depth of several kilometers, an excess of ^{136}Xe, ^{134}Xe, ^{132}Xe, and ^{131}Xe over ^{130}Xe was found [7] in comparison to the primary xenon from meteorites and from the moon. Also in those cases the fine

structure corresponds to ^{132}Xe (see Fig. 3). Xenon enriched by the same isotopes and having a clear fine structure at ^{132}Xe was determined by mass spectrometry in one of the most ancient rocks of the earth, namely in Greenland anorthosite [8].

Unless the similarity of the isotope composition of the xenon which is present in the low-temperature gas fractions from the natural nuclear reactor, the natural gas in the depth, the ancient rocks, and the terrestrial atmosphere is a coincidence by chance, one can assume the same source, namely the fission of nuclei, as the origin in the four cases.

However, the relative yields of the xenon isotopes and the clearly pronounced fine structure at ^{132}Xe, both effects observed in the natural nuclear reactor and in the above terrestrial objects, were not detected in the fission of known nuclei. Additional investigations are required for finally evaluating the possible relation between the anomalies of xenon and krypton in the natural nuclear reactor and fission processes.

The interaction of neutrons with Ba, Te, Se, and Sr isotopes is a similar explanation in terms of physics of the observed anomalies of xenon and krypton in the natural nuclear reactor. But at neutron fluxes of $\sim 10^{20}$ neutrons/cm^2, the required concentration of target nuclei is 10-100 times greater than the concentration really existing in the rock material. It is therefore impossible to explain the anomalies with nuclear reactions occurring directly at xenon and krypton isotopes, among them isotopes with large cross sections for the interaction with neutrons.

The authors sincerely thank Doctor R. Naudet (French Atomic Energy Commission) for providing them with the samples from the unique site.

LITERATURE CITED

1. Bul. Inform. Sci. Techn., No. 193, 5 (1974).
2. R. Drozd, C. Hohenberg, and C. Morgan, Earth and Planet. Sci. Lett., 23, No. 1, 28 (1974).
3. Yu. A. Shukolyukov, Fission of Uranium Nuclei in Nature [in Russian], Atomizdat, Moscow (1970).
4. T. Kennett and H. Thode, Canad. J. Phys., 38, No. 7, 945 (1960).
5. P. Kuroda, Nature, 187, 36 (1960).
6. Yu. A. Shukolyukov and L. K. Levskii, Geochemistry and Cosmochemistry of Noble Gas Isotopes [in Russian], Atomizdat, Moscow (1972).
7. G. Bennett and O. Manuel, Geochim. et Cosmochim. Acta, 34, No. 5, 593 (1970).
8. P. Jeffery, Nature, 233, No. 5317, 260 (1971).
9. O. Manuel, Geochim. et Cosmochim. Acta, 31, 2413 (1967).

COOPERATION NOTES

The Conference of Specialists from COMECON Member Countries on "Research on critical heat loads in rod bundles under stationary and nonstationary heat-transfer conditions" was held March 30-April 2, 1976 in Moscow.

The participants considered the state of researches in the member countries performed in accordance with the previous working plan on this topic. Papers were read and discussed by each of the delegations, and the resulting suggestions were incorporated in an agreed collaboration plan for this topic for 1976-1980.

The participants also expressed various recommendations on improved coordination of researches under this plan.

The 22nd meeting of the working group on reactor science and technology and nuclear power, COMECON Standing Commission on the Peaceful Use of Atomic Energy, was held in Predeal (Rumania) April 6-9, 1976.

Reports were read by delegations from COMECON member countries on progress in researches on "Dissociating gases as coolants for fast reactors," together with suggestions for future collaboration. A working plan for scientific collaboration on this topic was discussed and ratified.

Draft proposals from the USSR delegation were discussed as regards organization of scientific collaboration on the design of a water — water reactor for a nuclear boiler; the participants discussed the technical specifications for the design and construction of test beds for equipment for use on such reactors, and also suggestions on collaboration in this area.

A working plan for collaboration was discussed and ratified for "Research on critical heat loads in rod bundles under stationary and nonstationary heat-transfer conditions." There were also discussions on the results on the seminar of COMECON member countries on the construction and operation of VVÉR reactor systems (German Democratic Republic; March 23-26, 1976), together with proposals for future collaboration.

Information was also reported on the Conference of COMECON Member Countries on "Computerized monitoring and control systems for reactor installations of VVÉR-440 and VVÉR-1000 types."

There was also a discussion on working plans for major aspects of "The design and commissioning of power stations with water — water reactors of output around 1000 MW," which is included in the agreed plan for multilateral integrated research by COMECON member countries for 1976-1980, especially in relation to the preparation of proposals for detailed performance of these researches on the agreed basis.

There was also a discussion on suggestions on the main lines and forms of collaboration between COMECON and the International Atomic Energy Agency.

The 11th meeting of the Coordination Council on Radiation Engineering and Technology, COMECON Standing Commission on the Peaceful Uses of Atomic Energy, was held April 13-16, 1976, in Bucharest. The participants included members of the Council and experts from Bulgaria, Hungary, the German Democratic Republic, Poland, Rumania, the USSR, and Czechoslovakia, as well as members of the COMECON Secretariat. The Council discussed various topics and ratified decisions.

1. A draft prepared by the USSR delegation was agreed on forecasts for the major lines of development in radiation technology up to 1990, and it was considered possible to use this as a basis for developing the forecasts on the basis of the comments and suggestions made during the discussions.

2. The USSR delegation presented a second draft of "Unified methods in technical dosimetry involving isotope γ-ray sources"; comments and suggestions from the delegations were discussed, and the Council considered it desirable to change the title to "Recommendations on methods for technical dosimetry in radiation equipment containing isotope γ-ray sources."

Translated from Atomnaya Énergiya, Vol. 41, No. 1, pp. 56-58, July, 1976.

The Council ratified the above draft as incorporating the corrections and additions made during the discussion, and directed it to the Commission with a request for it to be recommended for use in COMECON member countries.

3. Information presented by the Bulgarian delegation was discussed as regards suggestions for research on the migration of toxic components from PVC tubes.

Such researches are of some interest in the choice of materials for blood-transfusion systems, so the Council requested the Bulgarian delegation to extend these researches and to report the results at the next conference of Specialists on Radiation Sterilization of Materials and Components for Medical Purposes.

4. There was discussion and agreement on the following prepared by the COMECON Secretariat: "Proposals and considerations on the main lines and forms of collaboration between COMECON and the International Atomic Energy Agency for 1976-1980."

The Council ratified the recommendations of the Secretariat on these topics, together with a formulation of a program for collaboration between COMECON and the International Atomic Energy Agency for 1976-1980 on radiation engineering and technology.

5. The following information items were also discussed:

a) From the Polish delegation on preparations for the symposium of COMECON member countries on modification of polymers by irradiation, which is to be held in September 1977 in Poland, and also on a temporary international team on radiation sterilization of biomedical components (VMK-RS) set up in Poland;

b) from the USSR delegation on its actions on the plan laid down by the Committee on Radiation Technology;

c) from the COMECON Secretariat and the USSR delegation on revision of the working plan of the Scientific Council on Radiation Engineering and Technology for 1976-1980; the Council concluded from the list of completed or current applied scientific and technical researches in member countries on this topic that the following promising lines of multilateral collaboration should be explored as not yet being covered by the working plan: synthesis of complex compounds for various purposes by radiation-chemical means; modification of inorganic materials by radiation (semiconductors, glass, rock crystal, and so on); and radiation disinfection of raw materials for light industry (wool, leather, etc.).

6. It was considered to be desirable that the 12th meeting should discuss improving the work of the Coordination Committee on Collaboration in Radiation Technology.

7. Suggestions from the USSR delegation on revision of the working plan of the Scientific Council were adopted as regards the part concerning radiation sterilization of materials and components for medical purposes and also the stages and times for performing individual studies on this topic, and it was considered desirable to continue revising this working plan in radiation technology for 1976-1980, in particular by linking it with suggestions mentioned above on improving the work of the Coordination Committee in this area.

8. The COMECON Secretariat reported a suggestion from the Czechoslovak delegation that COMECON standards should be drawn up on topic 9.1.4: "Radiation technology," which is part of the standardization plan within the framework of the above Committee, and the Council ratified a draft agenda for the 12th Session, which is to be held in September 1976 in Hungary.

The 9th Meeting of the Coordination Committee Fast Reactor Technology, COMECON Standing Commission on the Peaceful Uses of Atomic Energy, was held April 20-23, 1976, in Sofia; the Council finally ratified working plans for collaboration on "Researches on fast power reactors" for 1976-1980.

The Council also considered progress in executing the decisions taken at the Conference of COMECON Member Specialists on Nuclear Data.

The participants also discussed the drafting of suggestions on the design of facilities for proving designs and equipment for fast reactors. A program on the design of reliable sodium — water steam generators was discussed and ratified. There was also a discussion on preparations for a conference of COMECON member countries on sodium technology in the German Democratic Republic (March, 1977). Suggestions were also discussed on the main lines and forms of collaboration between COMECON and the International Atomic Energy Agency for 1976-1980. Communications were also presented from several dele-

gations on progress made with decisions of previous sessions of the Council.

Ratified decisions and recommendations were made by the participants on all these agenda topics.

The Conference of COMECON Member Countries' Representatives (Bulgaria, Hungary, Rumania, USSR, and Czechoslovakia) was held April 26-29, 1976, in Usti na Labe, Czechoslovakia, which discussed topics related to the formation of a temporary international team on radiation sterilization of materials and components for medical purposes (VMK-RS), which in Czechoslovakia is based on a branch of the State Textile Industry Research Institute (at Veverska-Bitishka).

As there are strong arguments for extending collaboration between COMECON members in this area, the conference ratified a suggestion from Czechoslovak representatives to consider in the near future the creation of a coordination center for COMECON members for research in this area, which should be based on the above Institute and replace VMK-RS.

The Conference of COMECON Member Countries in Radiation Shielding and Radiation Technology was held May 3-7, 1976, in Moscow. There were participants from Bulgaria, Hungary, the GDR, Poland, Rumania, and Czechoslovakia, together with members of the COMECON Secretariat, the COMECON Standardization Institute, and the International Nuclear Instrumentation Organization "Interatominstrument."

The conference discussed and ratified drafts for COMECON standards: terms, definitions, and classification features for laboratory furniture for work with radioactive substances (tables, cupboards, dust covers, floorings, and benching), and also transportable packing systems for shipping radioactive substances.

The conference suggested that no COMECON standard should be drawn up for stools for use in laboratories for work with radioactive substances, since such stools are not specific to laboratories for that purpose. Stools for laboratories where operations are performed with radioactive substances should correspond to the general technical specifications for furniture presented in the appropriate standard.

The conference also discussed the second draft for a COMECON Standard for lead shielding window blocks, which was presented by the Bulgarian delegation, and it ratified the name, the introductory part of the standard, and the major standard dimensions for such windows. The final agreement on the project is intended for March 1977.

The conference also discussed the draft of a program for general standardization during 1976-1980 of various components used in radiation shielding, together with proposals from member countries. The ratified draft envisages the formulation of about 20 COMECON standards in this period. At the same time, suggestions were discussed on a standardization program for 1976-1980 for components used in radiation technology. The conference considered it desirable to discuss and ratify the details of this project within the framework of the Coordination Council on Radiation Technology.

The conference also discussed and ratified the following:

a) a draft plan for the operations of the COMECON Standing Commission on Peaceful Uses of Atomic Energy for 1977-1978 as regards radiation shielding and radiation technology, including a draft plan for definition of COMECON standards in 1977; and

b) a report on work done and results from the collaboration program of COMECON members in radiation shielding during 1971-1975.

The conference observed that much work had been done on standardizing radiation-shielding components in COMECON members within the framework of the COMECON Standing Commission in this period, which has involved the drafting of standardization documents and the organization of routine production of certain forms of component in several countries. The report presented conclusions and suggestions for further improvement of these studies. The agenda was ratified for the next Conference of COMECON Members, which is to be held in the first quarter of 1977.

During the conference, the following information was presented by the Interatominstrument representative:

There is scope for holding conferences and seminars on the production of nuclear instrumentation in COMECON member nations and on experience with such instrumentation at the two exhibitions of nuclear technology held each year by Interatominstrument, which include radiation-protection and radiation-technology items; and

b) on specialization in producing radiation-protection equipment within Interatominstrument. Proposals on division of labor have been received from several countries. When the proposals have been thoroughly discussed in 1976-1977, it is proposed to sign agreements on the division of responsibilities between COMECON members for such components within an agreed range.

Agreement on COMECON Standards for nuclear-technology equipment will very considerably facilitate an early decision on specialization and cooperation between the interested participants.

The 7th session of the Coordination Council on Water Treatment in Nuclear Power Stations, COMECON Standing Commission on the Peaceful Uses of Atomic Energy, was held in Dresden (GDR) May 4-6, 1976.

The Council received reports from delegations on their actions under the working collaboration plan for 1971-1975 on "Water handling, water treatment, and fuel-rod leakage tests in nuclear power stations," and it ratified preliminary suggestions on the main lines of research for the period up to 1990. Drafts of the plan for the work of the Commission were discussed and ratified as regards water treatment in nuclear power stations for 1977-1978, as well as the Working Plan for COMECON collaboration on this topic.

The participants discussed a report on water handling and water treatment for VVÉR reactors during 1973-1974; agreement was reached on instructions for the formulation of reports on past runs with VVÉR reactors, in particular, water handling and water treatment.

Suggestions were discussed and agreed on regarding research on the performance of electromagnetic filters for treating heat carriers in the first and second loops of nuclear power stations, particularly to eliminate corrosion products.

The meeting also considered suggestions on the main lines and forms of collaboration between COMECON and the International Atomic Energy Agency for 1976-1980.

There was a discussion and agreement on the Draft Program for the Third Symposium on "Water handling, water treatment, and fuel-rod leakage monitoring at nuclear power stations," which is to be held November 2-5, 1976 in Neubrandenburg.

The 12th meeting of the Council of the International Nuclear Instrumentation Organization, Interatominstrument, was held may 11-15, 1976 in Warsaw, with K. Vancl as chairman, the General Director of the Tesla Electronics and Light-Current Engineering Organization.

The conference heard a report on the work performed by the organization in 1975 on "Programs for Interatominstrument for 1974-1980," and also action taken on Council decisions; it also considered a report on the achievement of the financial plan for 1975, a survey of the financial and economic activities, and a draft financial plan for 1977.

The Council took appropriate decisions on these topics, in particular as regards the future development of the direct economic activity of the organization and its subdivisions on support to nuclear technology in Bulgaria, Poland, and the USSR. There was a discussion on the economics of the proposed Interatominstrument plant for producing nuclear-physics equipment for nuclear power stations, and the Council agreed on further measures to be taken.

There were also discussions and decisions on Interatominstrument suggestions on division of labor in the production of certain nuclear items, and the Council undertook to draft an agreement on the basis of the recommendations made by the Executive Council of COMECON.

Surveys were also presented on coordination of internal trade in 1976-1980, with suggestions on joint planning within the Interatominstrument framework, and reports were received from directors of Interatominstrument branches, together with information on the coordination of research and design studies for semiconductor detectors.

In accordance with the Articles of Agreement of the organization, the Council appointed I. Traikov (Bulgaria) as Deputy Commercial Director, and V. Sinnitsyn (USSR) Deputy Technical Director.

The Council also ratified the agenda for the 13th meeting, which will be held November 16-20, 1976.

The meeting generated a friendly atmosphere, with complete mutual understanding.

39th SESSION OF THE SCIENTIFIC COUNCIL OF THE ALL-UNION INSTITUTE OF NUCLEAR RESEARCH

V. A. Biryukov

The 39th session of the Scientific Council of the All-Union Institute of Nuclear Research took place January 13-16, 1976 in Dubna. Opening the session, the director of the Institute, N. N. Bogolyubov, reported on the work of the management in fulfilling the resolutions of the Scientific Council. The director of laboratories gave reports on new scientific investigations and procedural developments achieved in 1975.

In the Theoretical Physics Laboratory (Report of D. I. Blokhintsev), during the investigation of power self-similar asymptotics in the interaction of particles with large momentum transfers, the energy and angular dependences of the differential scattering cross sections at large angles have been found. The conclusions from these studies recently have received experimental verification. A number of the low-energy characteristics of pions and kaons have been described by methods of nonlinear kiral and nonlocal field theory. The results are found to be in excellent agreement with experimental data. The feasibility was suggested and studied for describing the properties of the recently discovered vector mesons within the framework of color symmetry and the three-triplet quark model of N. N. Bogolyubov.

In connection with the study of the states of nuclei formed during neutron capture, the role of small quasiparticle components in the wave functions of highly excited states has been defined. A new method, in principle, has been suggested for calculating neutron force functions, and the behavior of S-wave force functions in the region of its minimum has been explained.

Investigations of the collective movements of a nuclear substance have been continued within the scope of the many-body theory. Interesting results were obtained in studies of the magnetic dipole and quadrupole excitations of nuclei, and also the theory of nuclear transformation and α decay. A method has been developed for regenerating the interaction potential of particles with nuclei, with respect to data concerning the energies of quasibound levels. The form-factors of nuclei in nucleon transfer reactions have been calculated. Corollaries have been produced and discussed for models describing dielectric-superconductor systems as the ferroelectric type and the binary solution type. The approach to the investigation of the model systems has been extended to a system with exchange forces and with Coulomb interaction.

Scientists of the High Energy Laboratories (Report of A. M. Baldin) have participated in conjunction with American physicists in an experiment to determine the elastic and inelastic pd scattering over the range of energies 50-400 GeV on the accelerator in Batavia. Processing of the measurement results has been completed. Work has been carried out within the scope of the Soviet-American scientific collaboration. By means of a 2-m propane chamber, irradiated in the Serpukhov accelerator, the coherent interaction of pions with carbon nuclei has been studied, and the mechanisms of charge exchange in pion — nucleon interactions with a momentum of 40 GeV/sec. Analysis of the inclusive single-particle spectra of secondary particles has been carried out on the basis of 7600 events in the Lyudmila 2-m hydrogen chamber, irradiated in a beam of separated antiprotons with a momentum of 22.4 GeV/sec. Elastic dd scattering and αp scattering were investigated at small angles, over the range of energies 6-11 GeV in the experiments on the synchrophasotron. Correlations were studied in processes of the direct disintegration of a deuteron in dp collisions with a momentum of 3.3 GeV/sec. Investigations of the cumulative formation of baryon systems — protons, deuterons, and tritons — by different nuclei have been continued.

In the laboratory, an assembly of physical apparatus has been set up for experiments on the accelerator in Batavia, where alignment of part of the plant already has been carried out, including the building in Dubna of a helium jet target. New drift and proportional chambers have been tested. Nonmetallic cryogenic targets

Translated from Atomnaya Énergiya, Vol. 41, No. 1, pp. 59-61, July, 1976.

of different types have been developed and made. A complex modernization of the synchrophasotron has been completed, as a result of which the intensity of the accelerated beams has been increased up to proton values of $1.5 \cdot 10^{12}$, $2.5 \cdot 10^{11}$ for deuterons and for α particles, 10^9 particles per cycle. A cryogenic source of polarized hydrogen and deuterium atoms has been developed.

In the Laboratory for Nuclear Problems (Report of V. P. Dzhelepov), experiments have been completed on the synchrocyclotron for a search for rare decays of $\mu^+ \rightarrow e^+e^+e^-$ and $\pi^+ \rightarrow e^+e^+e^-\nu_e$, carried out in order to verify the conclusions of the theory of weak interactions. An original procedure using cylindrical spark spectrometers has enabled the relative probability of meson decays to be estimated at the scale level of 10^{-9}. In the high-pressure helium streamer chamber, the elastic scattering of positively and negatively charge α pions by ^{4}He nuclei has been investigated in the region of the first baryon resonance, and for the first time detailed data were obtained on the elastic scattering of pions by ^{3}He nuclei in the energy range of 68-208 MeV. In studying the $\pi^-p \rightarrow e^+e^-n$ process, the pion and isovector nucleon form-factors were determined for five values of the time-like transfer of a four-dimensional momentum. One of the most accurate estimates of the radius of the pion has been made: $\langle r_\pi^2 \rangle^{1/2} = 0.75 \pm 0.06$ fermi.

In experiments on the beam of positively charged particles of the Serpukhov accelerator, with a momentum of 45 GeV/sec, polarizations in pp, π^+p, and K^+p scattering were measured, and also the spin rotation parameter in elastic pp scattering. Work has been undertaken by scientists of the All-Union Institute of Nuclear Research, together with specialists of the Institute of High-Energy Physics (IFVÉ), the Institute of Theoretical and Experimental Physics (ITÉF) and the institute at Saclay (France). A search has been completed for metastable particles with lifetimes in the range from 5 msec to 1 day, by recording the delayed radiation from lead screens irradiated by protons with energies of 60-70 GeV. The effect of delayed radiation was not observed. The upper limit of the creation cross section of long-lived particles has been estimated at a value of 10^{-34}-10^{-33} cm^2.

Polarization experiments have commenced on the synchrocyclotron by means of a new type of frozen polarized target, originated in the laboratory. A hydrogen polarization of about 90% is guaranteed in the target. The development of a procedure for self-shunting streamer chambers has led to the development of a hydrogen streamer chamber, in which tracks of particles suitable for photographing have been produced. All the systems of the U-120M accelerator have been manufactured and, after complex experiments in the All-Union Institute of Nuclear Research, will be installed in the Institute of Nuclear Physics of the Czechoslovakian Academy of Sciences (Rzhezh).

A cycle of investigations has been completed on the synthesis and study of the properties of new isotopes of the transfermium elements with Z-100, 102, 103, 104, and 105. Experiments have been carried out on the U-300 cyclotron in the Nuclear Reactions Laboratory (Report of G. N. Flerov), in which a method of synthesis developed here, using targets of stable elements in the vicinity of lead, was used. The results of the investigations have permitted a new classification to be given for the periods of spontaneous fission and α decay of heavy nuclei. During the irradiation of ^{209}Bi with accelerated ions of ^{54}Cr, a spontaneous fission was recorded with a half-life of ~2 msec. The results of numerous control experiments provided the authors with grounds to assume that they had observed the synthesis and decay of the isotope $^{261}107$ (80% α decay with $T_{1/2} \sim 2$ msec and 20% spontaneous fission with $T_{1/2} \sim 0.01$ sec). In the laboratory, work was continued on the search for superheavy elements in meteorites, using high-sensitivity methods — up to 10^{-16} wt. %. By means of an electromagnetic mass-separator, two new proton emitters have been obtained in the region of the rare-earth elements Sm-133 and Sm-135, and their radioactive decay has been studied. The results of a joint Dubna — Orse (France) experiment have been processed, in which reactions in heavy ions with the formation of a compound nucleus were studied.

Specialists of the Institute have worked out a procedure for preparing nuclear filters from plastic materials, which are capable of functioning in chemically corrosive media and at high temperatures. An investigation has been carried out in a beam of heavy ions, into the radiation swelling of samples of nickel and stainless steel. A beam of ^{48}Ca ions has been accelerated on the U-300 accelerator. Its use is most promising for the synthesis of superheavy elements with the minimum number of neutrons in the nucleus. Work has continued on the construction of a 4-m cyclotron for accelerating heavy ions.

On the pulsed reactor in the Neutron Physics Laboratory (Report of J. M. Frank), the magnetic moments have been measured of highly-excited compound-state nuclei of terbium and holmium by the method of resonance energy shift, due to a superfine magnetic interaction in nuclear targets oriented at ultralow temperatures. In accordance with statistical theory, the magnetic moments found for the series of rare-earth nuclei have revealed a significant fluctuation of their average values in comparison with the

expected values. By transmitting a polarized beam of electrons through a polarized target of metallic terbium, the spins of 66 resonances and the spin dependence of the averaged cross sections of terbium were determined. Despite the high accuracy of the measurements achieved by the improved procedure, no spin dependence of the force function was observed. In a joint project, scientists of the Joint Institute of Nuclear Research and the Institute of Atomic Energy (Moscow) have studied the storage of ultracold neutrons in copper and glass vessels. It has been established that their lifetime in glass vessels is independent of the temperature of the reflecting walls over the range from —100 to +300°C. Investigations in copper vessels have confirmed the previously observed anomalously large absorption. This anomaly is not associated with the usual inelastic scattering. Investigations of condensed media by means of neutrons produced a further development. Measurements were undertaken of paramagnetic scattering by metallic compounds of praesodymium, inelastic scattering of neutrons by methane molecules, and the diffraction of neutrons by iron oxide by the action of a pulsed magnetic field.

A spectrometer for scattering neutrons at small angles by the time-of-flight method has been tested. By means of it, a systematic study has been started of the structure of complex compounds and biological items.

The systems of the IBR-30 reactor and the LUÉ-40 injector have been improved, and the control and shielding system of the reactor has been improved. The power of the reactor in the booster mode has been increased from 7 to 15 kW by means of a new injector target.

In the Computer Technology and Automation Laboratory (report of M. G. Meshcheryankov) work has continued on the development of the measurement computer complex of the Joint Institute of Nuclear Research. Fitting out of the BÉSM-6 computer has been completed with eight memories on type ES-5052 magnetic disks with plug-in packs, and two BESM-4 machines have been completed by type ES-5012 magnetic tapes. In the BÉSM-6, the new Dubna-75 functional system has been brought into operation, which enables type ES-5012 magnetrons to be used, and also magnetic disks and Videoton-340 displays. The system currently guarantees a 95-98% loading of the BÉSM-6 central processor. The reproducibility of the CDC computer system has been increased by 20-30% due to the development of the CDC-6200 computer to the level of the CDC-6400 and the introduction of a new operating system. Conversion from the BÉSM-6 to the CDC-6400 program system for the processing of film data has been completed.

Development has been completed and experimental operation has started of graphical display systems based on the OSK-1 and OSK-2 point displays, and graphical displays on a memory electron-beam tube. Test samples of a BPS-3U-M2 scanning-measurement projector, developed in the Joint Institute for Nuclear Research, have been manufactured. The projector has been recommended for series industrial production.

In work on the development of methods of applied computations, the inverse problem of the theory of scattering has been solved, solutions of problems of molecular physics and the theory of the nucleus have been investigated, and also nonlinear problems associated with the acceleration of relativistic electron rings. A group of physicists from the laboratory have carried out a cycle of investigations on the synchrophasotron into the spectra of secondary charged particles in proton and deuteron collisions with nuclei of hydrogen, deuterium and carbon.

The Division of New Methods of Acceleration (Report of V. P. Sarantsov) in work on the alignment of a heavy ion accelerator (UTI), designed on the basis of the collective method of acceleration, has achieved beam capture on an equilibrium orbit with an efficiency of 50-70%. Investigations have been started with the first compression stage. A multichannel system for measuring the electrical parameters of the UTI has been introduced into an experimental operating cycle. The system operates on-line with a computer and provides in each cycle of operation, the measurement of the 36 parameters of the SILUND, the adhesator, and its multistage magnetic system.

Reconstruction of the LIU-3000 electron accelerator has been completed on models of the collective accelerator; at the exit of the accelerator, a beam of electrons with a diameter of 2 cm and a current of 250 A (1.5-MeV energy) has been obtained. The assembly of the first compression stage of the ring, with the parameters 30 kV, 30 kA and a pulse frequency of 1 Hz, has been constructed.

The cryogenic assembly, based on a large-scale helium liquifier with a refrigerating capacity of 250 W, has been started up. It will enable a closed refrigeration cycle to be achieved for the thermostatically controlled section of the ring at the temperature of liquid helium. The technology of sputtering of niobium — titanium coatings has been developed, with a controlled composition of the components and in resonators with this covering, a figure-of-merit of $5 \cdot 10^7$ at a frequency of 1.4 GHz has been achieved.

The Vice-Director of the Institute, K. Lanius, delivered a report on the International Scientific Collaboration of the Joint Institute for Nuclear Research with the research organizations of different countries. In 1975, together with the national physical centers of the associate countries of the Institute, the laboratories carried out investigations on 167 themes of the project. In connection with carrying out the joint tasks and in order to solve other problems, 1026 specialists from these countries arrived in the Institute and 226 specialists from other countries stayed for a time in Dubna in order to discuss scientific problems and to participate in the conferences. The Institute sent 600 of its own staff to the scientific centers of different countries in order to participate in joint tasks, and also in conferences, meetings, etc. Eleven scholarship students from five countries worked in the Institute.

During the year, the Institute organized 42 scientific and scientific-organizational meetings, including seven large-scale conferences and symposia and three schools. An International School of Physicists of OIYaI — CERN was held in Alushta, the Fifth International Symposium on High-Energy Physics was held in Warsaw, the Eighth International Symposium on Nuclear Electronics and an exhibition of electronic instruments was held in Dubna, etc.

The management presented for discussion, a plan for scientific meetings in 1976. The largest-scale undertaking of the Institute will be an International Conference on selected problems of the structure of the nucleus, which is being organized under the auspices of IYuPAP in June, in Dubna. In September, in Dubna, the Second Symposium on Collective Accelerators will be held, and in June a conference on the modular system of programs for the processing of experimental data will be held. The Institute is proposing to conduct 23 working conferences on the urgent problems of collaboration.

At the session of the Scientific Council, the work of the Institute during the Ninth Five-Year Plan (1971-1975) was summed up. The directions of the laboratories addressed brief reviews on the achievements of scientific research. In the concluding address, the Director of the Joint Institute of Nuclear Research, N. N. Bogolyubov, reported that a broad program of investigations had been achieved by the scientists of the Institute in the field of theoretical physics, the physics of elementary particles and the atomic nucleus, the physics of heavy ions, and also the physics of neutrons and condensed media. A large cycle of experiments had been carried out successfully on the 76-GeV Serpukhov accelerator. A base had been created in the Institute for investigations into the method of collective acceleration. Many tasks were associated with the improvement and reconstruction of the synchrophasotron and the synchrocyclotron, and also with the building of the U-200P cyclotron and the start of work on the U-400 facility. The planned complex of work on the building of the IBR-2 high-power pulsed reactor has been mainly achieved. The U-120M isochronous cyclotron has been developed and manufactured. The measurement-computational complex of the Institute has been expanded significantly, due to the addition of different classes of computers — from high-power to minicomputers.

The works of the scientists were honored with national prizes of the associate countries of the Institutes. Including the Soviet scientist-workers of the Joint Institute for Nuclear Research, four State prizes were awarded: for the work cycle "IBR Research reactor and the IBR reactor with injector" (1971); for the discovery and investigation of the shadow effect in nuclear reactions on monocrystals (1972); for the work cycle "Photocreation of pi mesons by nucleons" (1973); and for the work cycle on the synthesis and study of the properties of atomic nuclei near the limit of nuclear stability (1975). The State Committee on Inventions and Discoveries for the Council of Ministers of the USSR recorded 11 scientific discoveries made in the Joint Institute. The international collective body of the Joint Institute of Nuclear Research in 1972, for scientific achievements and service in the training of personnel specialists and the development of research centers in the Union Republics of the USSR, was rewarded with the Jubilee Honorable Decoration in honor of the 50th anniversary of the formation of the USSR.

SEMINAR ON THE PROSPECTS FOR DEVELOPMENT OF SECONDARY POWER SOURCES IN NUCLEAR INSTRUMENT CONSTRUCTION

A. F. Belov

On 14-17 March, 1976, at the Exhibition of Achievements of the National Economy of the USSR, a seminar was held by the All-Union Scientific Research Institute of Instrument Construction (SNIIP) — "The State and Prospects for the Development of Secondary Power Supply Sources in Nuclear Instrument Construction."

The role of secondary power supply sources is universally known. A characteristic feature of nuclear instrument construction is the use, besides low-voltage power sources of 300 V and below, of the high-voltage sources necessary for powering detector devices.

The All-Union Scientific-Research Institute of Instrument Construction, as the organizer of the seminar, presented nine reports with a description of unified sets of power units, which at present are familar to or are already used by factories. Structurally, high-voltage secondary power supply sources have been used in the well-known systems "Vishnya," "Chereshnya" and UTK. Their application for building into detector units was also discussed. These units find a wide application in conjunction with counters, photomultipliers and other detectors, remote from one another and from the power supply systems (Table 1).

TABLE 1. Parameters of High-Voltage Power Supply Sources

Type of detector	Structural use	Type of unit	Output voltage, V	Polarity	Lead current, mA	Stability from mains variation %	Output resistance, kΩ	Stability from temp. change, % per 10°C	Time drift, % / day	Voltage pulsations, mV	Primary power supply V
Photomultiplier + detector in the counting and spectrometric modes	"Vishnya"	BNV 3-02	2000—4000	Negative	25	0,1	1	0,3	0,3	400	Mains
		BNV 2-07	2000	Positive	10	0,05	1,2	0,15	0,2	20	»
		BNV 3-09	800—2500	Positive or negative	2,5	0,05	10	0,3	0,3	75	»
	"Chereshnya"	BNV -30	200—4000	Positive or negative	3	0,03	0,6	0,1	0,1	20	+24
		BNV 2-95	800—2500		2,5	0,05	10	0,3	0,3	50	Mains
	Built-in	BNV -49	800—1600	Positive	0,1	0,3	0,3	0,3	1	100	+12
		BNV -50	1250—2500	»	0,1	0,3	0,7	0,3	1	100	+12
		BNV -51	800—1600	Negative	0,1	0,3	0,3	0,3	1	100	+12
		BNV -52	1250—2500	»	0,1	0,3	0,7	0,3	1	100	+12
Corona counters	Built-in	BNV -50	1250—2500	Positive	0,1	0,3	0,7	0,3	1	100	+12
Geiger counter	Built-in	BNV -47	300—600	»	0,1	5	0,5	0,3	1	100	+12
		BNV -48	500—1000	»	0,1	5	2	0,3	1	100	+12
Ionization chambers, pulsed fission chambers	"Vishnya"	BNV 2-19	400—550	»	10	3	2,5	1	0,3	10	+27
		BNV 2-20	50—600	Negative	2,5	3	2,5	1	0,3	10	+27
	Built-in	BNV -51	800—1600	»	0,1	0,3	0,3	0,3	1	100	+24
	UTK	BNV -26	250	Positive	1	0,1	20	2	1	1	+24
		BNV -26	100—400	Negative	0,01	0,1	300	2	1	1	+24
		BNV -81	250	Positive	1	0,1	20	2	1	1	+24
		BNV -81	100—400	Negative	0,01	0,1	300	2	1	1	+24
Semiconductor diode (PPD)	"Vishnya"	BNV 3-06	50—2500	Positive or negative	0,001	0,1	Not regulated	0,3	0,3	5	Mains
	Chereshnya	BNV 2-97	50—2500	Positive or negative	0,01	0,1	The same	0,3	0,3	5	»
		BNV -31	100—4000		0,01	0,3	2	0,1	3	5	±12

Translated from Atomnaya Énergiya, Vol. 41, No. 1, pp. 61-63, July, 1976.

TABLE 2. Systems of Unified Low-Voltage General-Purpose Secondary Power Supply Sources

Type	Structural use	Output voltage, V	Lead current, A	Pulse voltage, mV	Stability, % of change of mains voltage	Stability, % of change of lead current	Specific output power, 10^3, W/m^3
BNN-150	"Chereshnya"	6	15	2	0,01	0,2	
		6	10	2	0,01	0,2	
BNN-153	UTK	24	3	2	0,01	0,1	18
		24	3	2	0,01	0,1	
BNN-151	"Chereshnya"	6	15	2	0,01	0,2	
		6	10	2	0,01	0,2	
		12	3	2	0,01	0,1	
BNN-154	UTK	12	3	2	0,01	0,1	18
		24	1,5	2	0,01	0,1	
		24	1,5	2	0,01	0,1	
BNN-152	"Chereshnya"	6	10	2	0,01	0,2	
		6	10	2	0,01	0,2	
BNN-156	UTK	6	10	2	0,01	0,2	18
		6	10	2	0,01	0,2	
BNN-2-90	"Chereshnya"	6	10	2	0,05	0,3	
		6	6	2	0,05	0,3	
		24	3	2	0,01	0,1	10
		24	3	2	0,01	0,1	
BNN-2-90-01	"Chereshnya"	6	10	2	0,05	0,3	
		6	6	2	0,05	0,3	
		12	2	2	0,01	0,1	
		12	2	2	0,01	0,1	10
		24	1,5	2	0,01	0,1	
		24	1,5	2	0,01	0,1	
BNN-2-92	"Chereshnya"	5	4	1	0,05	0,3	
		5	4	1	0,05	0,3	
		5	7	1	0,05	0,3	
		5	7	1	0,05	0,3	10
		12	0,7	1	0,01	0,1	
		12	0,7	1	0,01	0,1	
BNN-157	"Chereshnya"	5	3	2	0,01	0,1	
		12	0,5	1	0,01	0,1	13
		36	3	2	0,01	0,1	
BNN-159	UTK	6	0,5	1	0,01	0,1	
		12	0,5	1	0,01	0,1	
		12	0,5	1	0,01	0,1	5
		24	0,5	1	0,01	0,1	
BNN-158	UTK	6	1×3	1	0,01	0,3	
		6	1	1	0,01	0,3	
		12	0,5	1	0,01	0,1	
		12	0,5	1	0,01	0,1	5
		24	0,25	1	0,01	0,1	
		24	0,25	1	0,01	0,1	

In low-voltage sources of the third generation, devices which provide a power supply for the electronic units constructed according to the SAMAS and Vektor systems are being used (Table 2). Secondary power supply sources are calculated on a current of up to 40 A through a single bus-bar or 10-15 A with a set of different power supply bus-bars.

An interesting report was given by the representatives of the B. P. Konstantinov Institute of Nuclear Physics, Leningrad, on the development of a universal laboratory power supply source with programmed control. The power supply source is constructed on the modular type and has the possibility of parallel connection of several modules to a single load, which, undoubtedly, is a great achievement.

V. V. Lantsov, the representative of the All-Union Research Institute of Scientific Instruments, mentioned in his report that in future years a number of power supply devices of increased stability will be constructed and introduced into series production, which will guarantee the requirement of the institutes for such units.

In the report by O. I. Ogurtsev et al., "Voltage Stabilizers in Hybrid-Type Performance," methods were described for designing stabilizers and the results of investigations of their parameters. It can be said now, that such stabilizers find a wide application for supplying power to devices with particularly high demands on the power supply voltages, as they have small dimensions (24 × 36 × 5 mm) with a current of 400 mA, a potential of 6V, and high stability parameters. Their instability does not exceed 0.001% of all destabilizing factors, and therefore they can be installed immediately near the power consumer, excluding external pickup in the coupling circuit.

The seminar took place with high activity and attention on the part of the audience. The specialists received a large volume of information about the commercially used power supply devices for nuclear instrument construction.

CONFERENCE OF EXPERTS OF THE INTERNATIONAL ATOMIC ENERGY AGENCY (IAEA) ON THE TREATMENT OF RADIOACTIVE WASTES

M. K. Pimenov

At the conference, held on December 8-12, 1975 in Vienna (Austria), the following document was discussed: "Factors determining the choice of region for the prolonged storage or burial of consolidated, highly radioactive and α-active wastes in geological formations." The document was prepared on the instructions of the IAEA secretariat by a group of consultants.

Twenty experts from Belgium, Canada, Czechoslovakia, France, Federal German Republic, USA, USSR, Great Britain, India, Japan, and Switzerland and other countries and representatives of international organizations participated in the conference.

The principal source of highly radioactive wastes are the fission products separated from uranium and plutonium during chemical reprocessing of irradiated nuclear fuel. Plutonium and uranium, during reprocessing, are not recovered completely and therefore traces of them, and also of other α-emitting transuranic elements, remain in the wastes and make them also α-active. This entails the necessity for isolating these wastes from the biosphere for a prolonged time (up to hundreds of thousands of years).

The final removal of the radioactive wastes and, in the first place, of highly active and α-active wastes, is a complicated and complex problem. The solution of the problem of their storage is the immediate problem standing today before nuclear science and technology.

In recent years, a number of countries have studied the possibility of using geological formations for the long-term storage of radioactive wastes, resulting from two main reasons:

Geological formations have existed in protogenic form for a very long time, tens of millions of years, and therefore, the probability is large that some of them will exist for an even longer time in the future.

Geological formations exist, in which filtration of underground water is absent or is negligibly small. By thorough investigations, sections could be found where the circulation of underground water is completely excluded.

Consequently, correctly chosen geological formations, almost without inspection and monitoring, could guarantee the complete isolation of buried radioactive wastes during the decay time of the isotopes to permissible safety levels. The latter requirement can be met also by the use of deep water-bearing levels in zones with a stagnated cycle, where the flow-rate of the underground water either is equal to zero or is very small.

In the document discussed, different types of geological formations, which are recommended for study, are considered, and also the complex of geological and hydrogeological investigations in order to confirm their suitability. Additionally, other factors were discussed — ecological, economical, and social aspects, potential resources, transportation of wastes, previously exhausted mineworkings, etc.

Basic criteria have been formulated, to which the formations which are suitable for storage or burial should conform. However, the majority of the criteria in the text of the document were of a qualitative nature and required considered efforts of the experts from a number of countries (USSR, France, Great Britain, USA, etc.) for their definition and to work out approved quantitative values (thickness, horizontal spread, permissible values of the porosity of the rock formation, strength and permeability of the overburden and underlying rocks, etc.).

Translated from Atomnaya Énergiya, Vol. 41, No. 1, pp. 64-65, July, 1976.

The document, discussed in its final approved form, should make possible competent elements for assessing the suitability of geological formations for the reliable storage or burial of consolidated highly active and α-active wastes.

Depending on the origin, three arbitrary groups of geological formations are considered: chemogenic, sedimentary, and volcanic and metamorphic. According to the degree of conformity of the rock to the basic criteria of suitability, they may be represented in the following way: chemogenic rocks: rock salt, anhydrites, gypsums, potassium salts; sedimentary rocks: argillaceous sedimentary deposits, limestones, sandstones; volcanic and metamorphic rocks: granites, basalts, tuffs, gneisses and aspidic-shales.

But although chemogenic rocks also are sedimentary, in view of the special importance of one of the members of this group – rock salt – they are distinguished separately.

Each specifically chosen geological formation which conforms to the basic criteria should be investigated in detail by a special program and procedure as, in consequence of the complexity of geology, it is unique.

The USSR experts at the conference said that, e.g., for salt formations the Council for Mutual Economic Aid (CMEA), within the scope of the Permanent Commission on the Peaceful Uses of Atomic Energy, has worked out and approved "A Procedure for investigating the foundation of health-hydrogeological and radiation safety of burial of radioactive wastes in salt formations," and the decision was taken to include this procedure in the literature references to the document being considered. The term "storage" used in the document implies such distribution of wastes which will permit, in the case of necessity, their recovery (removal) after the lapse of a certain time. As applied to geological formations, it is assumed that storage will be accomplished either in previously worked-out mines or in specially created cavities. The term "burial" signifies operations to dispose of the wastes without consideration of the possibility of their future recovery. Burial does not require a constantly operating and guaranteed service, e.g., refrigeration, observation, repair, etc. In other words, burial can take place only in situations where an assurance can be guaranteed that, in the absence of constant monitoring on the part of human beings, the radioisotopes contained in the wastes could never reach the biosphere in concentrations which exceed the safety standards of radiation exposure for separate individuals or for groups of the population.

Hence, it follows that the solution of the problem of safe burial of highly active and α-active wastes, at least during the next 10–20 years, obviously must be based on the use of geological formations, the integrity of which can be predicted to hundreds of thousands of years. Such long periods are stipulated by the presence in the wastes of α-active elements, e.g., ^{239}Pu, with a half-life of 24,000 years. If these elements were to be removed from the wastes, then the remaining fission products would represent a hazard only during a few hundreds of years which, in its turn, would permit the choice of geological formations suitable for the safe burial of wastes to be so much simplified.

In taking account of the long periods of burial of wastes, the conference experts posed the problem of studying the question of marking the storage and burial sites of radioactive wastes, the reliability of which must be comparable with the periods of burial.

The IAEA experts discussed and approved all the changes, refinements and additions to the document being considered. The conference made a request to the Secretariat to complete the work of correcting the document and after this, to distribute it for final approval in the countries concerned.

The conference confirmed that, from the point of view of the IAEA, and also from the point of view of the countries represented by the experts, there is a clear understanding of the necessity for the speediest solution to the problem of the safe removal of highly active and α-active wastes.

THE SECOND SESSION OF THE SOVIET — AMERICAN COORDINATION COMMISSION ON FAST REACTORS

V. B. Lytkin and E. F. Arifmetchikov

The Second Session of the Joint Soviet — American Coordination Commission for cooperation in the field of fast breeder reactors was held November 12-14, 1975 in Washington.

At the session, the results of cooperation since the time of the first session (September 1974, in Moscow) were given and the program in 1976-1977 was worked out.

During the period between the sessions, two joint seminars had taken place: on steam generators for fast reactors (Los Angeles, December 1974), and on the experience and problems of construction and operation of these reactors (Obninsk, June 1975), at which an exchange took place of results of calculations of the breeding factor of a standard reactor and data on the various physics aspects.

The program for Soviet — American Cooperation on fast reactors with sodium coolant in 1976-1977 provides for the organization of bilateral seminars on the most important technological problems, such as the reliable operation of the sodium — water type of steam generators, the strength properties of fuel element cladding materials, and also on problems of physics. An exchange of samples of the steam generator and intermediate heat exchanger tubes, and fuel element claddings has been proposed.

At the session, the principal aspects of the American program of work on fast reactors and the state of its achievement at the present time were recounted. As the most important constituents of the program may be named operating experience, physics, fuel and materials, safety, and components.

Design, Construction and Operation of Fast Reactors. The only functional reactor, EBR-II, of the National Reactor Testing Station in Idaho, continues to be used for radiation investigations of fuel and structural materials. The load factor in 1975 amounted to 64%. Work on the construction of the FFTF reactor has reached 48% (construction — 90%, assembly of plant — 32%, electrical assembly — 30%, and installation of instruments — 13%). Almost all the plant has been delivered to the site, 70% has passed functional tests, and 60% has passed life tests. At the beginning of 1976, it is proposed to start testing of the first circuit with nitrogen for leak-tightness.

TABLE 1. Design Fuel Characteristics

Characteristic	Oxide, current	Oxide, improved	Carbides (nitrides), improved
Diam. of fuel element, mm	5,84	6,35—7,60	7,85—9,40
Tablet density, %	90	95	various
Cladding material	stainless steel 316	stainless steel 316, improved	
Thickness of cladding, mm	0,38	0,25—0,38	0,38—0,51
Maximum depth of burnup, MW·day/ton	80 000	150 000	150 000
Doubling time, yr	30	10—15	10—15

Translated from Atomnaya Énergiya, Vol. 41, No. 1, pp. 65-67, July, 1976.

TABLE 2. Material Requirements for the Cladding of Fuel Elements and Fuel Assemblies

Characteristic	Stainless steel 316, current	Improved alloy
Swelling, %	18 with an integrated flux of $2.5 \cdot 10^{23}$ neutrons /cm^2	5 with specified integrated flux $2 \cdot 10^{-7}$
Radiation creep (105 kg/cm^2, 650°C), mm/mm/h	$6,2 \cdot 10^{-7}$	
Tensile strength on stretching (long-term stability: tests at 20,000 h and 650°C) kg/mm^2	13	32

An administrative structure has been drawn up for controlling the CRBRP reactor project at Clinch River. The principal contractor for the reactor installation is Westinghouse Electric, the subcontractors for the steam power plant are General Electric and Rockwell International, and for the architectural-design — Berns and Rowe, for maintenance construction — Stone and Webster Engineering. The draft plan of the reactor project was approved in August 1974. The total cost of the already concluded contracts amounts to $115 million, of which on the main plant are: reactor vessel — 13.1; main circulating pumps — 34.9; protective casing of the reactor — 24.4; safety and control instruments — 9.0; and the turbogenerator — 16.7. A contract has been concluded with Atomics International for the design and manufacture of the steam generators. It is expected that testing of them will be started in 1977. In the autumn of 1976, it is proposed to start additional work on the floor. Constructional work will be expanded to full scale in 1977, criticality is planned to be achieved in 1982 and startup in 1983, after which will follow a five-year demonstration period.

The resolution to construct a facility for testing the components of the PCTF is a verification of the concept associated with the renunciation of the gradual increase of power of the nuclear power stations in service with fast reactors. Preliminary draft planning of the facility started at the Structural Center for Liquid Metals (LMEC) in 1974. It is intended in the first place for testing steam generator modules with a capacity of 300 MW (th.), but later its task will be extended. Installation of the PCTF is expected in October 1977 and it will be completed in November 1981. In this case, testing of components could be started in 1982. It had been previously intended to bring into operation several demonstration fast reactors in order to substantiate the type and develop the design of the future commercial reactor. Now, it is proposed to concentrate efforts on the testing of components for a "precommercial" nuclear power station with a capacity of 1000-1500 MW (el.), which it is contemplated to build after the Clinch River reactor. This nuclear power station is the next important element of the fast reactor program. In September 1975, contracts were concluded for a draft design with the firm of General Electric, Rockwell International, Westinghouse Electric, and for construction, with Bechtel, Berns and Rowe, and Stone and Webster Engineering. The contracts are being subsidized jointly by ERDA and the Electric Power Generation Institute, and the plans should be ready after 30 months.

The "precommercial" nuclear power station with NCBR may comprise separate units, which will be modernized in a commercial version. It is proposed that NCBR can be installed at the end of the 1980's, opening the route to commercial operations by the sale of fast reactors.

Reactor Physics. Based on calculations on the fast reactor program, experiments were undertaken on the critical assemblies ZPR-9 and ZPPR in order to determine the critical mass, the void sodium coefficient and the Doppler coefficient, measurements of the neutron flux distributions, the effects of heterogeneity and the interference of the control rods. At the same time, work was continued on the refinement of nuclear data and the improvement of computational methods. At present, active zones are being studied, the configurations of which correspond to gas-cooled fast reactors. Later, active zones with carbide and nitride fuel will be modelled on them. The ZPPR is being reconstructed and the diameter of the assembly has been increased from 300 to 420 cm in order that in future it will be possible to simulate the active zones of large fast reactors, including the screens and shielding. At present, assemblies of the CRBRP reactor are being studied on ZPPR, which correspond to its initial and transient states.

TABLE 3. Characteristics of Versions of the Steam Generator

Characteristic	"High-temperature"	"Low-temperature"
Type	Straight through	
Sodium temp.,°C:		
at reactor inlet	510	440
at reactor outlet	540	470
Steam temp.,°C	480	415
Steam pressure, atm.	168	70—87
Material	2.25%Cr+1%Mo	2.25%Cr+1%Mo
Type of intermediate superheat	Sodium	—
Loop power, MW	1000	1200

Fuel and Materials. In the FFTF reactor and in the first charges of the CRBRP reactor, plutonium oxide fuel will be used. At present, work is being carried out for the purpose of reducing the doubling time in fast breeder reactors down to 10-15 years. The fuel is being made on a carbide and nitride base, for which testing is being carried out on ever-increasing scales (Table 1).

At the same time, work is being carried out on the production of improved alloys (Table 2), the possibilities are being studied of preventing the chemical interaction of the oxide fuel with the cladding, due to the use of buffer antioxygen layers, internal coating of the cladding, and the reduction of the oxygen content of the fuel.

Safety. The main problems in this field are the prevention of accidents, their localization within the confines of the primary circuit, limitation of the damage to the active zone, and their radiobiological consequences.

A large volume of numerical studies is being carried out on various emergency situations, including the maximum hazard with melting of the active zone. In the TREAT reactor, the behavior of fuel under transient conditions is being studied. In 1975, 12 capsule experiments and four experiments in the loop were carried out. The installation has been completed of the SLSF liquid — metal loop in the ETR reactor, designed for testing fuel with hazards created by a reduction of the coolant flow rate. An assembly of 37 full-scale fuel rods can be installed in the loop. The cost of an experiment is $5 million and up to four experiments per year can be carried out. It is planned to install a SAREF facility (completion of construction in 1983) for investigating the probability of the formation of a secondary critical mass in the case of melting of the fuel. The "active zone" of the facility consists of four full-scale fuel assemblies, in each of which are 271 rod-shaped fuel elements. The cost of the facility is $350-650 million, the proposed cost of an experiment is $25 million, and the number of experiments will be four per year. The overwhelming majority of the problems of safety require solutions which will satisfy the demands of the community, with a guarantee of the safety of construction of the nuclear power station.

Plant Development. In the USA, a program of construction is being achieved for fast reactor components — steam generators, pumps, pipelines and valves. At present, this is already restricting somewhat the construction of fast reactors; however, it promises great advantages at the stage of bringing commercial reactors into operation.

The program of work on steam generators includes developments which are dependent on and independent of the final concept of the steam generator. This involves methods of detecting leaks, materials, and investigations of the sodium — water reaction. For a commercial fast reactor, the parameters of which still have not been determined finally, it is proposed to go ahead with the development of "high-temperature" and "low-temperature" versions of the steam generator (Table 3).

In planning the equipment, the principal attention is being paid to increasing the reliability and reducing costs. Failures in operation of the steam generators must not lead to a reduction of the readiness factor of nuclear power stations by more than 5%; the cost of the steam generators must be at the level of $30 million/kW (el.). It is desirable to have the pumps of the smallest possible dimensions and of the simplest construction. They must operate with a minimum pressure at the intake without generating cavitation,

and their cost must not exceed $3 million. Attention is being paid to the possibility of reducing the flow rates in the pipelines, on account of a reduction of the compensation loops, and to the necessity for reducing the production costs of the accessories.

It was noted at the session that the construction of commercial fast reactors requires the solutions of a number of important technical problems. The Soviet – American cooperation in the field of fast reactors should be capable of successfully solving these problems.

SOVIET – AMERICAN SEMINAR ON THE SAFETY OF FAST REACTORS

Yu. E. Bagdasarov

The seminar took place January 12-15, 1976 at the Argonne National Laboratory (ANL). Each side presented 12 reports. In addition to the issues and discussions at the seminar, the Soviet delegation visited the Argonne and Hanford Laboratories and the Idaho Nuclear Center.

Great interest was shown in the Soviet reports and to the seminar as a whole by the American side. This interest was governed by and associated with the successes of the Soviet Union in the construction of nuclear power stations with fast reactors. The USA program differs significantly from that accepted in the Soviet Union: Construction of the first nuclear power station with fast reactors is planned to start in the next few years at Clinch River. However, at present large resources are being assigned for the construction of test rigs and reactors for special purposes in order to carry out experimental work, especially on safety. Included in these large-scale experimental reactors are the FFTF, with a thermal capacity of 400 MW, which is intended to start up in 1978. The heat will be discharged into the surrounding medium through air heat exchangers.

Approach to the Safety of Fast Reactors. The opinion of the majority of American specialists 10 to 15 years ago was that a number of well-known specific features of fast reactors require a demonstration of their safety. At the present time, there is a degree of credence in safety and the principal problem of future work is to demonstrate it before the general public.

The results of the first series of experimental investigations influenced the change of opinions of the American specialists. Thus, local boiling of sodium in an individual cluster (as a result of local blocking of a small part of a section of the latter), as a rule is due to the formation and "collapse" of individual steam bubbles even during the initial heating up of the coolant. Rapid spread of boiling to the entire fuel bundle does not take place, and damage to the fuel element claddings, located in the zone of bubbles, is extended in time, and with the presence of a system for indicating the process, further development of a hazard can be prevented. The passage of gas bubbles through the fuel cluster, either because they reach the inlet section of the circuit, or in the case of bursting of the fuel element claddings with the discharge of gaseous fission products, does not lead to a dangerous superheating of the fuel elements and their rapid destruction. The interaction of the molten fuel with the sodium is characterized by a relatively low heat transfer due to the relatively small degree of dispersion of the fuel. For this reason, the probability and scale of the danger of a steam explosion are reduced sharply in comparison with previously made assumptions. The mechanical energy amounts to an insignificant part (less than 1%) of the total energy released during maximum hazards.

Requirements on Structural Safety Measures during Planning. The principal requirements imposed for the safety of fast reactors can be formulated in the following way.

The integrated sodium void reactivity factor must be negative or slightly positive. In reactor projects, including FFTF and Clinch River, de-energizing of the installation with simultaneous failure of the system,

Translated from Atomnaya Énergiya, Vol. 41, No. 1, pp. 67-69, July, 1976.

total rupture of the main pipeline of the primary circuit, and the introduction of positive reactivity with maximum speed, are considered as hypothetical hazards.

All the radioactive plant and systems of the primary circuit, together with the reactor, are installed in the leaktight protective vessel. However, it is not designed for a hazard of an explosive nature, but is a kind of barrier for the prevention of leaks of aerosols and active gases during unsealing of the circuit, including also causes not connected with a hypothetical hazard. As the maximum possible hazard is considered before all possible conditions, intrareactor devices are being planned for a melted fuel assembly, the prevention of burning-through of the reactor vessel, and the assurance of posthazard removal of the residual heat release. It is considered to be compulsory to monitor the sodium temperature at the outlet from each fuel cluster, for which a central outlet for the coolant is provided, and an outlet in the gas void for tracer xenon atoms. However, these parameters are not included in the scram system.

In order to assess the safety of the installation in the case of an emergency in the steam generators, for the maximum hypothetical hazard is assumed the instantaneous total rupture of one coolant feed pipeline and its surrounding poles, with a buildup of the water flow rate in the sodium in the latter up to the limiting value during 0.1 sec.

Containers with radioactive sodium are being designed compact, filled with nitrogen (oxygen content less than 4-5%) with a closed ventilation system. It will be specified that the inside of the compartment be lined with steel, and the floor divided into trays. On the outer face, between the steel lining and the concrete, a layer of firebrick is proposed, 15 cm thick and a gap of several cm between the steel and the firebrick for drawing off water vapor which may be released from the concrete in the case of a hazard or in other situations. The layer of firebrick is required in view of the severe consequences of the sodium reaching the concrete. Containers of nonradioactive sodium also will have a steel lining. The collection of overflowed sodium will be provided for in special tanks. In the case of an emergency, it is proposed to replace the air in the containers with nitrogen.

Functional Experimental Assemblies and Test-Rigs. The TREAT pulsed reactor, with a sodium loop, was constructed in Idaho for carrying out experiments to test fast reactor fuel elements under emergency conditions. The reactor is provided with a special sodium loop with its own pump. Up to seven fuel elements of the FFTF reactor type can be tested simultaneously, and data can be obtained about melting of the fuel, its interaction with sodium, the characteristics of the fuel element breakdown process, the dynamics of the coolant as a result of a rapid increase of energy release or a reduction of the flow rate, and movement of the melted fuel. A special device is provided — a hodoscope, for photography and teledisplay in a real-time scale of the process of void formation and the movement of steel and fuel in the test section. This is a 334 collimated beam of neutrons, each of which "illuminates" its own section of the channel (continuous neutronography). At the present time, 13 experiments have been carried out simulating abrupt power increase, and 10 experiments simulating instantaneous reduction of flow rates. In addition to the continuous recording of the process by the devices mentioned, after each experiment the loop in the assembly was transferred to a hot laboratory for breaking down and investigation.

The sodium loop for the intrareactor investigations of the safety of SLSF in the assembly is installed in the thermal reactor ETR with a capacity of 175 MW (th.). The facility and the loop characteristics permit the conditions of heat release which are nominal for fast power reactors to be provided in an assembly containing up to 61 fuel elements. However, in the next two and one-half years, it is proposed to increase the number of fuel elements in the assembly up to 127. The main trend of the investigations is to study the consequences of hazards from a reduction of the sodium flow rate through the fuel assembly according to different causes: external causes; local or total blocking of the assembly at different points of it; simulation of a hazard with failure of the pumps, etc. The program for 1976-1980 provides for 12 experiments (three/year). At the present time, one experiment has been carried out on an assembly of 19 fuel elements. Research cycle: reduction of the sodium flow rate from 100 to 15% with a speed of 100%/sec. A power reduction from 100% to zero during 0.3 sec was carried out 0.5 sec after the start of the process (at this time boiling commenced). The loop still did not split, and neutronography showed no visible cracks in the fuel elements.

The OPERA test rig in Argonne National Laboratory is designed for outside reactor investigations of processes as a result of deeply perturbed flow rates. The test rig has a working section, where assemblies of seven full-scale fast reactor fuel elements can be tested. Heat is released in the fuel elements as a result of electrical heating with a Nichrome wire, separated from the stainless steel cladding by an

insulator of boren nitrate. The test rig is used for the investigation of surge processes and the reentry of sodium by the simulation of an accident with pump breakdown and blocking, and also instruments for detecting accidents are being tested.

In Oakridge National Laboratory, a high-temperature test rig FFM has been constructed for out-of-reactor investigations of processes with deep sodium flow rate perturbations, in which at present assemblies of up to 91 fuel elements can be tested, and in the future, up to 217. The electric power fed to the fuel elements in 2MW at present. Since 1970, five assemblies of up to 19 fuel elements each have been investigated on the test rig. The rig has operated for 15,000 h with sodium and 1700 h with heat release in the fuel assemblies. The sodium boiling cycle has lasted for about 13 min.

On a test rig for investigating the interaction of melted fuel with sodium in the Argonne National Laboratory, an experiment is being set up with a single-fuel element channel: A single fuel element is surrounded by an annular space, through which sodium flows with a velocity of 8 m/sec. Inside the fuel element a mixture of molybdenum trioxide and metallic uranium is installed. A chemical reaction is initiated electrically, which proceeds with velocities which are characteristic for hypothetical accidents of melting of the active zone, and which concludes with the formation of molten uranium oxide at a temperature of 3200°C. At a previously marked spot, the fuel element cladding bursts and the molten fuel is ejected into the sodium. The process is recorded both by the usual instruments and by x-ray cinephotography. After carrying out this experiment, a similar experiment will be set up but on an assembly of seven fuel elements.

There are 12 experimental test rigs with tanks or leaktight vessels with volumes of 1-1000 m^3 with a permissible pressure of up to 7 kg/cm^2, where a small flow of pure sodium or sodium contaminated with fuel under industrial conditions is simulated, in order to investigate the consequences of sodium fires. Fires are studied, and the behavior of aerosol products of sodium and fuel with time, their concentration, and rate of deposition originated at this temperature and pressure.

In order to choose and demonstrate the efficiency of the fire extinguishing systems of the FFTF facility, three experiments have been carried out. Sodium, heated to 600°C in amounts of 300, 350, and 1110 kg, was discharged into trays of a leaktight compartment with dimensions $5 \times 5 \times 8$ m. In one of the experiments, the interaction of high-temperature sodium (350 kg) with concrete placed on the tray was studied. The thickness of the concrete layer was about 10 cm, with a tray depth of 30 cm. The atmosphere in the compartment was air. At the end of the process (15 min), when nitrogen started to feed in, there was 25% of hydrogen in the compartment. Almost all the discharged sodium interacted. In two other experiments, the sodium was discharged into trays without concrete. The fire extinguishing efficiency was investigated by means of inert gases. In this experiment, not more than 5% of the discharged sodium burned. The nitrogen in the compartment started to enter also 15 min after the start of the experiment; at this time, the combustion process almost finished. All the experiments showed the high efficiency of the fire extinction in the leaktight compartments. The trays, when the sodium flowed out, were distorted by the temperature stresses, but the leaktightness was not lost. No cracking of the cement floor below the lining was observed.

SEMINAR ON GENERAL PURPOSE AND SPECIAL ACCESSORIES FOR NUCLEAR POWER STATIONS

G. V. Kiselev

The firms of Steel Accessories of Perst GMbH-KG and Babcock and Wilcox AG, at the end of March, held a seminar in Moscow for Soviet specialists on the general-purpose and special accessories for various purposes manufactured by them. Over the last half-year this was the second meeting with representatives of the West German firms [see At. Énerg., Vol. 40, No. 2, 192 (1976)]. Twenty reports and communications were presented at the seminar, which contained data on the technology of manufacture, organization of industrial production, construction and purposes of the accessories, and their quality control, and an account was given of the general and special requirements on construction.

It should be mentioned that in 1975 accessories worth 15 million rubles were delivered by these firms to the Soviet Union.

These firms specialize in the manufacture of general-purpose and special accessories, but accessories for conventional and nuclear power stations received preferential development. In the technological production cycle, drop-forging of individual units is widely used: reactor vessel, bonded branch pipes, shutoff sections such as wedges, etc. At the factory of Steel Accessories Perst GMbH-KG it is possible to forge complex complete housings with an internal diameter of 300 mm and a mass of up to 465 kg. The forgings are prepared by electric spark erosion. For this purpose, the part to be worked is placed in an oil bath, into which graphite electrodes of the required shape are lowered. The forging made in this way requires hand finishing. Treatment of the individual units (housings, covers, etc) is carried out on automatic machine tool lines, and also by the use of machines with programmed control. In connection with the use of drop-forged parts, great importance is attached to the method of welding and quality inspection of the welded seams. A considerable part of welded joints is effected with an arc weld under a flux. Accessories for nuclear power stations, manufactured from drop-forged blanks of austenitic steel, are welded by electron-beam welding in vacuo without additional material. Welding by means of electron beams has a number of advantages in comparison with other types — in the first place, in the quality of the welded joints, times of effecting the weld, and the absence of finishing of the part. Inspection for the quality of the accessories commences with examination of the materials supplied by other firms. In the manufacturing process, the individual items and accessories are tested according to a special plan, which provides for control of the drawings and specifications; methods of nondestructive testing during welding and verification of the measuring instruemnts. Welded joints are checked by the usual (x-ray inspection, luminescent and magnetic-powder) methods. Stress after welding is reduced by heat-working of the part.

The following requirements are imposed on the construction of accessories: maximum standardization and unification of components; maximum possible compaction in a shutoff unit (depending on a considerable extent on the material of the valve seat and the treatment of its surface); leaktightness of the joint between cover and housing, and also the shaft of slide gates.

The last requirement is very important when the accessories are used in pipelines with highly corrosive, radioactive and toxic media.

The leaktightness of the cover and housing of the accessories of the firm Babcock and Wilcox AG is ensured by flanged and self-sealing joints. There are three types of packing for the first of these: by bolts and gaskets; with intermediate suction and with welded collar or membrane sealing. In the first case, resilient metallic gaskets are used with a stressed soft or asbestos covering. Spirally wound gaskets also are used.

Translated from Atomnaya Énergiya, Vol. 41, No. 1, pp. 69-70, July, 1976.

In the second case, two double seals form an intermediate chamber for pumping out the effluent medium. The latter represents the well-known joint by welding.

A representative of the firm Steel Accessories Perst GMbH-KG reported that they have developed and can supply an equipment for sharp mitering of seams, the drawings for which have been transmitted to the Soviet external commerce society Mashinoimport. Thanks to remote control, the cutter allows shearing of an annular mitered seam during a single pass. A special feature of a self-sealing joint is that the sealing force increases with increase of the internal pressure. As a result of this, the cover clamps the special gasket of graphitized asbestos with wedge-shaped nickel plates to a segmented collar, located in the gap of the housing.

There are also new designs of gaskets in the factories of this same firm. Thus, e.g., a gasket for a flanged joint, consisting of a Niconel wire spiral, is enclosed in austenitic steel sheaths. The Niconel wire spiral imparts the necessary stability and elasticity and the austenitic steel sheaths achieve the sealing. Sylphons, together with packing glands, are required, as a rule, in regulating accessories and check valves, and mainly multilayered sylphons are used (six- or two-layered) of stainless steel. Sylphons for shutoff and controlling accessories will endure 20 and 10 thousand cycles of double lifts, respectively, and, moreover, 20 and 50 thousand cycles with a 30% lift. During the experiments, it was established that in the case when the specified number of working cycles is exceeded, the sylphons lose leaktightness.

For sodium slide valves, a freezing gasket is considered to be more preferable, as the use of sylphons leads, in this case, to difficulties in their manufacture and to an increase of the dimensions of the housing, due to the relatively large stroke of the shaft. One of the structural characteristics of certain types of the manufactured accessories, due to the technology of forging the housings, is the use of a valve seat with a close threaded fit in the slide valve housing or the check-valve housing. For this purpose, the inside surface of the valve seat has lugs for screwing-in with a special tool. This method of securing the valve seat ensures, first of all, a quite simple replacement in the case of necessity and, secondly, it facilitates grinding of the surface because the main bulk of the work on grinding can be done outside the housing. This structural characteristic is extremely important.

All kinds of designs of tapered shutoff devices, types of valve seats, and forms of weld seams are of interest. No fewer than 35 types of shutoff slide valves, regulating valves, and check valves have been developed and offered for supplying by the firm of Babcock and Wilcox AG. The high-speed cutoff valves deserve mention with a diameter of up to 800 mm, designed on a steam pressure of up to 83 bar and a temperature of 300°C. Their time of operation is ~2 sec. The firm of Steel Accessories Perst GMbH-KG has developed more than 40 types of different accessories, including sodium accessories for the SNR-300 fast reactor (Federal German Republic). The housing of this armature consists of upper and lower parts, made by drop forging and joined to one another by electron beam welding. The inner part is Z-shaped in order to ensure its complete drainage while maintenance work is carried out on the pipelines. Moreover, the sodium pipelines have a slope of 2-5° for total drainage of the sodium. Together with the freezing gasket, multilayer sylphons are used widely for which Niconel-600 is used as the material. Sodium slide valves with a diameter of up to 300 mm can be supplied.

In the activities of both firms there exists the practice of including contracts for service maintenance during operation, when accessories are supplied, for which there are suitable servicing personnel. The seminar, organized by the All-Union Association Vneshtorgreklam created interest among the Soviet specialists.

engineering science

continued
from back cover

Title	# of Issues	Subscription Price
Metallurgist *Metallurg*	12	$225.00
Metal Science and Heat Treatment *Metallovedenie i termicheskaya obrabotka metallov*	12	$215.00
Polymer Mechanics *Mekhanika polimerov*	6	$195.00
Problems of Information Transmission *Problemy peredachi informatsii*	4	$175.00
Programming and Computer Software *Programmirovanie*	6	$95.00
Protection of Metals *Zashchita metallov*	6	$195.00
Radiophysics and Quantum Electronics (Formerly Soviet Radiophysics) *Izvestiya VUZ. radiofizika*	12	$225.00
Refractories *Ogneupory*	12	$195.00
Soil Mechanics and Foundation Engineering *Osnovaniya, fundamenty i mekhanika gruntov*	6	$195.00
Soviet Applied Mechanics *Prikladnaya mekhanika*	12	$225.00
Soviet Atomic Energy *Atomnaya energiya*	12 (2 vols./yr. 6 issues ea.)	$235.00
Soviet Journal of Glass Physics and Chemistry *Fizika i khimiya stekla*	6	$ 95.00
Soviet Journal of Nondestructive Testing (Formerly Defectoscopy) *Defektoskopiya*	6	$225.00
Soviet Materials Science *Fiziko-khimicheskaya mekhanika materialov*	6	$195.00
Soviet Microelectronics *Mikroélektronika*	6	$135.00
Soviet Mining Science *Fiziko-tekhnicheskie problemy razrabotki poleznykh iskopaemykh*	6	$225.00
Soviet Powder Metallurgy and Metal Ceramics *Poroshkovaya metallurgiya*	12	$245.00
Strength of Materials *Problemy prochnosti*	12	$295.00
Theoretical Foundations of Chemical Engineering *Teoreticheskie osnovy khimicheskoi tekhnologii*	6	$195.00
Water Resources *Vodnye Resursy*	6	$190.00

Back volumes are available. For further information, please contact the Publishers.

SEND FOR YOUR FREE EXAMINATION COPIES

Plenum Publishing Corporation

Plenum Press • Consultants Bureau
• IFI/Plenum Data Corporation

227 WEST 17th STREET
NEW YORK, N. Y. 10011

United Kingdom: Black Arrow House
2 Chandos Road, London NW10 6NR England

Declassified and Approved For Release 2013/09/23 : CIA-RDP10-02196R000700080001-9

breaking the language barrier

WITH COVER-TO-COVER
ENGLISH TRANSLATIONS
OF SOVIET JOURNALS

in engineering science

Title	# of Issues	Subscription Price
Automation and Remote Control *Avtomatika i telemekhanika*	24	$260.00
Biomedical Engineering *Meditsinskaya tekhnika*	6	$195.00
Chemical and Petroleum Engineering *Khimicheskoe i neftyanoe mashinostroenie*	12	$275.00
Chemistry and Technology of Fuels and Oils *Khimiya i tekhnologiya topliv i masel*	12	$275.00
Combustion, Explosion, and Shock Waves *Fizika goreniya i vzryva*	6	$195.00
Cosmic Research (Formerly Artificial Earth Satellites) *Kosmicheskie issledovaniya*	6	$215.00
Cybernetics *Kibernetika*	6	$195.00
Doklady Chemical Technology *Doklady Akademii Nauk SSSR*	2	$65.00
Fibre Chemistry *Khimicheskie volokna*	6	$175.00
Fluid Dynamics *Izvestiya Akademii Nauk SSSR mekhanika zhidkosti i gaza*	6	$225.00
Functional Analysis and Its Applications *Funktsional'nyi analiz i ego prilozheniya*	4	$150.00
Glass and Ceramics *Steklo i keramika*	12	$245.00
High Temperature *Teplofizika vysokikh temperatur*	6	$195.00
Industrial Laboratory *Zavodskaya laboratoriya*	12	$215.00
Inorganic Materials *Izvestiya Akademii Nauk SSSR, Seriya neorganicheskie materialy*	12	$275.00
Instruments and Experimental Techniques *Pribory i tekhnika éksperimenta*	12	$265.00
Journal of Applied Mechanics and Technical Physics *Zhurnal prikladnoi mekhaniki i tekhnicheskoi fiziki*	6	$225.00
Journal of Engineering Physics *Inzhenerno-fizicheskii zhurnal*	12 (2 vols./yr. 6 issues ea.)	$225.00
Magnetohydrodynamics *Magnitnaya gidrodinamika*	4	$175.00
Measurement Techniques *Izmeritel'naya tekhnika*	12	$195.00

SEND FOR YOUR FREE EXAMINATION COPIES

Back volumes are available.
For further information,
please contact the Publishers.

continued on inside back cover

Declassified and Approved For Release 2013/09/23 : CIA-RDP10-02196R000700080001-9